



International Ocean Discovery Program Expedition 390 Preliminary Report

South Atlantic Transect 1

7 April–7 June 2022

Rosalind M. Coggon, Jason B. Sylvan, Damon A.H. Teagle, Julia Reece, Gail L. Christeson, Emily R. Estes, Trevor J. Williams, and the Expedition 390 Scientists

Publisher's notes

Core samples and the wider set of data from the science program covered in this report are under moratorium and accessible only to Science Party members until 23 January 2024.

This publication was prepared by the *JOIDES Resolution* Science Operator (JRSO) at Texas A&M University (TAMU) as an account of work performed under the International Ocean Discovery Program (IODP). This material is based upon work supported by the JRSO, which is a major facility funded by the National Science Foundation Cooperative Agreement Number OCE1326927. Funding for IODP is provided by the following international partners:

National Science Foundation (NSF), United States
Ministry of Education, Culture, Sports, Science and Technology (MEXT), Japan
European Consortium for Ocean Research Drilling (ECORD)
Ministry of Science and Technology (MOST), People's Republic of China
Korea Institute of Geoscience and Mineral Resources (KIGAM)
Australia-New Zealand IODP Consortium (ANZIC)
Ministry of Earth Sciences (MoES), India

Portions of this work may have been published in whole or in part in other IODP documents or publications.

Disclaimer

The JRSO is supported by the NSF. Any opinions, findings, and conclusions or recommendations expressed in this material do not necessarily reflect the views of the NSF, the participating agencies, TAMU, or Texas A&M Research Foundation.

Copyright

Except where otherwise noted, this work is licensed under the Creative Commons Attribution 4.0 International (CC BY 4.0) license (<https://creativecommons.org/licenses/by/4.0/>). Unrestricted use, distribution, and reproduction are permitted, provided the original author and source are credited.



Citation

Coggon, R.M., Sylvan, J.B., Teagle, D.A.H., Reece, J., Christeson, G.L., Estes, E.R., Williams, T.J., and the Expedition 390 Scientists, 2022. Expedition 390 Preliminary Report: South Atlantic Transect 1. International Ocean Discovery Program. <https://doi.org/10.14379/iodp.pr.390.2022>

ISSN

World Wide Web: 2372-9562

Expedition 390 participants

Expedition 390 scientists

Rosalind M. Coggon

Co-Chief Scientist Expedition 390
School of Ocean and Earth Science
University of Southampton
United Kingdom
R.M.Coggon@soton.ac.uk

Jason B. Sylvan

Co-Chief Scientist Expedition 390
Department of Oceanography
Texas A&M University
USA
jasonsylvan@tamu.edu

Damon A.H. Teagle*

Co-Chief Scientist Expedition 393
School of Ocean and Earth Science
National Oceanography Centre Southampton
University of Southampton
United Kingdom
Damon.Teagle@southampton.ac.uk

Julia Reece*

Co-Chief Scientist Expedition 393
Department of Geology and Geophysics
Texas A&M University
USA
jreece@geos.tamu.edu

Gail L. Christeson*

Site Survey Data Lead
Marine Geology and Geophysics
National Science Foundation
USA
gchriste@nsf.gov

Also at
University of Texas Institute for Geophysics
USA
glchristeson@utexas.edu

Emily R. Estes

Expedition Project Manager/Staff Scientist Expedition 390
International Ocean Discovery Program
Texas A&M University
USA
estes@iodp.tamu.edu

Trevor J. Williams*

Expedition Project Manager/Staff Scientist Expedition 393
International Ocean Discovery Program
Texas A&M University
USA
williams@iodp.tamu.edu

Masataka Aizawa

Inorganic Geochemist
Graduate School of Engineering and Science
University of the Ryukyus
Japan
masataka-aizawa@apr.email.ne.jp

Chiara Borelli*

Micropaleontologist (benthic foraminifera)
Department of Earth and Environmental Sciences
University of Rochester
USA
cborelli@ur.rochester.edu

Joshua D. Bridges

Paleomagnetist
Department of Earth and Environmental Sciences
University of Rochester
USA
jbridge2@ur.rochester.edu

Elliot J. Carter

Petrologist
School of Earth and Environmental Sciences
University of Manchester
United Kingdom
elcarter@tcd.ie

Jaume Dinarès-Turell

Paleomagnetist
National Institute of Geophysics and Volcanology (INGV)
Italy
jaume.dinares@ingv.it

Justin D. Estep

Physical Properties Specialist/Core-Log-Seismic Correlator
School of Earth and Sustainability
Northern Arizona University
USA
justin.estep@nau.edu

William P. Gilhooly III

Organic Geochemist
Department of Earth Sciences
Indiana University/Purdue University, Indianapolis
USA
wgilhool@iupui.edu

Lewis Grant

Physical Properties Specialist/Stratigraphic Correlator
School of Ocean and Earth Science
University of Southampton
United Kingdom
l.grant@soton.ac.uk

Michael R. Kaplan

Sedimentologist
Lamont-Doherty Earth Observatory
Columbia University
USA
mkaplan@ldeo.columbia.edu

Pamela D. Kempton

Petrologist
Department of Geology
Kansas State University
USA
pkempton@ksu.edu

*Shore-based participant

Walter Kurz*

Petrologist

Institute of Earth Sciences
University of Graz
Austria
walter.kurz@uni-graz.at

Christopher M. Lowery

Micropaleontologist (planktic foraminifera)

Institute for Geophysics
University of Texas at Austin
USA
cmlowery@utexas.edu

Andrew McIntyre

Physical Properties Specialist/Stratigraphic Correlator

School of Environment, Earth and Ecosystem Sciences
The Open University
United Kingdom
Andrew.mcintyre@open.ac.uk

Muthusamy Prakasam*

Micropaleontologist (planktic foraminifera)

Biostratigraphy
Wadia Institute of Himalayan Geology
India
prakasam@wihg.res.in

Claire M. Routledge

Micropaleontologist (nannofossils)

Institute of Geosciences
Christian-Albrechts-University of Kiel
Germany
claire.routledge@ifg.uni-kiel.de

Angela L. Slagle

Physical Properties/Downhole Measurements

Lamont-Doherty Earth Observatory
Columbia University
USA
aslagle@ldeo.columbia.edu

Outreach

Marlo Garnsworthy

Outreach Officer

Icebird Studio
USA
icebirdstudio@outlook.com

Mako Takada

Microbiologist/Organic Geochemist

Graduate School of Frontier Sciences
University of Tokyo
Japan
mako-takada@g.ecc.u-tokyo.ac.jp

Leonardo Tamborrino

Sedimentologist

MARUM—Center for Marine Environmental Sciences
University of Bremen
Germany
ltamborrino@marum.de

Liyan Tian*

Petrologist

Institute of Deep-sea Science and Engineering
Chinese Academy of Sciences
China
lytian@idsse.ac.cn

Yi Wang

Inorganic Geochemist

Department of Geology and Geophysics
Woods Hole Oceanographic Institution
USA
ywang@whoi.edu

Kiho Yang

Sedimentologist

Department of Oceanography
Pusan National University
Republic of Korea
kyang@pusan.ac.kr

Tiantian Yu*

Microbiologist/Organic Geochemist

School of Oceanography
Shanghai Jiao Tong University
China
yutiantian@sjtu.edu.cn

Laura Guertin

Outreach Officer

Earth Science
Penn State Brandywine
USA
guertin@psu.edu

Operational and technical staff

Siem Offshore AS officials

Jake Robinson
Master of the Drilling Vessel

Mark Robinson
Drilling Supervisor

JRSO shipboard personnel and technical representatives

Matthew Allen
Development Engineer

Aidan Leetz
Marine Laboratory Specialist

Alejandro Avila Santis
Marine Laboratory Specialist

Daniel Marone
Marine Laboratory Specialist

Timothy Blaisdell
Applications Developer

Brittany Martinez
Curatorial Specialist

William Cary
Applications Developer

Aaron Mechler
Marine Laboratory Specialist

David Fackler
Marine Computer Specialist

Stephen Midgley
Operations Superintendent

Fabricio Ferreira
Marine Laboratory Specialist

Beth Novak
Assistant Laboratory Officer

Clayton Furman
Logging Engineer

Chieh Peng
Laboratory Officer

Randy Gjesvold
Marine Instrumentation Specialist

Jessica Riekenberg
Marine Laboratory Specialist

Sandra Herrmann
Imaging Specialist

Alyssa Stephens
Publications Specialist

Mark Higley
Marine Laboratory Specialist

Steven Thomas
Marine Computer Specialist

Myriam Kars
Marine Laboratory Specialist

Garrick Van Rensburg
Marine Instrumentation Specialist

Abstract

The South Atlantic Transect (SAT) is a multidisciplinary scientific ocean drilling project that comprises four International Ocean Discovery Program (IODP) expeditions: engineering Expeditions 390C and 395E as well as Expeditions 390 and 393. Altogether, the expeditions aim to recover complete sedimentary sections and the upper 100–350 m of the underlying oceanic crust along a slow/intermediate spreading rate Mid-Atlantic Ridge crustal flow line at $\sim 31^{\circ}\text{S}$. The sediments along this transect were originally spot cored more than 50 y ago during Deep Sea Drilling Project Leg 3 (December 1968–January 1969) to help verify the theories of seafloor spreading and plate tectonics. Given dramatic advances in drilling technology and analytical capabilities since Leg 3, many high-priority scientific objectives can be addressed by revisiting the transect. The SAT expeditions target six primary sites on 7, 15, 31, 49, and 61 Ma ocean crust, which fill critical gaps in our sampling of intact in situ ocean crust with regards to crustal age, spreading rate, and sediment thickness. Drilling these sites is required to investigate the history of the low-temperature hydrothermal interactions between the aging ocean crust and the evolving South Atlantic Ocean and quantify past hydrothermal contributions to global biogeochemical cycles. Samples from the transect of the previously unexplored sediment- and basalt-hosted deep biosphere beneath the South Atlantic Gyre are essential to refining global biomass estimates and examining microbial ecosystems' responses to variable conditions in a low-energy gyre and aging ocean crust. The transect is located near World Ocean Circulation Experiment Line A10, providing access to records of carbonate chemistry and deepwater mass properties across the western South Atlantic through key Cenozoic intervals of elevated atmospheric CO_2 and rapid climate change. Reconstruction of the history of the deep western boundary current and deepwater formation in the Atlantic basins will yield crucial data to test hypotheses regarding the role of evolving thermohaline circulation patterns in climate change and the effects of tectonic gateways and climate on ocean acidification.

Engineering Expeditions 390C and 395E cored a single hole through the sediment/basement interface with the advanced piston corer/extended core barrel system at five of the six primary proposed SAT sites and installed a reentry system with casing either into basement or within 10 m of basement at each of those five sites. Expedition 390 (7 April–7 June 2022) conducted operations at three of the SAT sites, recovering 700 m of core (77% recovery) over 30.3 days of on-site operations. Sediment coring, basement drilling, and logging were conducted at two sites on 61 Ma crust, and sediment coring was completed at the 7 Ma crust site. At Site U1557 on 61 Ma crust, the drill bit was deposited on the seafloor prior to downhole logging, leaving Hole U1557D available for future deepening and to establish a legacy borehole for basement hydrothermal and microbiological experiments. Expedition 390 scientists additionally described, and analyzed data from, 792 m of core collected during Expeditions 390C and 395E. Expedition 393 plans to operate at four sites, conducting basement drilling and downhole logging at the 7 Ma site, in addition to sediment coring, basement drilling, and logging at the sites intermediate in age.

1. Introduction

Together, the multidisciplinary South Atlantic Transect (SAT) expeditions, comprising International Ocean Discovery Program (IODP) Expeditions 390 and 393 and supported by preparatory engineering Expeditions 390C and 395E, will drill a transect along a crustal flow line across the western flank of the southern Mid-Atlantic Ridge (MAR) at $\sim 31^{\circ}\text{S}$ to investigate the hydrothermal evolution of the aging ocean crust, sediment- and basement-hosted microbial community variation with increasing substrate age, the paleoceanographic evolution of the South Atlantic Ocean, and the deep-ocean and subtropical gyre responses to changing global climate. The SAT expeditions revisit an area first cored in 1968, when Deep Sea Drilling Project (DSDP) Leg 3 accomplished one of the great achievements of scientific ocean drilling: recovering sediments from a transect of spot cored holes across the South Atlantic between $\sim 28^{\circ}$ and 30°S (Figure F1) to demonstrate that basal sediment age increases with distance from the ridge axis. This provided definitive proof for the theory of seafloor spreading (Scientific Party, 1970). The SAT expeditions have been designed to take advantage of the dramatic advances in drilling technology and analyti-

cal capabilities since the earliest days of scientific ocean drilling to address many high-priority scientific objectives by revisiting the Leg 3 transect region.

Although there have been more than 50 y of scientific ocean drilling since Leg 3, major gaps remain in our observations of the evolving Earth system. These gaps include drill cores of ocean crust of different ages and formed at contrasting spreading rates, virtually unexplored biogeographic microbial provinces, and continuous samples of key times in Earth's climate, changing ocean chemistry, or geomagnetic field history. Transects of drill holes, sampling both the sediment cover and the uppermost oceanic crust, can provide essential knowledge of how interconnected processes have evolved over Earth's history and responded to changes in external drivers such as atmospheric CO₂ concentrations, oceanic gateways, or major ocean currents. Transects can provide important information about the duration of hydrothermal exchange by sampling tens of millions of years of ocean crust formed at the same mid-ocean ridge (MOR). However, sampling both the sediment and the underlying basaltic basement in a specific ocean region has rarely been undertaken in a systematic manner, and the few transects previously accomplished cover relatively short intervals of Earth history (e.g., Juan de Fuca Ridge, 0–3.5 Ma [Shipboard Scientific Party, 1997; Expedition 301 Scientists, 2005; Expedition 327 Scientists, 2011] and Costa Rica Rift, 0–7 Ma [Shipboard Scientific Party, 1985]).

Comparison of predicted and observed conductive heat flow through the ocean crust reveals a discernible conductive heat flow deficit out to 65 Ma crust on average (e.g., Stein and Stein, 1994; Figure F2), indicating that there is significant advection of heat from the cooling of the oceanic lithosphere out to this age. However, basement hydrological flow can occur in crust of all ages if sufficient hydrologic heads can be established because crustal age is only one of a suite of interlinked parameters that influence the duration, depth, and intensity of off-axis hydrothermal fluid flow, including: basement topography; volcanic stratigraphy and flow morphology; and sediment type, thickness, and completeness of basement blanketing. Simple relationships may not exist between crustal age, fluid flow, thermal and chemical exchange, and biological activity.

Hence, the SAT expeditions were designed to recover complete sediment sections and the uppermost ~100–350 m of basaltic ocean crust produced between ~7 and 61 Ma at the slow/intermediate-spreading MAR, returning to the Leg 3 transect region to achieve the following objectives:

1. Quantify the timing, duration, and extent of ridge flank hydrothermal fluid-rock exchange;
2. Investigate sediment- and basement-hosted microbial community variation with substrate composition and age; and
3. Investigate the responses of Atlantic Ocean circulation patterns and the Earth's climate system to climate change, including elevated atmospheric CO₂ during the Cenozoic.

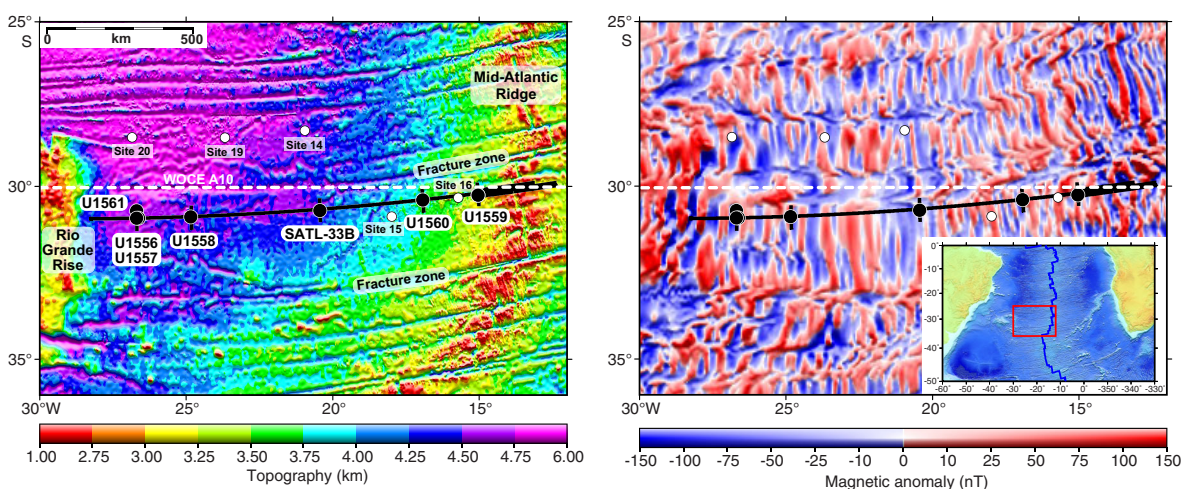


Figure F1. SAT study region. Left: topography (Ryan et al., 2009). Right: magnetic anomalies (Maus et al., 2009). Inset shows regional setting. Black lines = locations of Crustal Reflectivity Experiment Southern Transect seismic reflection profiles, black circles = SAT sites, white dashed line = World Ocean Circulation Experiment (WOCE) Line A10, white circles = DSDP Leg 3 sites.

Expeditions 390 and 393 were delayed because of the COVID-19 pandemic. However, engineering and sediment coring operations during Expeditions 390C and 395E (Estes et al., 2021; Williams et al., 2021), which sailed without science parties, cored initial sediment sections and installed reentry cones and casing systems at most sites to maximize science operations during Expeditions 390 and 393. The SAT expeditions targeted six primary sites on 7, 15, 31, 49, and 61 Ma ocean crust (Figure F1) to fill critical gaps in our sampling of intact in situ ocean crust with regards to crustal age, spreading rate, and sediment thickness (Figures F2, F3; Table T1).

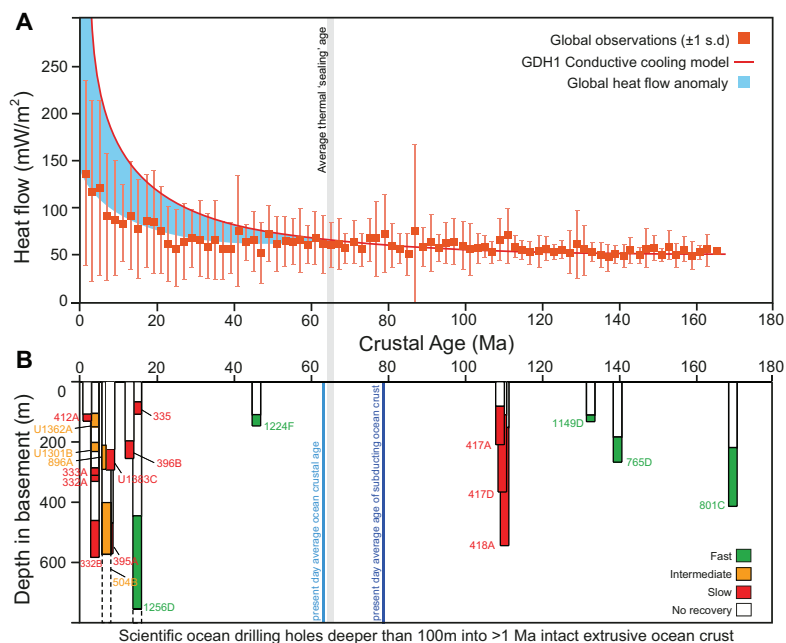


Figure F2. A. Discrepancy between observed and predicted conductive heat flow. Global heat flow anomaly indicates hydrothermal circulation persists across ridge flanks for ~65 My on average (modified from Stein and Stein, 1994). B. Compilation of all scientific ocean drilling holes that penetrate >100 m into intact upper (basaltic) ocean crust vs. crustal age, excluding drill holes that penetrated seamounts, oceanic plateaus, back-arc basement, hydrothermal mounds, or passive continental margins (after Michibayashi et al., 2019). Colors show spreading rate each crustal section formed at, and proportion of cored interval that is colored indicates average core recovery. Dashed lines = two holes that penetrated through entire upper ocean crust into underlying sheeted dikes.

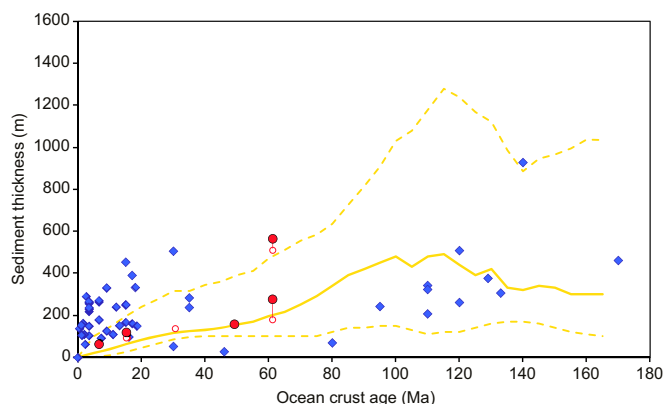


Figure F3. Sediment cover vs. crustal age for Expedition 390 and 393 sites. Solid circles = observed sediment thickness, open circles = sediment thickness expected based on site survey data, diamonds = sediment thicknesses at all DSDP/ODP/Integrated Ocean Drilling Program/IODP drill holes that cored more than 100 m into basement in intact oceanic crust and tectonically exposed lower crust/upper mantle, solid yellow line = global average sediment thickness vs. age, calculated as 25 My moving average of median sediment thickness of 5 Ma binned global compilation of sediment thickness vs. lithospheric age of Spinelli et al. (2004), yellow dashed lines = 25 My moving average of 25th and 75th percentiles of 5 Ma binned data.

These sections of upper ocean crust will enable us to quantify the magnitude and duration of low-temperature chemical exchange with the overlying oceans; investigate the impact of changing ocean conditions on hydrothermal exchange; determine the critical thermal, hydrogeologic, chemical, and microbial transitions across the ridge flank; and evaluate hydrothermal contributions to global biogeochemical cycles. Expeditions 390 and 393 will also sample the sedimentary and upper crustal deep biosphere along the transect, allowing exploration of the microbial ecosystems' responses to variations in habitat conditions in a low-energy gyre and aging ocean crust. Sediments recovered during the SATL expeditions will include Cenozoic stratigraphic sections required to investigate the Earth system's past responses to high atmospheric CO₂ and temperatures and to improve predictions of the impacts of projected future anthropogenic increases in atmospheric CO₂. The transect also provides a paleoceanographic record near World Ocean Circulation Experiment (WOCE) Line A10, enabling reconstruction of the history of the deep western boundary current and the sources of deepwater formation in the Atlantic basins.

Table T1. Summary of planned South Atlantic Transect Expedition 390 and 393 primary and alternate sites, crustal ages, spreading rates, and sediment thicknesses as well as operations accomplished during engineering Expeditions 390C and 395E. * = alternate site adopted as primary in preference to Site SATL-54A during Expedition 390C due to operational considerations, † = not planned for either Expedition 390 or 393.

Site	Proposed site	Proposed primary/alternate site	Expedition		Latitude	Longitude	Water depth (m)	Age (Ma)	Half spreading rate (mm/y)	Estimated sediment thickness (m)
			Completed operations	Planned operations						
Drilled/Planned sites										
U1559	SATL-13A	Primary	390C	390	30°15.6336'S	15°2.0941'W	3055.7	6.6	17.0	50
U1560	SATL-25A	Primary	395E	393	30°24.2064'S	16°55.3718'W	3723.7	15.2	25.5	104
	SATL-33B	Primary		393	30°42.6174'S	20°26.0340'W	4193.0	30.6	24.0	138
U1558	SATL-43A	Primary	390C	393	30°53.7728'S	24°50.4970'W	4336.9	49.2	19.5	148
U1556	SATL-53B	Primary	390C	390	30°56.5244'S	26°41.9472'W	5006.4	61.2	13.5	180
U1557	SATL-56A	Alternate*	390C, 395E	390	30°56.4651'S	26°37.7892'W	5012.3	61.2	13.5	510
U1561	SATL-55A	Alternate	395E	†	30°43.2902'S	26°41.7162'W	4909.5	61.2	13.5	126
Alternate sites										
	SATL-11B	Alternate		†	30°13.3398'S	15°2.2902'W	3057	6.6	17.0	104
	SATL-12A	Alternate		†	30°6.2256'S	15°2.8992'W	3373	6.6	17.0	96
	SATL-23A	Alternate		†	30°23.7210'S	16°52.7844'W	3819	15.2	25.5	162
	SATL-24A	Alternate		†	30°24.0126'S	16°55.8318'W	3676	15.2	25.5	94
	SATL-31A	Alternate		†	30°45.8436'S	20°25.9530'W	4188	30.6	24.0	183
	SATL-35A	Alternate		†	30°37.9506'S	20°26.1516'W	4157	30.6	24.0	93
	SATL-41A	Alternate		†	30°0.1992'S	24°49.1478'W	4408	49.2	19.5	203
	SATL-44A	Alternate		†	30°53.8218'S	24°52.1706'W	4283	49.2	19.5	176
	SATL-54A	Primary		†	30°56.5452'S	26°43.3128'W	4991	61.2	13.5	639

Site	Proposed site	APC/XCB cored hole				Installed reentry system			
		Hole	Expedition	Observed sediment thickness (m)	Average sediment accumulation rate (m/My)	Total penetration (m)	Hole	Expedition	Casing shoe depth (mbsf)
Drilled/Planned sites									
U1559	SATL-13A	A	390C	64.0	9.70	66.2	B	390C	55.3
U1560	SATL-25A	A	395E	120.0	7.89	122.5	B	395E	122.0
	SATL-33B				4.51				
U1558	SATL-43A	A	390C	158.9	3.23	163.9	D	390C	146.1
U1556	SATL-53B	A	390C	278.0	4.54	283.8	B	390C	284.2
U1557	SATL-56A	B	390C	564.0	9.22	574.0	D	390C/395E	571.6
U1561	SATL-55A	A	395E	46.0	0.75	49.0			
Alternate sites									
	SATL-11B								
	SATL-12A								
	SATL-23A								
	SATL-24A								
	SATL-31A								
	SATL-35A								
	SATL-41A								
	SATL-44A								
	SATL-54A								

2. Background

2.1. Geological setting

The SAT expeditions operate in the Leg 3 transect region (~31°S) but occupy a transect of new sites that were selected to (1) target basement formed along the same crustal flow line at similar rates (~13–25 mm/y half rate; Table T1) and (2) recover sections of slow-spreading crust of comparable ages to the ocean crust reference sections in Ocean Drilling Program (ODP) Hole 504B at the Costa Rica Rift (7 Ma; Shipboard Scientific Party, 1993) and ODP Hole 1256D on the Cocos plate (15 Ma; Shipboard Scientific Party, 2003b; Expedition 309/312 Scientists, 2006; Expedition 335 Scientists, 2012), which are located in intermediate- and superfast-spreading crust, respectively.

The site locations were chosen to optimize the recovery of material required to achieve our multi-disciplinary objectives. Thick sediment cover is typically targeted by scientific ocean drilling to maximize the resolution of paleoceanographic records. Thick sediment sequences are also often required to install the seafloor infrastructure required for deep subseafloor drilling. This has led to a bias in DSDP/ODP/Integrated Ocean Drilling Program/IODP sampling of in situ upper ocean crust (for depths >100 m into basement) toward regions with anomalously thick sediment (Figure F3). Rapid deposition of sediment in such areas seals the crust from the oceans, resulting in anomalously hot basement temperatures, and may result in premature cessation of hydrothermal circulation. Consequently, the SAT sites target locations where the sediment cover is close to the global average for their crustal ages (Spinelli et al., 2004; Figure F3), even though this decision reduces the resolution of the paleoceanographic records. However, because seafloor roughness is greater in slow-spreading ocean basins than in fast-spreading basins (Spinelli et al., 2004), there are significant variations in sediment thickness and the continuity of coverage along the SAT. Basement crops out at all ages along the transect (Estep et al., 2019), and these topographic variations likely impact the crustal hydrogeology. Therefore, the SAT includes two sites on 61 Ma crust to investigate the variability in duration and extent of hydrothermal alteration due to basement topography at a given crustal age: Site U1556, which is blanketed by 278 m of sediment, and Site U1557 in a more thickly sedimented (564 m) portion of the same local sediment basin (Figure F4). Site U1557 also provides a higher resolution paleoceanographic record at this crustal age, the oldest among our drill sites.

The sediment sections at the 61 Ma sites (U1556, U1557, and U1561) cover key Paleogene hyperthermals, including the Paleocene/Eocene Thermal Maximum (PETM), and the underlying basement records the cumulative hydrothermal alteration of the uppermost crust across the entire SAT. The 7 Ma site (U1559) provides the young end-member for investigating the evolution of hydrothermal and microbiological systems with crustal age and allows comparison with similar-aged intermediate spreading rate crust from Hole 504B (Shipboard Scientific Party, 1993). The 31 Ma (proposed Site SATL-33B) and 49 Ma (Site U1558) sites fill critical gaps in our ocean crust and deep biosphere sampling with respect to basement age and major changes in ocean chemistry (Coggon et al., 2010). The 15 Ma site (U1560) was chosen for comparison to superfast spreading rate crust from Hole 1256D (Shipboard Scientific Party, 2003b; Expedition 309/312 Scientists, 2006; Expedition 335 Scientists, 2012).

2.1.1. DSDP Leg 3 drilling results

During Leg 3, ten sites were drilled in the equatorial and South Atlantic Ocean between Senegal and Brazil (Scientific Party, 1970), including seven sites along a transect across the MAR that penetrated to basement (Sites 14–20; Figure F1). The basal sediment ages are within a few million years of the inferred magnetic anomaly ages, which are consistent with a half spreading rate of ~20 mm/y since 76 Ma. Recovery in the cored intervals was typically high (>98%), but the sediments were only spot cored, and there are significant gaps between cored intervals. The cores recovered along the Leg 3 transect make up an almost continuous Lower Cretaceous to Pleistocene composite stratigraphic section. All sites yielded calcareous sediments with calcareous nannoplankton and planktic foraminifera. Basalts (0.05–2 m penetration) were recovered from each site, and they comprise variably altered extrusive rocks with common glass and some calcium carbonate veins.

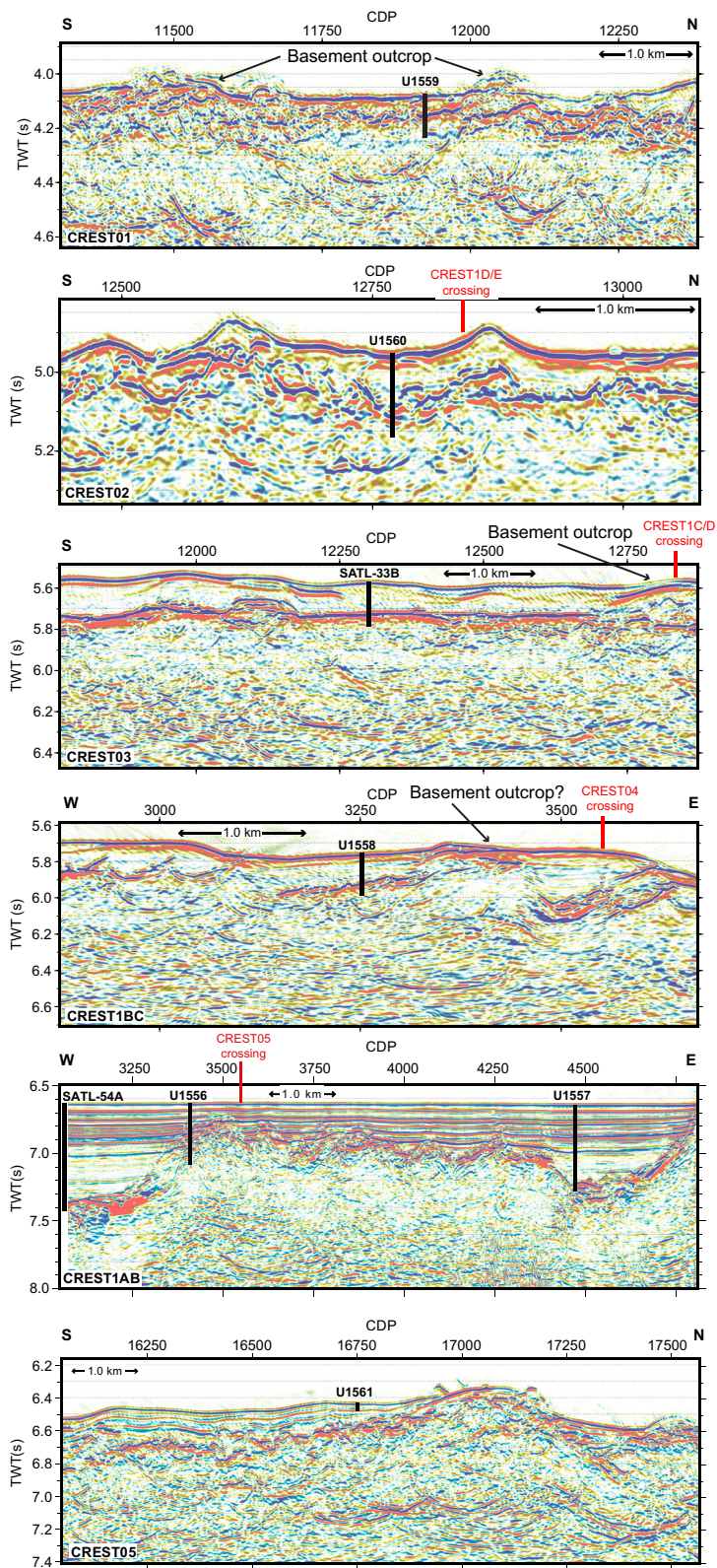


Figure F4. Seismic reflection profiles for all SAT sites, including proposed Site SATL-33B, which will be first occupied during Expedition 393. Site U1557 was relocated from proposed Site SATL-54A, given the thicker than expected sediment layer at Site U1556 and consequent reinterpretation of seismic data for this area, to ensure casing could be installed to basement at Site U1557 without exceeding the maximum deployable casing string length of ~600 m in that water depth (~5 km). TWT = two-way travelttime, CDP = common depth point.

2.2. Seismic studies and site survey data

The SAT is located along a crustal flow line at $\sim 31^\circ\text{S}$ where fracture zones are far apart and magnetic lineations are clear (Figure F1). The Crustal Reflectivity Experiment Southern Transect (CREST) cruise aboard the research vessel (R/V) *Marcus G. Langseth* conducted a detailed geophysical survey across the western MAR flank along this crustal flow line (Reece et al., 2019). The CREST survey included a 1500 km multichannel seismic reflection profile from the ridge crest to the Rio Grande Rise (RGR) spanning 0–70 Ma crust, two shorter ridge-crossing profiles spanning 0–7 Ma crust, and five ridge-parallel profiles. Ocean-bottom seismometer profiles were acquired coincident with the ridge-parallel profiles. Gravity, magnetics, multibeam bathymetry, and backscatter data were also acquired.

The present-day MAR axis at $30^\circ\text{--}32^\circ\text{S}$ has a well-defined axial valley with two inferred active vents (Schmid et al., 2019). The CREST seismic survey crossed a ridge segment that is ~ 100 km long and bounded to the north and south by ridge offsets $\sim 16\text{--}22$ km in width. Crustal accretion along the northern MAR is complex and there are significant regions where spreading is accommodated by amagmatic extension by detachment faults that exhume sections of deep lithosphere to form oceanic core complexes (OCCs; Mallows and Searle, 2012) with a characteristic domal structure. However, a survey of the modern southern MAR during Cruise MSM25 of the R/V *Maria S. Merian* in 2013 found no OCCs between 25° and 33°S (Devey, 2014). This finding, combined with the relatively well defined marine magnetic anomalies on the southern MAR flanks (Maus et al., 2009), is consistent with accretion of intact magmatic crust. Because the $\sim 31^\circ\text{S}$ SAT follows a crustal flow line through a relatively long spreading segment away from major transform faults, we expect a Penrose-type stratigraphy of lavas overlying dikes and gabbros to have been accreted along the transect (Penrose Conference Participants, 1972).

Kardell et al. (2019) calculated ages and spreading rates from magnetic data acquired during the CREST cruise (Figure F5). Ages of the SAT sites are estimated at 6.6, 15.2, 30.6, 49.2, and 61.2 Ma with half spreading rates of 17.0, 25.5, 24.0, 19.5, and 13.5 mm/y, respectively (Table T1). If a half spreading rate of 20 mm/y is used to define the transition between slow and intermediate spreading rates (Perfit and Chadwick, 1998), then the SAT sites formed at slow to intermediate spreading rates.

Seismic imaging along the CREST transect shows an abundance of unsedimented, exposed basement outcrops that may allow the ingress and egress of seawater and ridge flank hydrothermal fluids at all crustal ages from 0 to 65 Ma. This suggests that the crust is never fully sealed by sediment at these ages (Estep et al., 2019) and that there may be long-lived and ongoing connection between the oceans and uppermost basaltic crust with implications for biogeochemical exchanges and subsurface microbial activity. Seismic Layer 2A, which corresponds to the porous and permeable uppermost igneous portion of the oceanic crust based on seismic velocities, is imaged in 0–48 Ma crust but not in older crust (Estep et al., 2019). Velocities at the top of basement increase rap-

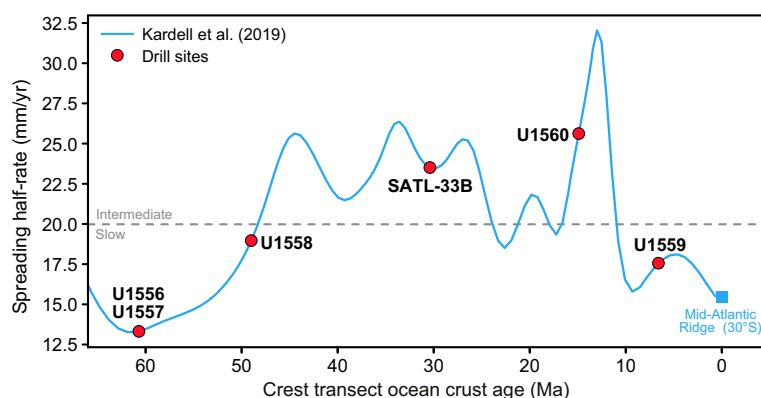


Figure F5. Ages and spreading rates along CREST transect. Blue line = cubic interpolation of rates calculated from table S3 in Kardell et al. (2019), red circles = estimated values at SAT drill sites.

idly from 2.4 km/s at 0 Ma to 4.2 km/s at 6 Ma and then continue to increase gradually to 4.9 km/s at 58 Ma (Kardell et al., 2019). The presence of unsedimented basement outcrops, persistent imaging of Layer 2A, and continued velocity increase at the top of basement are consistent with fluid circulation within the upper crust that continues to at least 48–58 Ma (Estep et al., 2019; Kardell et al., 2019). The seismic transect ends just east of the eastern margin of the RGR, which may have affected the thermal history of the lithosphere and the structure of the crust to the east. Careful reconstruction of the Tristan de Cunha hotspot history (O'Connor and Duncan, 1990) indicates that ~70 My ago the spreading axis migrated westward, terminating formation of the RGR, and normal spreading resumed directly to the east of the RGR between 30° and 34°S.

The SAT sites were all positioned in localized sedimentary basins imaged on the seismic reflection profiles with unsedimented basement ridges within 1–2 km of most sites (Figure F4). Sediment thicknesses were calculated at each proposed drill site prior to drilling using a constant sediment velocity of 1.8 km/s (Table T1).

3. Scientific objectives

3.1. Objective 1 (primary): quantify the timing, duration, and extent of ridge flank hydrothermal fluid-rock exchange.

Hydrothermal circulation at MORs and across their vast ridge flanks influences tectonic, magmatic, and microbial processes on a global scale; is a fundamental component of global biogeochemical cycles of key elements and isotopes (e.g., O, S, Mg, Fe, Li, B, Tl, and ⁸⁷Sr); and facilitates geological CO₂ sequestration within the ocean crust. The chemical and isotopic composition of seawater reflects the dynamic balance between riverine inputs from the continents, burial of marine sediments, and hydrothermal exchanges with the ocean crust (e.g., Palmer and Edmond, 1989). Ocean crust is young and chemically relatively homogeneous compared to continental crust, and its chemical exchanges with seawater are limited to a few relatively well-known reactions (e.g., Alt, 1995). Consequently, hydrothermal contributions to ocean chemistry are simpler to reconstruct than riverine inputs (Coggon and Teagle, 2011; Davis et al., 2003; Vance et al., 2009; Antonelli et al., 2017). Knowledge of the rates and magnitudes of hydrothermal exchanges will help us to decipher the changing global conditions responsible for past variations in seawater chemistry such as mountain building, changes in seafloor spreading rate, large igneous province emplacement, changing climate, and evolution of biological systems. Building this knowledge requires ocean basin-wide transects across ridge flanks with different hydrogeologic histories.

Conductive heat flow deficits indicate that, on average, hydrothermal exchange persists at low temperatures (generally $\ll 100^\circ\text{C}$) to 65 Ma on the ridge flanks (Stein and Stein, 1994; Figures F2, F6). Given the vast extent of the ridge flanks, the hydrothermal fluid flux through them is many orders of magnitude greater than that through high-temperature ($\leq 400^\circ\text{C}$) axial systems (Mottl, 2003) and is likely important for elements for which fluid-rock exchange occurs at low temperatures (e.g., Mg, K, S, Li, B, C, and H₂O). Hydrothermally altered ocean crust provides a time-integrated record of geochemical exchange with seawater manifested through changes in its chemical and isotopic composition, mineral assemblages, and physical properties (e.g., porosity, permeability, and seismic properties). The intensity of seawater-basalt exchange depends on the crustal age, architectural and thermal history, sediment cover, and spreading rate. Consequently, hydrothermal contributions to global geochemical cycles depend on the global length of slow-, intermediate-, and fast-spreading ridges and the age-area distribution of the ridge flanks, which have varied significantly throughout the Phanerozoic (Müller et al., 2008). However, the impact of these variations on geochemical cycles is uncertain because the magnitude and spatial and temporal distribution of crust-seawater hydrothermal exchanges are poorly quantified. For example, the role of MOR spreading in controlling past atmospheric CO₂ and hence climate remains controversial (Alt and Teagle, 1999; Berner et al., 1983; Gillis and Coogan, 2011; Staudigel et al., 1989) because of uncertainties regarding the rate, extent, and duration of hydrothermal CaCO₃ precipitation due to our sparse sampling of intermediate age ocean crust (Figure F6). The hydrothermal carbonates that sequester CO₂ in the ocean crust also record the composition of the fluids from which they precipitate (Coggon et al., 2004) and provide an exciting opportunity to develop medium-resolu-

tion records of past ocean chemistry (e.g., Mg/Ca and Sr/Ca) (Coggon and Teagle, 2011; Coggon et al., 2010; Rausch et al., 2013), which integrates past changes in major Earth system processes such as plate tectonics, mountain building, and climate. However, this approach is limited by sparse sampling of ocean crust of a variety of ages.

Knowledge of the controls on the extent, rate, and duration (Coogan et al., 2016; Harris et al., 2014) of natural CO₂ sequestration along the SAT will assist efforts to assess the feasibility of geo-engineered CO₂ sequestration within the ocean crust (Marieni et al., 2013). The permeable upper ocean crust is of particular interest because it constitutes a vast potential reservoir for CO₂ trapping in areas where the crust is isolated from the oceans by low-permeability sediments (e.g., Marieni et al., 2013) or permanent storage through carbonate mineralization (e.g., Matter et al., 2016).

Drilling experiments on the Juan de Fuca Ridge flank were a key investigation of hydrothermal evolution across a ridge flank but were restricted to young (<3.6 Ma), intermediate-spreading (29 mm/y half spreading rate) crust (Shipboard Scientific Party, 1997; Expedition 301 Scientists, 2005; Expedition 327 Scientists, 2011). There is a dearth of holes in 20–140 Ma intact in situ MOR crust and no significant penetrations (>100 m) of 46–110 Ma crust (Figure F2; Expedition 335 Scientists, 2012). Consequently, the critical thermal, hydrogeologic, chemical, and microbial transitions across the ridge flanks remain unknown (Figure F6). Our current sampling of in situ upper ocean crust (>100 m) is biased toward areas with anomalously thick sediment for their crustal ages (Figure F3). The majority of holes in ocean crust older than 35 Ma penetrate intermediate or fast spreading rate crust. The recovery of uppermost basement sections along the SAT across slow/intermediate-spreading MAR crust was planned to address these sampling gaps with respect to age, spreading rate, and sediment thickness. In addition, knowledge of the controls on the

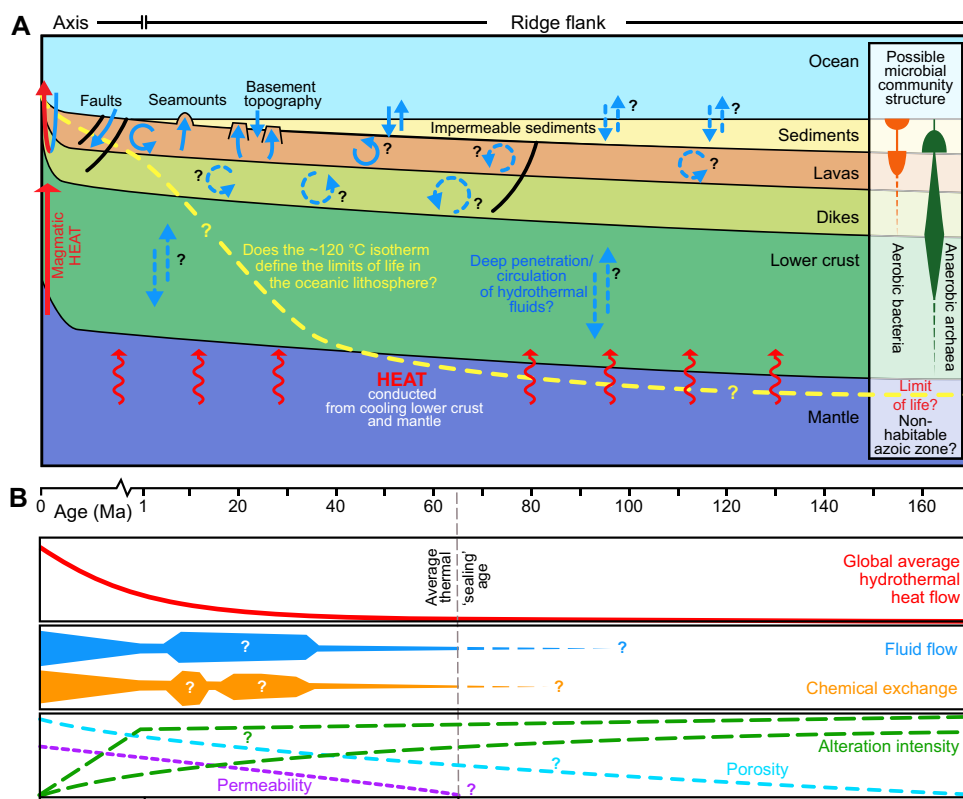


Figure F6. A. Schematic architecture of mid-ocean ridge flank (not to scale) illustrating parameters that may influence intensity and style of hydrothermal alteration and hypothetical trajectory of 120°C isotherm with crustal age. Arrows indicate heat (red) and fluid (blue) flow. B. Calculated global hydrothermal heat flow anomaly, which decreases to 0 by 65 Ma on average, and hypothetical variations in fluid flow and chemical exchange and crustal properties that could be measured to investigate intensity and style of ridge flank hydrothermal circulation (e.g., porosity, permeability, and two possible scenarios for alteration intensity). (After Coggon and Teagle, 2011; Expedition 335 Scientists, 2012; and an original figure by K. Nakamura, AIST.)

extent, rate, and duration of natural CO₂ sequestration along the SAT will assist in assessing the properties and processes that govern the flow and storage of carbon in the subseafloor.

The hydrothermal alteration of thinly sedimented slow/intermediate-spreading ocean crust recovered along the SAT will be investigated using a combination of petrological and geochemical analyses, radiometric dating, and detailed quantitative core logging of rock types, alteration features, and veins integrated with continuous wireline geophysical data with the following aims:

- To determine the nature, rates, magnitudes, distribution, and duration of hydrothermal alteration across the ridge flank;
- To investigate the effect of titanomagnetite/titanomaghemite alteration on the magnetic anomaly signal to elucidate its origin;
- To compare hydrothermal alteration of the uppermost slow/intermediate-spreading crust with crust of similar ages produced at faster spreading ridges (e.g., Holes 504B and 1256D);
- To evaluate the effect of changes in global spreading rates and the age-area distribution of the seafloor on hydrothermal contributions to global biogeochemical cycles; and
- To investigate signatures of changing ocean chemistry in the hydrothermal record and develop medium-resolution records of past ocean chemistry using hydrothermal minerals (following Coggon et al., 2010).

Shipboard description and analyses combined with detailed postexpedition research will allow us to address the following hypotheses:

- Hydrothermal chemical exchange persists beyond 20 My of crustal formation.
- Basement topography and sedimentation history affect the rate and duration of hydrothermal alteration.

3.2. Objective 2 (primary): investigate sediment- and basement-hosted microbial community variation with substrate composition and age.

Scientific ocean drilling has revealed that microorganisms, including Archaea, Bacteria, viruses, and eukaryotic fungi and protists are present, intact, and metabolically active in uncontaminated deep subsurface sediment and basalt. Knowledge about subseafloor microbial communities has grown exponentially since the initial microbiological investigations by DSDP in the 1980s, but only ~4% of ODP/Integrated Ocean Drilling Program/IODP sites have been sampled, documented, or archived for microbiological purposes (Figure F7) (Kallmeyer et al., 2012; Orcutt et al., 2014). Determining microbial community composition and physiological capabilities along the SAT will provide insights into the role of microbes in mineral alteration, hydrocarbon formation, and global biogeochemical cycles.

In sediments, the number of microbial cells present is estimated to equal that in the entire oceanic water column (Kallmeyer et al., 2012). However, the amount of biomass stored in the deep subsurface remains contentious because microbial cell abundance in subseafloor sediment varies by approximately five orders of magnitude (Figure F7) with significant geographic variation in the structure of subseafloor communities (Inagaki et al., 2006). Most studies have focused on relatively high biomass continental shelf systems (Inagaki and Orphan, 2014). Holocene efforts, including Integrated Ocean Drilling Program Expeditions 329 (South Pacific Gyre; Expedition 329 Scientists, 2011) and 336 (North Pond; Expedition 336 Scientists, 2012), investigated lower biomass sedimentary systems underlying oceanic gyres. Crucially, no data have been collected from the South Atlantic Gyre (Figure F7). Hence, postexpedition analyses of the cores recovered during the SAT expeditions will refine the global biomass census and improve our understanding of the global carbon cycle.

The presence or absence of oxygen in marine sediments has profound implications for the quantity, diversity, and function of microbial communities. Oxygen penetration depth varies between oceanic regions and settings, ranging from only a few millimeters in areas with high rates of microbial respiration, such as on continental shelves, to the entire sediment column in extremely low biomass sediments, such as the relatively thin sediments beneath the South Pacific Gyre

(D'Hondt et al., 2015). Extrapolation of an observed global relationship between oxygen penetration and sedimentation rate and thickness indicates South Atlantic Gyre sediment may be oxic to basement (D'Hondt et al., 2015). During Leg 3, oxygen was not measured, but pore water sulfate was detected near the basement. However, sediment organic carbon concentrations along the SAT are intermediate to those of North Pond, where oxygen penetrated tens of meters below seafloor and nitrate was present to basement, and Nankai Trough, where oxygen was depleted by 3 meters below seafloor (mbsf) and sulfate was depleted by 19 mbsf (Figure F8; Expedition 336 Scientists, 2012; Tobin et al., 2009; Orcutt et al., 2013; Reese et al., 2018). These results indicate that oxygen is unlikely to extend to the basement at sites along the SAT, contrary to model predictions (D'Hondt et al., 2015), and that the classical redox succession of oxygen respiration followed by nitrate reduction, potentially followed by metal reduction, may be present. However, oxygen may be reintroduced at the bottom of the sediment column because of oxygenated fluid flow from the uppermost volcanic basement, which is the case at North Pond (Expedition 336 Scientists, 2012). The recovery of the sediment package across the South Atlantic Gyre allows us to investigate the relationships between oxygen penetration, biomass, and carbon limitation of microbial activity.

Drilling allows us to compare the phylogenetic diversity, functional structure, and metabolic activity of South Atlantic Gyre communities with results from previously studied regions. By exploiting the variations in sediment carbon composition expected across the subsiding MOR flank, we can examine the response of autotrophy versus heterotrophy to carbonate chemistry. Additionally, previous studies of the sedimentary deep biosphere have explored community diversity based on site-to-site or downhole (age) comparisons, often implicitly assuming a similar “starter community” that colonized the seafloor and whose structure and function subsequently changed in response to evolving geochemical conditions or burial depth. However, energy limitation may preclude replication (Lever et al., 2015; Lomstein et al., 2012) and thus limit community changes. The SAT age-transect approach allows us to test this assumption directly by investigating the impact of burial depth and chemical zonation on sediment of the same age and hence the same starter community.

Given the dearth of basement holes in ocean crust of intermediate age, there were no microbiological samples across the critical ridge–flank transitions in basement properties that may affect microbial communities prior to the SAT expeditions (Figure F6). Most of the biological alteration of subseafloor basalts is thought to occur within 20 My of crustal formation (Bach and Edwards,

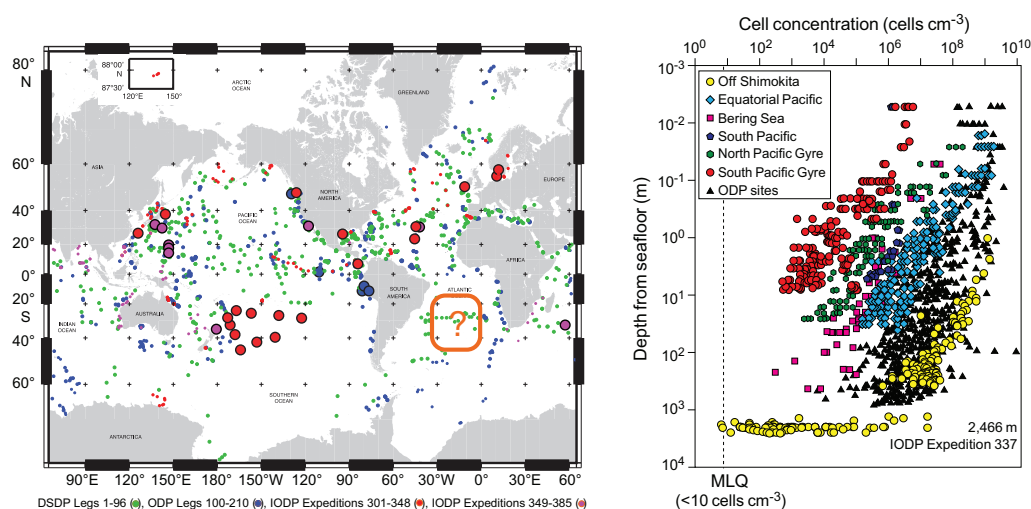


Figure F7. Left: global distribution of DSDP/ODP/Integrated Ocean Drilling Program/IODP drill sites. Larger circles = sites where microbiological samples were taken (through IODP Expedition 385). Right: microbial cell abundance vs. depth at sampled sites, which reveals over five orders of magnitude of variation in biomass–depth trends, depending on the geographic origin of samples (after D'Hondt et al., 2019). MLQ = minimum quantifiable limit. The South Atlantic represents a crucial gap in knowledge (orange box with question mark), and sampling proposed here will be used to groundtruth models predicted from current biomass database. Note that symbol colors between diagrams are not related because they are derived from different sources.

2003). However, microbiological investigations of oceanic basement have focused on young (<10 Ma) crust (Jungbluth et al., 2013; Lever et al., 2013; Mason et al., 2010; Orcutt et al., 2011) or older (>65 Ma) lava associated with hotspot volcanism along the Louisville Seamount Trail (Expedition 330 Scientists, 2012; Sylvan et al., 2015). Basement outcrops that penetrate the relatively impermeable sediment provide permeable conduits that facilitate seafloor fluid circulation in older basement (Wheat and Fisher, 2008). Fluid flow across the sediment/basement interface can produce redox gradients that provide recharge of depleted electron acceptors (e.g., oxygen and nitrate) to basal sediments, as observed above 3.5 and 8 Ma ocean crust on the Juan de Fuca Ridge flank (Engelen et al., 2008) and at North Pond (Orcutt et al., 2013), respectively. However, the extent and duration of fluid flow through this interface across the ridge flanks remains unknown (Figure F6). The recovery of the uppermost basaltic basement from 7 to 61 Ma along the SAT will allow us to determine whether microbial populations are indeed present in basement older than 20 Ma where hydrothermal flow persists across the ridge flanks and to investigate the nature, extent, and duration of communication between the sedimentary and crustal biosphere for the first time.

The SAT expeditions were designed to sample seafloor populations of Bacteria, Archaea, viruses, and microbial eukaryotes in both the sedimentary and upper crustal ecosystems across the aging MAR flank, quantify their biomass by cell enumeration, identify them using molecular biology methods, measure the stable isotopic composition (C, N, and S) of sediment and basement to relate processes to geochemistry, measure their metabolic activities using a variety of incubation assays, and resolve their physiological adaptations with omics-based approaches with the following aims:

- To evaluate cell abundance and community activity in the low-energy seafloor biosphere of the South Atlantic Gyre and refine estimates of global seafloor sedimentary microbial abundance;

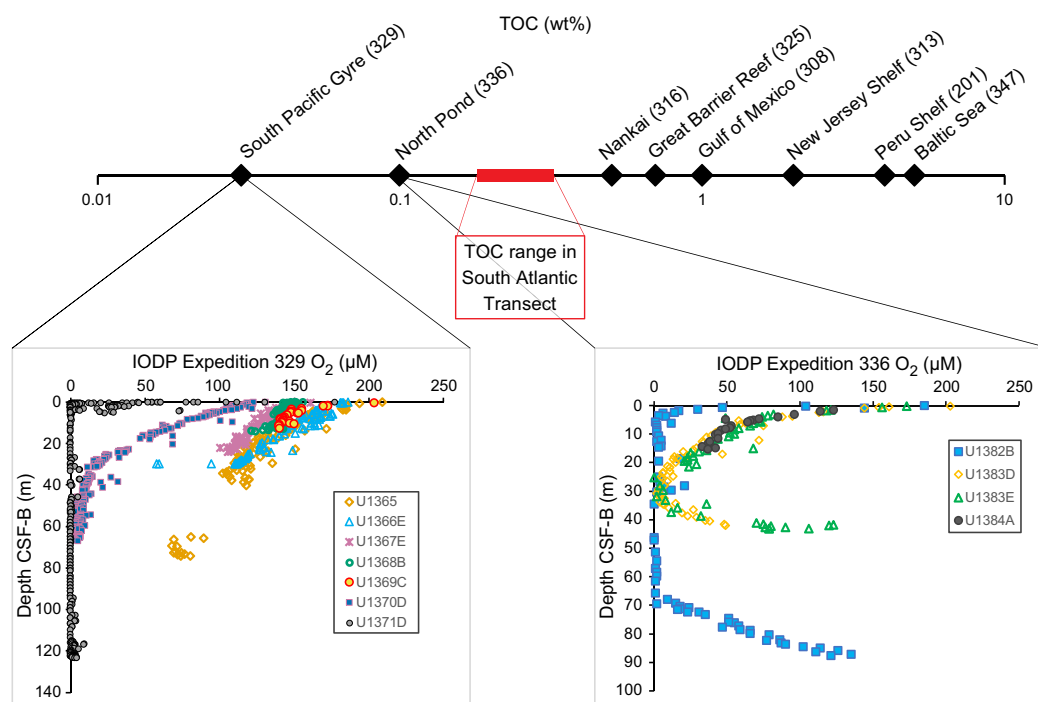


Figure F8. Comparison of predicted range of weight percent TOC for proposed SAT study area with other areas where scientific ocean drilling has conducted microbiological investigations (expedition numbers in brackets; data following Andrén et al., 2015; Shipboard Scientific Party, 2003a; Expedition 329 Scientists, 2011; Expedition 336 Scientists, 2012; Expedition 308 Scientists, 2006; Tobin et al., 2009; Expedition 313 Scientists, 2010; Expedition 325 Scientists, 2011). Proposed drill sites have higher TOC concentrations than South Pacific Gyre, where oxygen penetrated to basement, and North Pond, where oxygen penetrates tens of meters into the seafloor in Holes U1383D, U1383E, and U1384A, but lower than Nankai Trough, where pore water oxygen is consumed less than 5 m below seafloor, based on pore water Mn concentrations.

- To resolve model predictions about the depth of oxygen penetration into sediment from overlying seawater and into the bottom of the sediment package from oxygenated fluid in basement;
- To evaluate the role of subseafloor microbes in sediment biogeochemistry and basement alteration and hence global biogeochemical cycles; and
- To investigate how aging of the ocean crust influences the composition of the crustal biosphere, particularly the effects of changing oxidation state and permeability on microbial abundance, diversity, and function.

The SAT samples will also allow us to test the following hypotheses:

- South Atlantic Gyre microbial communities share membership and function with both oligotrophic sediments, like those found at North Pond, and open-ocean systems with higher organic matter input, such as Nankai Trough, given the intermediate organic carbon content of the SAT sites.
- Microbial community structure and diversity depends on the starter community (and hence sediment age) rather than subsequent selection driven by burial or chemical zonation.
- Crustal biomass decreases with increasing basement age, and communication between the sedimentary and crustal biosphere ceases with the cessation of hydrothermal flow and sealing of the basement.
- Microbial diversity increases within subseafloor basalts with basement age as previously demonstrated in basalts exposed on the seafloor (Lee et al., 2015; Santelli et al., 2009).

3.3. Objective 3 (secondary): investigate the responses of Atlantic Ocean circulation patterns and the Earth's climate system to rapid climate change, including elevated atmospheric CO₂ during the Cenozoic.

Climate change due to anthropogenic CO₂ emissions poses significant and imminent threats to global society and the biosphere. Knowledge of past ocean circulation patterns and temperatures is essential to understand the operation of Earth's climate system and required to improve the efficacy of numerical models in simulating intervals of high *p*CO₂. High *p*CO₂ intervals are commonly characterized by relatively shallow lysocline and calcite compensation depths (CCDs) resulting in poor preservation of calcareous microfossils used to generate paleoceanographic records and reconstruct past climates. This problem can be overcome by coring sediment deposited on basement slightly older than the targeted sediment age that accumulated prior to thermal subsidence of the seafloor below the CCD. More continuous composite stratigraphic sequences can be obtained by drilling multiple sites along a crustal age transect, a strategy successfully employed during ODP Leg 199 (Shipboard Scientific Party, 2002) and Integrated Ocean Drilling Program Expedition 320/321 (Pälike et al., 2012). The Walvis Ridge depth transect sampled during ODP Leg 208 demonstrated the dynamic nature of the Cenozoic CCD and lysocline in the eastern South Atlantic (Shipboard Scientific Party, 2004) and the value of re-drilling DSDP transects to collect more complete records of Earth's history. Although spot cored, Leg 3 sites in the western South Atlantic demonstrated moderate to excellent carbonate preservation along the SAT (Scientific Party, 1970) and the area's suitability for high-resolution paleoclimatic and paleoceanographic reconstructions through key intervals of rapid climate change (Figure F9; Cramer et al., 2009; Zachos et al., 2001, 2008), including the PETM and other short-lived hyperthermals, early and middle Eocene climatic optima, the onset of Antarctic glaciation across the Eocene–Oligocene Transition (EOT), multiple Oligocene and the Miocene glaciation events (Oi and Mi events), the Miocene climatic optimum and Monterey Carbon Excursion, the middle Miocene climate transition, Pliocene warmth, and the onset of Northern Hemisphere glaciation.

Global ocean circulation transfers heat and nutrients around the globe, both influencing and responding to changes in Earth's climate system (Broecker, 1991; Stommel, 1961; Wunsch, 2002). The western intensification of ocean currents means that by characterizing western portions of major ocean basins using drilling transects, records of deepwater mass properties and thus the development of modern thermohaline circulation can be constructed. The western South Atlantic

is the main northward flow path of Antarctic Bottom Water (AABW) and southward flow path of North Atlantic Deep Water (NADW) and their precursor water masses. Consequently, the SAT expeditions will provide complementary data needed to constrain the evolution of thermohaline circulation patterns and climate change as the Drake Passage and Southern Ocean opened, the northern NADW gateway opened, and the Tethys Ocean became restricted to thermohaline circulation. In particular, the SAT cores will assist in establishing how high-latitude sea surface (and hence deep ocean) temperatures and the CCD varied in response to $p\text{CO}_2$ changes and ocean acidification (Barker and Thomas, 2004; Barrera et al., 1997; Billups, 2002; Bohaty et al., 2009; Cramer et al., 2009; Frank and Arthur, 1999; Kennett and Stott, 1991; Scher and Martin, 2006; Thomas et al., 2003; Wright et al., 1991). Together the complementary records from western North Atlantic sediments (Expedition 342; Norris et al., 2014) and the SAT will provide an exceptional record of the evolution of Atlantic overturning circulation through the Cenozoic.

A novel, direct way to compare paleoceanographic reconstructions of past high $p\text{CO}_2$ to modern conditions is to recover sediments along transects of water column data collected by the WOCE. The SAT constitutes a “paleo-WOCE” line following the western portion of WOCE Line A10 (Fig-

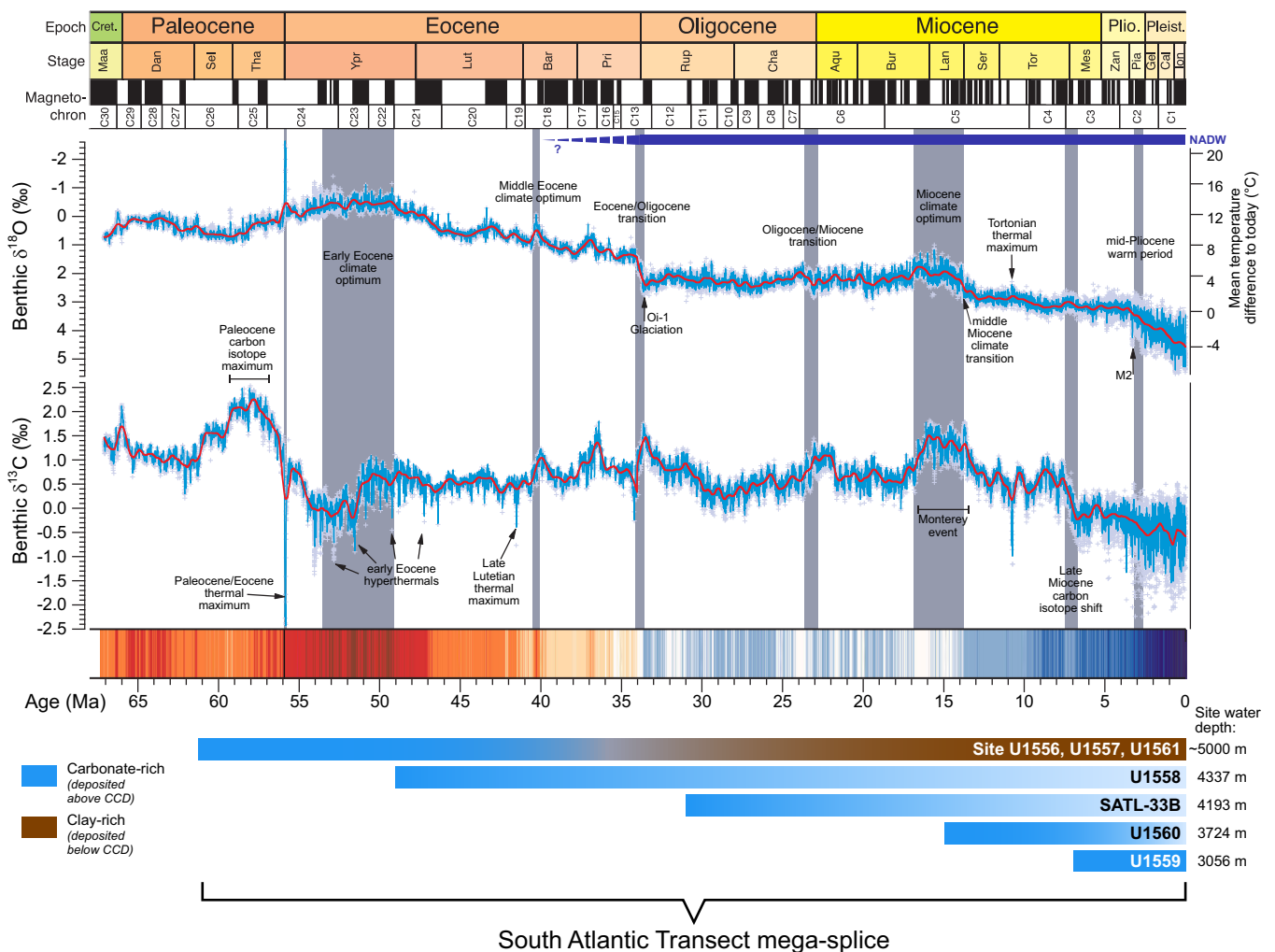


Figure F9. Composite deep-sea benthic foraminiferal $\delta^{13}\text{C}$ and $\delta^{18}\text{O}$ records showing both gradual and abrupt changes in global climate during Cenozoic, with key events highlighted by vertical bars (modified from Westerhold et al., 2020). Red and blue “climate stripes” show departure from average Cenozoic temperature in 100 ky time bins, with red representing warmer than average temperatures and blue colder than average. A rich paleoceanographic record of these changes will be accessed by drilling the SAT sites. A rich paleoceanographic record of these changes will be accessed by drilling the SAT sites. Bars on the bottom show the 7 SAT sites, present water depth (Site U1556, U1557, and U1561 water depths range 4910–5012 m; see Table T1), and intervals of Cenozoic climate history they are expected to sample. The deepest sites will generally contain carbonate-rich sediments (blue) in the older part, deposited when site was closer to ridge crest and shallower than CCD, transitioning up to poorly preserved carbonate sediments (light blue to white) or carbonate-poor sediment (brown) in the younger part as each site subsided below CCD. Sites on younger oceanic crust will recover younger carbonate-rich sediments. Together, these sites represent a “megasplice” recovering last 61 My of Earth’s climate history from an understudied region of the ocean.

ure **F10**), providing access to paleoceanographic records of southern- and northern-sourced deep and bottom waters. We will test models of bipolar deepwater evolution (e.g., Borrelli et al., 2014; Cramer et al., 2009; Katz et al., 2011; Tripathi et al., 2005) using stable and radiogenic isotope analyses of sediments recovered from these key western South Atlantic sites.

The Walvis Ridge depth transect (Shipboard Scientific Party, 2004) revealed a dramatic 2 km shoaling of the CCD during the PETM due to the acidification of the ocean from massive carbon addition followed by a gradual recovery (Figure **F11**) (Zachos et al., 2005; Zeebe et al., 2008). Given chemical weathering feedbacks, the recovery of the CCD should have resulted in a transient overdeepening of the CCD (Dickens et al., 1997). Collectively, the SAT sites will provide additional data for reconstructing changes in the position of the lysocline and CCD in the western South Atlantic that are essential for constraining the timing of gateway events and the history of Northern Component Water (NCW) and Southern Component Water (SCW), which were the precursors to NADW and AABW, and the nature of Atlantic basin responses to climate change relative to the Pacific.

Microfossils provide a critical archive of ocean and climate history, including long-term changes (e.g., early Eocene warmth, Cenozoic cooling, and Pliocene warmth) and abrupt events (e.g., early Paleogene hyperthermals and multiple glaciation events). The SAT expeditions were designed to recover complete sedimentary sections along paleo-WOCE Line A10, exploiting the thermal subsidence of the ocean crust along the transect to provide material for high-resolution proxy records including benthic and planktic foraminiferal geochemistry, micropaleontological assemblages, orbitally tuned age models, neodymium isotopes, and alkenone $\delta^{13}\text{C}$ and boron isotope $p\text{CO}_2$ reconstructions with the following aims:

NADW and AABW Along the South Atlantic Transect

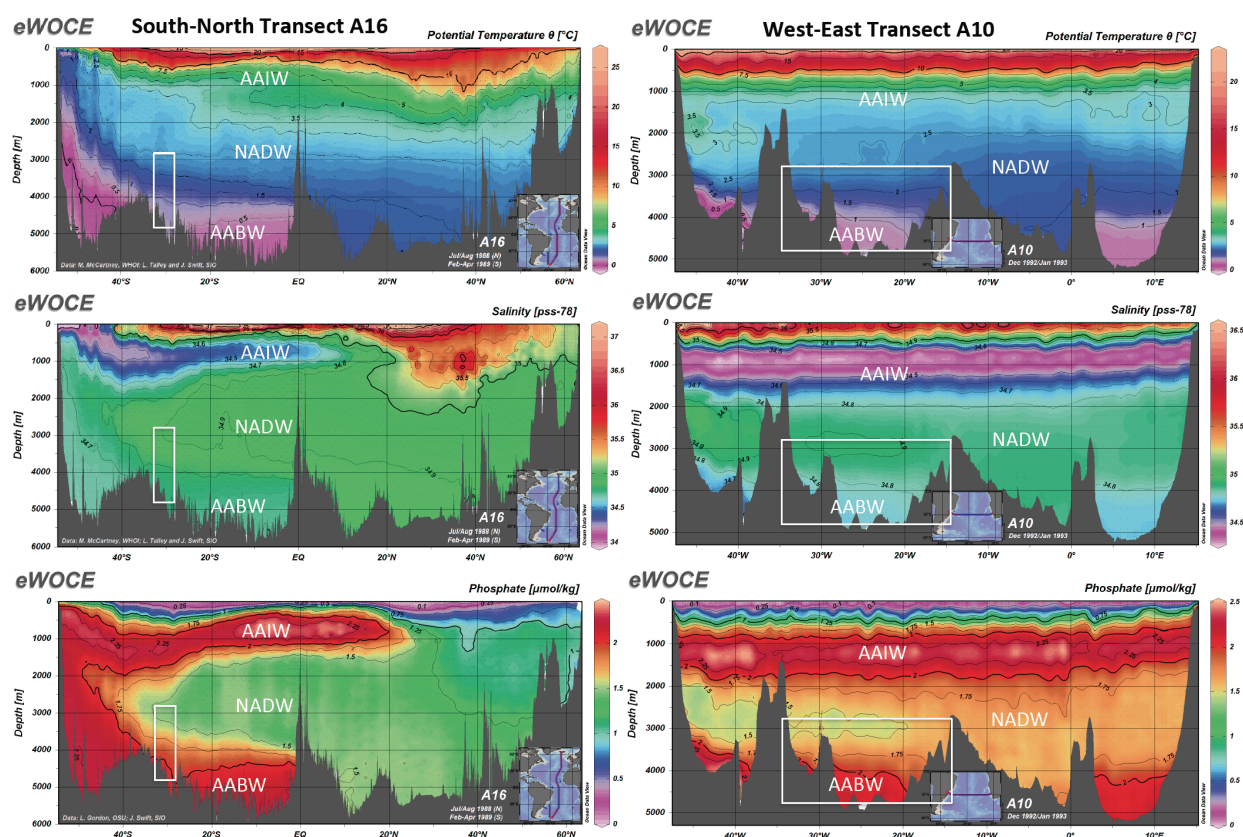


Figure F10. WOCE temperature, salinity, and phosphorus profiles along south–north Transect A16 through western South Atlantic Basin and west–east Transect A10 at 30°S near the location of the SAT (data from World Ocean Circulation Experiment; <http://www.ewoce.org>). Rectangles show approximate coverage of SAT. AAIW = Antarctic Intermediate Water.

- To reconstruct the evolution of deepwater masses over the past 61 My to assess contributions of NCW and SCW in the early Paleogene western South Atlantic (Kennett and Stott, 1990), document the influence of the openings of the Drake and Tasman Passages on South Atlantic deepwater circulation, and reconstruct the overall development of modern thermohaline circulation;
- To provide high-resolution constraints on CCD and carbonate chemistry changes of the deep western Atlantic, particularly during transient hyperthermals and other intervals of global warmth;
- To reconstruct the Cenozoic history of the South Atlantic subtropical gyre by monitoring proxies of productivity and paleobiogeography of plankton, rates of speciation/extinction relative to the equatorial zone and higher latitudes, and changes in biodiversity and subtropical ecosystem dynamics; and
- To evaluate the response of subtropical planktic and benthic biota to changing environmental conditions such as global warming, ocean acidification, or fertility patterns during intervals of rapid climate change through the Cenozoic.

The recovered sediment sections will also allow us to test the following hypotheses:

- Low-latitude sites were potential sources of deepwater formation at times of global warmth and high atmospheric $p\text{CO}_2$.

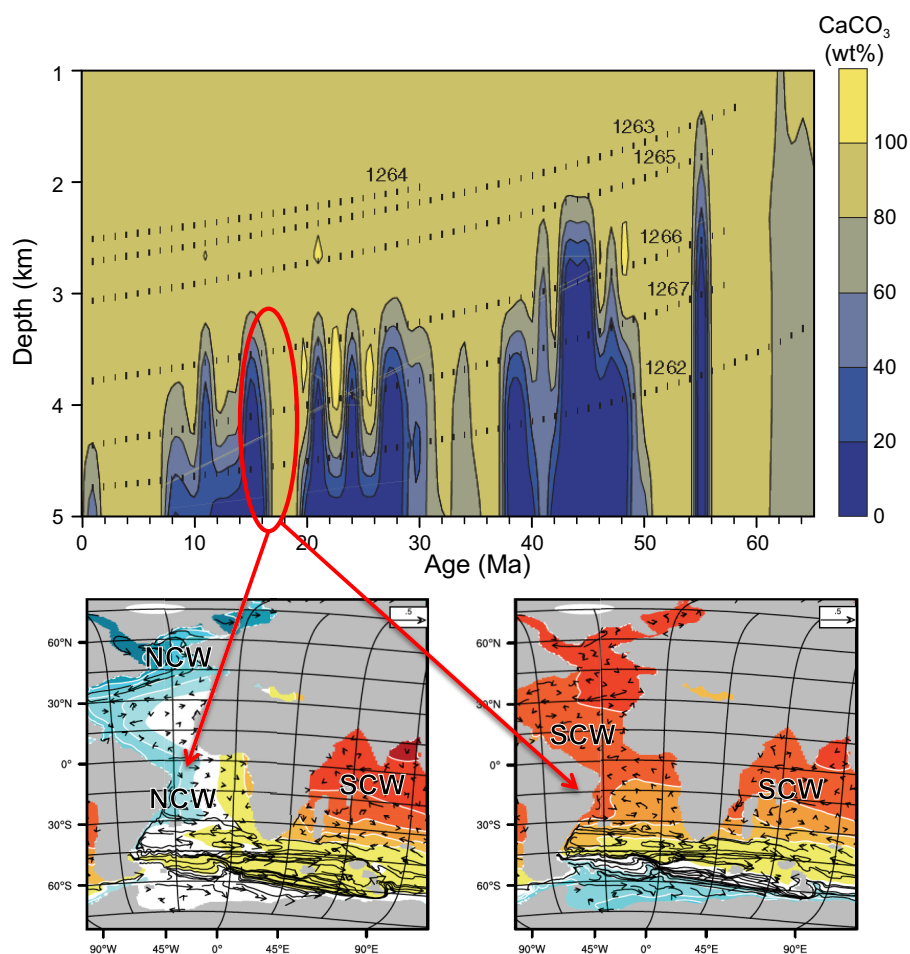


Figure F11. Top: percent carbonate in depth transect of drill sites recovered during Leg 208 on Walvis Ridge, eastern South Atlantic (Shipboard Scientific Party, 2004). Position of lysocline and CCD were dynamic during Cenozoic related to changing deepwater circulation, productivity, and ocean acidification associated with PETM. Bottom: modeled relative water mass age during mid-Miocene climatic optimum (Coggon et al., 2016). Red oval = correlative changes in carbonate chemistry on Walvis Ridge. Colors represent benthic “age,” which is a $\delta^{13}\text{C}$ -like tracer; red = old water, blue = young water. Left: mode with NCW “on.” Right: NCW “off.” The SAT, near 31°S, is expected to capture changes in these two modes of deepwater formation.

- The strength of the coupling between the climate and the carbon cycle varied through the Cenozoic.
- The lysocline and CCD responded differently on the western side of the MAR compared to the Walvis Ridge record due to changing deep/bottom water sources, gateway configurations, and flow paths.
- The subtropical gyre cut off the delivery of heat to Antarctica as the Antarctic Circumpolar Current developed through the late Eocene–Oligocene.

3.4. Connections to the 2050 Science Framework

Given its multidisciplinary essence, the SAT campaign will advance the full spectrum of the 2050 Science Framework including each of the seven interconnected Strategic Objectives (SOs) and five Flagship Initiatives (FIs) (Koppers and Coggon, 2020). For example, SAT Objective 1 explores hydrothermal alteration and fluid-rock exchange during crustal aging through the recovery of upper crustal sections (>100 m) along a crustal age transect. This aspect of the project directly relates to the 2050 Science Framework SO2 The Oceanic Life Cycle of Tectonic Plates and SO6 Global Cycles of Energy and Matter, as well as FI2 Probing the Deep Earth. Documenting the impact of fluid-rock exchange on the composition and physical properties of the crust as a function of its age provides insights into key properties of old crust entering subduction zones, such as hydration state, seismic velocity, and strength, to inform studies of hazards generated along convergent plate margins (SO7 Natural Hazards Impacting Society and FI3 Assessing Earthquake and Tsunami Hazards).

Quantifying the abundance and diversity of microbial life in ocean crust and the overlying nutrient-limited sediment environments (SAT Objective 2) will help determine the impact of biological activity in geochemical cycles and improve our understanding of the limits of life in the lithosphere. This knowledge will contribute to SO1 Habitability and Life on Earth, SO6 Global Cycles of Energy and Matter, and FI5 Exploring Life and its Origins. SAT Objective 3 investigates the responses of Atlantic Ocean circulation patterns and the Earth's climate system to rapid climate change. This objective relates to SO3 Earth's Climate System, SO4 Feedbacks in the Earth System, and SO5 Tipping Points in Earth's History, as well as FI1 Ground Truthing Future Climate Change and FI4 Diagnosing Ocean Health by examining the ocean's past responses to climate events, including hyperthermals, changes in oxygenation, and acidification, to look ahead to future impacts on Earth's climate and ecosystems.

The SAT project also embraced new technologies and approaches to core description and objective quantification of recovered cores through the analysis of high-resolution images of external core surfaces and the application of machine learning approaches (e.g., Enabling Element 4 Technology Development and Big Data Analytics). The ambitious operational goals of the SAT project align with the 2050 Science Framework and emphasize, as stated in the framework, that achieving these scientific objectives “requires continued developing of drilling, coring, logging, observatory, and laboratory tools and techniques.” Overall, the mission of the 2050 Science Framework for scientific ocean drilling is to guide “multidisciplinary seafloor research into the interconnected processes that characterize the complex Earth system and shape our planet's future.” The breadth of the interrelated science addressed by the SAT project exemplifies such investigation of the interconnected Earth by IODP.

4. Operational strategy

The original operational strategy for Expeditions 390 and 393 is described in detail in the *Scientific Prospectus* (Coggon et al., 2020) and was updated in the *Scientific Prospectus Addendum* (Coggon et al., 2022) following the completion of engineering Expeditions 390C and 395E. In brief, the SAT intended to drill six sites located at five different crustal ages (~7, 15, 31, 49, and 61 Ma), with two of the sites located in the same localized sedimentary basin on 61 Ma crust where significant basement topography results in variable sediment thickness (~180 and 640 m thick at proposed Sites SATL-53B and SATL-54A, respectively). At each of the six sites, we planned the following opera-

tions to achieve our scientific objectives and establish legacy boreholes for future basement experiments:

1. Recover a complete sediment section by coring three advanced piston corer/extended core barrel (APC/XCB) sediment holes at each crustal age to allow compilation of complete paleo-oceanographic records across core breaks in the sediment sections using stratigraphic correlation and to provide sufficient material for whole-round microbiological and pore water sampling,
2. Recover the sediment/basement interface using the XCB system,
3. Install a drill-in reentry cone and casing to ~5 meters subbasement (msb),
4. Core to ~250 msb, and
5. Collect wireline geophysical logging data through the basement sections.

4.1. Depth of basement drilling

To fully quantify the extent and duration of ridge flank hydrothermal exchange, we required our sampling of the upper basement to be as representative as possible of the entire extrusive crust. A systematic downward decrease in the extent of oxidative hydrothermal alteration is not observed through all previously drilled upper crustal sections (Shipboard Scientific Party, 2003b), and the permeability of the extrusive crust is highly heterogeneous and not always greatest at the top of the basement (Becker et al., 2013; Shipboard Scientific Party, 2003b). Commonly, fluid flow in the upper crust is channeled along specific horizons of enhanced permeability (Harris et al., 2015; Neira et al., 2016). At many drill sites globally, the fluid temperature–depth distribution recorded by hydrothermal carbonate veins, typically one of the last hydrothermal phases to form, indicates the circulation of cool (<100°C) ridge flank fluids through at least the upper 300 m (Coggon et al., 2010). If there is a depth limit to off-axis fluid circulation, sufficient basement drilling is required to establish what it is and how it varies across the ridge flanks; therefore, we need to achieve the maximum possible basement penetration. Consequently, our target was to core ~250 m into the uppermost basaltic ocean crust at each site along the transect.

5. Preexpedition engineering and coring operations

SAT Expeditions 390 and 393 were originally scheduled for October–December 2020 and April–June 2021, respectively. In 2020 and 2021, the global COVID-19 pandemic resulted in the postponement of several IODP expeditions, including Expeditions 390 and 393. In response, the ship was used to conduct preparatory work for postponed expeditions that did not require a science party aboard but could be carried out by the ship's crew and a team of technicians from the *JOIDES Resolution* Science Operator (JRSO). Two of these expeditions (Expeditions 390C and 395E) were in service of the SAT drilling project to reduce the operational risks and expedite basement drilling during the postponed Expeditions 390 and 393 by coring one hole through sediment to basement and installing a cased reentry system <5 m into basement in a second hole at each of the six proposed primary SAT sites. All basement drilling was deferred to Expeditions 390 and 393.

During Expedition 390C, which sailed in October–December 2020 (Estes et al., 2021), the sediment section at four of the SAT sites (U1556–U1559) was cored. The contact with basalt was slightly deeper than estimated at all sites (Table T1), likely because of a slight underestimation of the in situ seismic velocities. At 61 Ma Site U1556, basalt was encountered at 278 mbsf, significantly deeper than expected (180 mbsf). If the sediment had also been thicker than expected (640 m) at proposed Site SATL-54A ~2.5 km west of Site U1556, the casing length required would have exceeded the drill string weight limit for the water depth (~5 km). Therefore, alternate proposed Site SATL-56A replaced Site SATL-54A and was drilled as Site U1557. The site is ~6.5 km east of Site U1556 in the same localized sedimentary basin, where the basement contact was estimated to be 510 mbsf and encountered at 564 mbsf.

The reentry systems were to be installed using the Dril-Quip running tool, which permits later extension of casing. However, there were difficulties installing casing into basement with this system (Estes et al., 2021). The extra time taken for troubleshooting meant that reentry installations

could not be completed at all sites, and a second expedition was planned. Expedition 395E (April–June 2021; Williams et al., 2021) completed additional SAT preparatory work at Sites U1556, U1557, and U1560. Following installation of reentry systems at Sites U1556 and U1560 and extending casing at Site U1557, there was insufficient time to core and install a reentry system at proposed Site SATL-33B (on 31 Ma crust). Instead, a single APC/XCB hole was cored at an alternate site adjacent to Sites U1556 and U1557, overlying 61 Ma crust (Site U1561; proposed Site SATL-55A; Figure F4; Table T1). Proposed Site SATL-33B was the only primary SAT site at which no operations were conducted prior to Expeditions 390 and 393.

6. Expedition 390C and 395E principal results

Because there was no shipboard science party on the ship during engineering Expeditions 390C and 395E, no cores were described during the expeditions. Instead, the Expedition 390C and 395E cores are considered part of the joint Expeditions 390 and 393. The Expedition 390 shipboard scientists described all engineering expedition cores from sites occupied during Expedition 390, including Site U1561. Expedition 393 scientists will describe the remainder of the engineering expedition cores. A range of physical properties and chemical analyses were conducted during Expeditions 390C and 395E, but microbiological sampling was not possible. Core catcher samples were collected for distribution to the Expedition 390 and 393 micropaleontologists to develop preliminary biostratigraphic age models on shore ahead of Expeditions 390 and 393. A summary of the engineering expedition shipboard data is provided in the Expedition 390C and 395E *Preliminary Reports* (Estes et al., 2021; Williams et al., 2021), but all data generated during the preexpedition engineering operations along with the descriptions of the Expedition 390C and 395E cores made during Expeditions 390 and 393 are combined with the results of Expeditions 390 and 393 and presented in the relevant site reports. The Expedition 390C and 395E geochemical data provided a valuable guide for chemical and microbiological sampling during Expeditions 390 and 393.

7. Revised Expedition 390 and 393 operational strategy

The successful installation of five of the six planned reentry systems along the SAT prior to Expeditions 390 and 393 significantly decreased the operational risk of the SAT expeditions. The time savings due to operations already completed were partially offset by the need to sail to and from Cape Town, rather than from Cape Town to Montevideo for Expedition 390 and from Montevideo to Montevideo for Expedition 393, which added additional transit time to both expeditions. Extra time was also required to recore the thicker than expected sediments. The operations plans for the rescheduled Expeditions 390 and 393 were revised to account for these changes (Coggon et al., 2022; Figure F12).

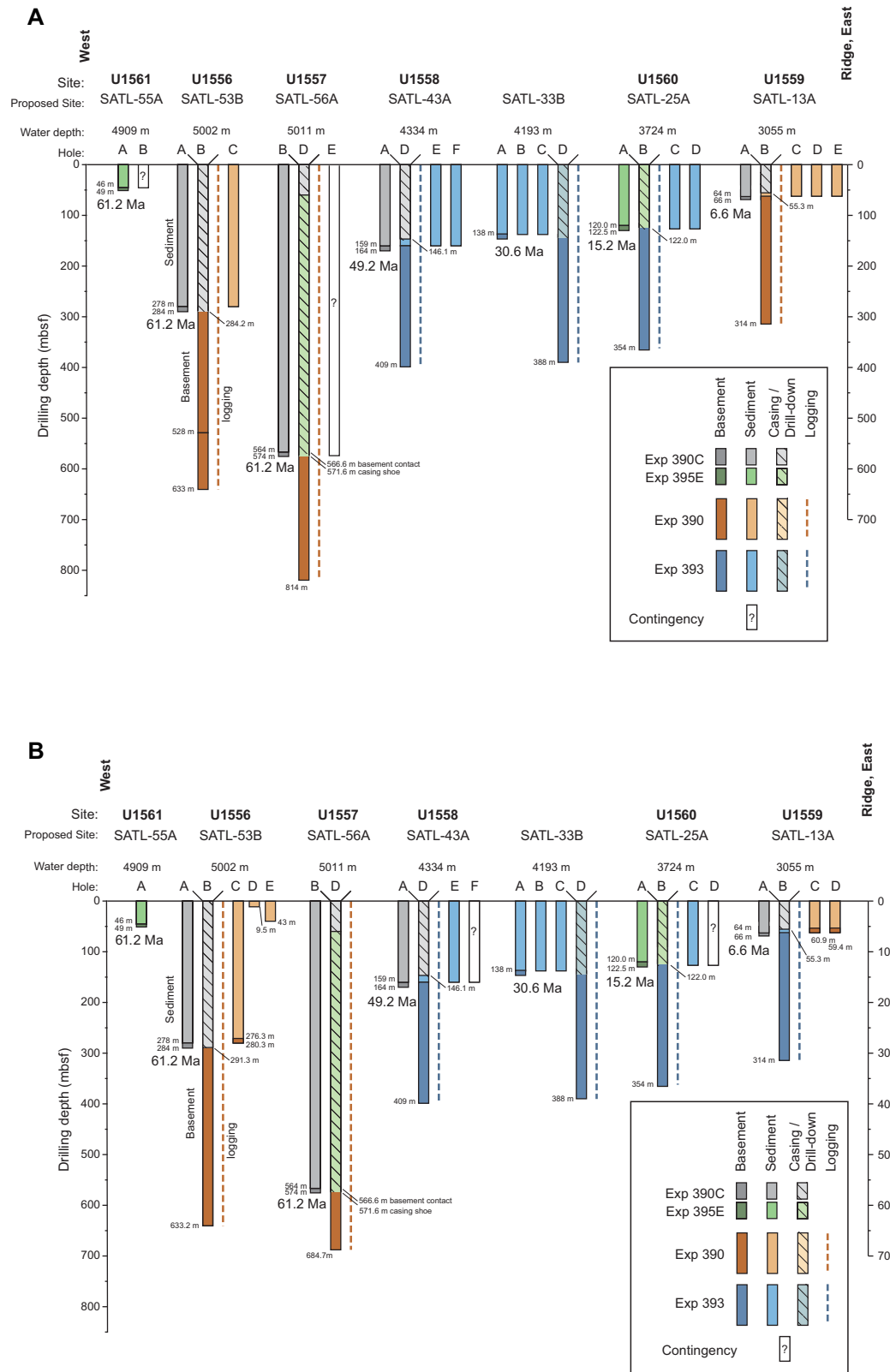


Figure 12. A. Engineering operations completed during Expeditions 390C and 395E and planned operations for Expeditions 390 and 393. B. Panel A modified to show operations completed during Expeditions 390C, 395E, and 390 and planned operations for Expedition 393. Water depths are for cased hole at each site, except for Sites U1561 (Hole U1561A) and SATL-33B (not yet occupied).

8. South Atlantic Transect drill sites

The SAT drilled during Expeditions 390C, 395E, 390, and 393 comprises the following seven sites from youngest to oldest:

- Site U1559 (proposed Site SATL-13A; Expeditions 390C, 390, and 393) is located nearest to the MAR on 6.6 Ma crust formed at a half spreading rate of 17 mm/y and overlain by ~64 m of sediment. This site provides a comparison to young intermediate spreading rate ocean crust drilled at reference Hole 504B (6.9 Ma; spreading rate of 36 mm/y; 275 m of sediment).
- Site U1560 (proposed Site SATL-25A; Expeditions 395E and 393) is located on 15.2 Ma crust formed at 25.5 mm/y and overlain by ~120 m of sediment. This site provides a comparison to reference superfast spreading rate ocean crust at Site 1256 (15 Ma; spreading rate of 220 mm/y; 250 m of sediment).
- Proposed Site SATL-33B (Expedition 393) is located on 30.6 Ma crust formed at 24 mm/y and overlain by an estimated 138 m of sediment.
- Site U1558 (proposed Site SATL-43A; Expeditions 390C and 393) is located on 49.2 Ma crust formed at 19.5 mm/y and overlain by ~159 m of sediment.
- Site U1556 (proposed Site SATL-53B; Expeditions 390C, 395E, and 390) is located on 61.2 Ma crust formed at 13.5 mm/y and overlain by ~278 m of sediment.
- Site U1557 (proposed Site SATL-56A; Expeditions 390C, 395E, and 390) is located on ~60.7 Ma crust 6.7 km east of Site U1556 in the same localized sedimentary basin and has a sediment thickness of ~564 m.
- Site U1561 (proposed alternate Site SATL-55A; Expeditions 395E and 390) is located on ~61.2 Ma crust ~22 km north of Site U1556 and has a sediment thickness of ~46 m.

9. Site summaries

9.1. Site U1556

9.1.1. Background and objectives

Site U1556 is in the western South Atlantic Ocean ~1250 km west of the MAR at a depth of ~5000 meters below sea level (mbsl). Site U1556 was previously occupied during engineering Expeditions 390C and 395E, during which the sediment succession and uppermost <6 m of basement were cored with the APC/XCB system (Hole U1556A). A reentry system with casing that extends almost to the sediment/basement interface was installed in Hole U1556B. The main objectives for visiting Site U1556 during Expedition 390 were to (1) core a second hole with the APC/XCB system to recover the complete sediment succession (via stratigraphic correlation with Hole U1556A) and sample the sediment/basement interface and (2) core 350 m into basement with the rotary core barrel (RCB) system in Hole U1556B (Figure F12). Sediment and interface cores provide samples that address the microbiological, geochemical, and paleoceanographic objectives of the SAT expeditions, and basement cores provide material that addresses the petrological, geochemical, and microbiological objectives of the SAT expeditions.

Site U1556 is located 6.7 km west of Site U1557 with basement predicted to have formed at ~61.2 Ma at a half spreading rate of ~13.5 mm/y. Oceanic crust at these sites is the oldest of all sites drilled during the SAT expeditions. The mineralogy and extent of alteration of the basement rocks at Site U1556, changes in physical properties such as porosity, and the composition of the microbial communities will be compared to the same characteristics at the other sites along the transect to investigate the development of hydrothermal circulation and crustal aging of the upper oceanic crust formed at slow to intermediate spreading rate MORs. The sedimentary succession at Site U1556 is about half as thick as it is at Site U1557, and contrasts between these closely spaced sites will allow exploration of the blanketing effect of sediment thickness on hydrothermal circulation.

9.1.2. Operations

Site U1556 was first visited during engineering Expedition 390C, with the goal of coring a single APC/XCB hole to basement for gas safety monitoring and installing a reentry system with casing

through sediment to ~5 m into basement; however, failure of the subsea camera system prevented installation of the reentry system at Site U1556. Engineering Expedition 395E returned to Site U1556 and installed a hydraulic release tool (HRT) reentry system with 284.2 m of 10% inch casing in Hole U1556B (Table T1). Casing did not extend into basement in Hole U1556B because of thicker sediment resulting from either a shallower seafloor or deeper basement.

During Expedition 390, the R/V *JOIDES Resolution* completed its 2296 nmi voyage from Cape Town, South Africa, to Site U1556 on 20 April 2022, arriving at 2330 h (UTC + 2 h). Overall, the vessel averaged 11.1 kt and took 8.6 days to complete the transit. Operations at Site U1556 started with reentry in Hole U1556B and basement coring with the RCB system. Reentry was made at 0405 h on 22 April, and the hole was washed down to 291.0 mbsf, where the bit contacted a hard layer. This depth is deeper than the 286.2 mbsf hole bottom observed during Expedition 395E; whether this discrepancy is due to subsidence of the reentry system, tidal variation in water depth, or another factor remains undetermined. During the first reentry, we observed that the cone was below the sediment surface, making this reentry and subsequent reentries challenging. Poor recovery and low penetration rates led to the decision to primarily drill half-length cores in Hole U1556B.

Coring progressed smoothly from Cores 390-U1556B-2R through 28R, at which time the bit had completed 61 h of drilling time and we conducted a bit change. Core 35R experienced high pump pressures (>2400 pounds per square inch [psi]), and the core barrel was retrieved so that we could attempt to restore circulation. The deplugger tool was deployed, and several mud sweeps were run, which successfully returned circulating pressure to normal coring values. Core 59R was the last core for the hole. The RCB bit, having completed 78 h of drilling time without failure, was dropped at the bottom of the hole using the mechanical bit release. We then pulled out of the hole, setting the pipe depth to 41 mbsf to prepare for logging operations. This hole was not preserved as a legacy hole because of the subsidence of the reentry cone. RCB drilling in Hole U1556B overall advanced 342.2 m to 633.2 mbsf and recovered 191.87 m of basement material (56%; Table T2; Figure F12). Microbial contamination tracer was pumped with the drilling fluid throughout RCB coring in Hole U1556B.

To assist with logging, the hole was cleaned by pumping twice the hole's volume of seawater. The triple combo logging tool string, including tools for measuring natural gamma radiation (NGR), borehole diameter, formation density, resistivity, and magnetic susceptibility, was lowered until it tagged hole bottom. Tool string telemetry failed after only a few meters of logging, and the string was pulled back to the surface and recovered. The Hostile Environment Natural Gamma Ray Sonde (HNGS) was identified as the issue, and a spare tool was substituted into the string. The second attempt at logging was successful. Two additional tool strings were then run: the Ultrasonic Borehole Imager (UBI) and Accelerator Porosity Sonde (APS) tool string, and the Formation MicroScanner (FMS) tool string, which logged two upward passes. Following completion of logging, the ship was repositioned 30 m south of Hole U1556B to prepare to drill Hole U1556C. Hole U1556B used 16.2 days of operational time in total (Table T2).

Table T2. Expedition 390 hole summary. * = drilled during Expeditions 390C and 395E; total penetration includes these drilled intervals. NA = not applicable.

Hole	Latitude	Longitude	Water depth (m)	Total penetration (m)	Drilled interval (m)	Cored interval (m)	Core recovered (m)	Recovery (%)	Total cores (N)	APC cores (N)	XCB cores (N)	RCB cores (N)	Start date (2022)	Start time UTC (h)	End date (2022)	End time UTC (h)	Time on hole (h)	Time on hole (days)
U1556B	30°56.5244'S	26°41.9472'W	5001.8	633.2	291.0*	342.2	191.87	56	58	0	0	58	20 Apr	2330	7 May	0400	388.50	16.20
U1556C	30°56.5406'S	26°41.9472'W	5005.7	280.3	NA	280.3	283.81	101	32	16	16	0	7 May	0400	10 May	1915	87.25	3.60
U1556D	30°56.5514'S	26°41.9472'W	5003.1	9.5	NA	9.5	9.67	102	1	1	0	0	10 May	1915	10 May	2115	2.00	0.10
U1556E	30°56.5622'S	26°41.9472'W	5003.1	43.1	NA	43.1	43.30	100	5	5	0	0	10 May	2115	11 May	1530	18.25	0.80
Site U1556 totals:				966.1	291.0*	675.1	528.65	78	96	22	16	58					496.00	20.70
U1557D	30°56.4651'S	26°37.7892'W	5010.8	684.7	575.6*	109.1	71.28	65	13	0	0	13	11 May	1530	19 May	0615	182.75	7.60
Site U1557 totals:				684.7	575.6*	109.1	71.28	65	13	0	0	13					182.75	7.60
U1559C	30°15.6505'S	15°2.0911'W	3058.0	60.9	NA	60.9	56.81	93	7	6	1	0	21 May	1845	22 May	1615	21.50	0.90
U1559D	30°15.6593'S	15°2.0906'W	3057.7	59.4	NA	59.4	43.60	73	8	6	2	0	22 May	1615	23 May	1945	27.50	1.10
Site U1559 totals:				120.3	NA	120.3	100.41	83	15	12	3	0					49.00	2.00
Expedition totals:				1771.1	866.6*	904.5	700.34	77	124	34	19	71						

Three APC/XCB sediment holes were cored at Site U1556 during Expedition 390: Hole U1556C was cored to 280.3 mbsf, Hole U1556D was terminated after a missed mudline core, and Hole U1556E resampled the top 43.1 m of sediment for microbiology and geochemistry objectives (Table T2; Figure F12). In Hole U1556C, coring progressed through Core 390-U1556C-30X, which recovered basalt fragments in the core catcher. Overall, Cores 1H–30X penetrated to 276.3 mbsf and recovered 281.74 m of sediment (102%). Cores 31X and 32X advanced another 4 m into basement to 280.3 mbsf, recovering 2.07 m (52%). APC cores in Hole U1556C (Cores 1H–16H) were collected using nonmagnetic core barrels and oriented for paleomagnetic research using the Icefield MI-5 core orientation tools. Formation temperature measurements were made while collecting Cores 4H, 7H, 10H, and 13H using the advanced piston corer temperature (APCT-3) tool. In Hole U1556E 40 m south of Hole U1556C, coring progressed through Core 390-U1556E-5H in a water depth of 5003.1 m, achieving a final hole depth of 43.1 mbsf and recovering 43.33 m (100.5%). Cores from Hole U1556E were not oriented, and no temperature measurements were made. APC/XCB coring in Holes U1556C–U1556E took 4.5 days of operations time overall (Table T2).

9.1.3. Principal results

9.1.3.1. Stratigraphic unit summary

Site U1556 cores comprise two sedimentary units as well as 13 basement units, identified on the basis of macro- and microscopic visual observations combined with mineralogical analyses (by X-ray diffraction [XRD] for sediment), color reflectance, and magnetic susceptibility data. The units are numbered from the top of the hole, with units in the sedimentary section designated by Roman numerals and basement units designated by Arabic numerals; subunits are designated with letters. The sediment/basement interface was recovered at three different depths below seafloor in Holes U1556A–U1556C. Differences in basement depth are likely attributable to basement topography and subsequently different sediment thicknesses but may also be due to differences in seafloor height. For stratigraphic correlation across holes and reporting, basement was defined at 290.29 mbsf based on the first occurrence of basalt in Hole U1556B, the hole with the reentry system and casing where we conducted basement drilling.

9.1.3.2. Sedimentology

In the five holes cored at Site U1556, a mixture of biogenic and siliciclastic sediments were recovered (Figure F13). The former typically consists of pinkish white or light gray calcareous nannofossil ooze that lithifies to chalk downhole. Variable but minor amounts of foraminifera are present throughout. Siliciclastic sediment consists of silty clays that range from brown/dark brown where carbonate is absent to reddish brown where the carbonate content is higher. Two lithologic units (I and II) are defined based on a combination of visual observations of sedimentological characteristics, microscopic examination of smear slides and bulk mineralogical analysis by XRD, integrated with magnetic susceptibility, and color reflectance observations. Lithologic Unit I is composed of ~235 m of upper Oligocene to Pleistocene sediments, mainly silty clay and calcareous nannofossil ooze. Lithologic Unit II is composed of ~42 m of Paleocene or Eocene sediments, predominantly nannofossil-rich calcareous chalk or calcareous nannofossil chalk. Differences in mineral assemblages are relatively small with increasing burial depth within the respective silty clay and ooze/chalk phases. Below the sediment/basement interface is a transitional unit that comprises both pelagic sedimentary material and volcanic clasts where the sediment matrix is composed of calcareous chalk with clay.

9.1.3.3. Sediment biostratigraphy

Calcareous nannofossil and planktic foraminifera biostratigraphy was performed on core catcher samples recovered from Hole U1556A (collected during Expedition 390C and examined on shore) and at a higher resolution (utilizing both core catchers and additional samples from the working half of each core) from Hole U1556C. Additional calcareous nannofossil and planktic foraminifera samples were taken from Hole U1556A archive halves and Hole U1556C working halves to refine the biostratigraphic zonation. Calcareous nannoplankton are present in the oozes and chinks but are mostly absent from the clays; planktic and benthic foraminifera are also mostly absent from the clays and have variable abundance in the nannofossil oozes of Unit I, in which they commonly comprise depauperate assemblages of mostly very small specimens (Figure F14).



Figure F13. Stratigraphic summary of representative sediment holes at each Expedition 390 site, Holes U1556C, U1557B, U1561A, and U1559C. For epoch, see Figure F15. a* (red to green) is smoothed with 100 point moving average. cps = counts per second. NGR and magnetic susceptibility (point source) are plotted on CSF-B depth scale.

Sedimentation rates appear to be relatively continuous from the Holocene through the early Oligocene (Figure F15). A ~44 m thick condensed interval or unconformity composed of dark brown pelagic clay spans the early Oligocene to early Eocene at Site U1556. Below this unconformity, the Eocene extends from ~216 to 266 m core depth below seafloor, Method B (CSF-B). Eocene assemblages contain significant reworking of Paleocene calcareous nannofossils and foraminiferal taxa that appear to be principally or entirely sourced from the middle Paleocene planktic foraminifera Zone P4a and calcareous nannoplankton Zones NP5/CNP8–CNP7, including a coherent slump deposit that contains an entirely Paleocene assemblage. Increasing reworking downhole makes precise age determinations difficult, but the middle Eocene (likely below planktic foraminifera Zone E5 and calcareous nannofossil Zones NP11/CNE3) unconformably overlies the middle Paleocene in the lowermost part of the sediment section, representing an interval of missing time spanning at least 5 My and up to 10 My. Samples directly above the in-place Paleocene sediments contain an increased proportion of benthic foraminifera and broken planktic foraminifera. Samples below the Paleocene–Eocene unconformity are middle Paleocene in age (planktic foraminifera Zone P4a and calcareous nannofossil Zones NP5/CNP8–CNP7).

To constrain the age of basement at Site U1556, samples were taken as close to the sediment/basement interface as possible and comprise the same middle Paleocene assemblages of planktic foraminifera and calcareous nannofossils. A thin section from a sediment lens in the deepest core in Hole U1556B (~633 m CSF-B) recorded a planktic foraminifera assemblage in Zone P4a. This suggests that the entire 341 m sequence of basalt cored at Site U1556 must have been erupted within 220 ky, or between 60.54 and 60.76 Ma (based on the global calibration for the duration of Zone P4a by Gradstein et al., 2020) because sediments at the sediment/basement interface and at the bottom of the basement were deposited within the same planktic foraminifera zone.

Benthic foraminifera indicate that Site U1556 was at lower bathyal depths in the Paleocene and early Eocene before subsiding to its present abyssal depth by the Pliocene. Subsidence likely occurred even earlier, but the lack of benthic foraminifera in the intervening samples makes a precise determination impossible.

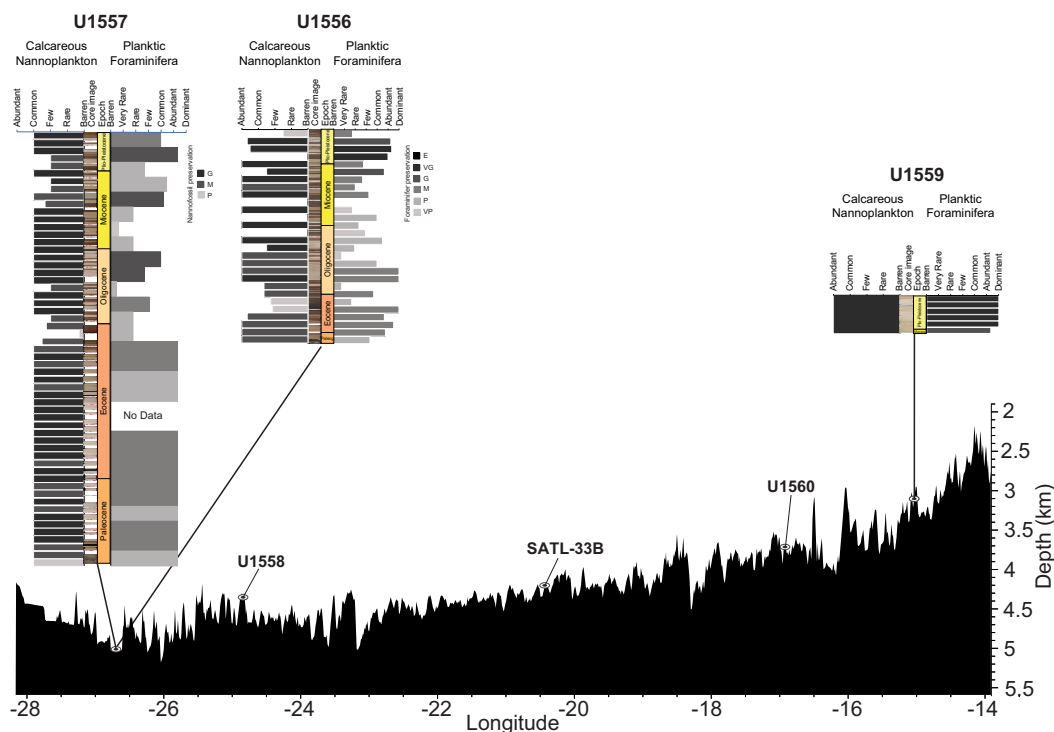


Figure F14. Summary of calcareous nannoplankton and planktic foraminifera abundance and preservation across the SAT and plotted in 10 m thick bins, (except Site U1557 foraminifera, which are binned at 20 m because of sample resolution) and shown above seafloor bathymetry measured during CREST cruise. Preservation: E = excellent, VG = very good, G = good, M = moderate, P = poor, VP = very poor.

Sieved residues from Site U1556 contain varying abundances of broken fish debris (most abundant in pelagic clays), siliceous microfossils (diatoms, radiolarians, and sponge spicules), and authigenic manganese (Mn) oxide. Siliceous material is most common in the Pliocene–Pleistocene and then again in the middle Oligocene. Mn oxides are primarily found in the Neogene.

9.1.3.4. Sediment paleomagnetism

Paleomagnetic investigation of Site U1556 sediments included remanence analysis of cores split during engineering Expedition 390C alongside Expedition 390 analyses of the archive halves of Sections 390C-U1556A-30X-1 through 30X-4 (the portion of Core 30X above basement) and Cores 390-U1556C-1H through 30X, 390-U1556D-1H, and 390-U1556E-1H through 5H on the superconducting rock magnetometer (SRM) and 59 discrete sediment samples primarily from Hole U1556C. We use these data to establish a magnetostratigraphy for the sediment package at Site U1556, which will be refined with additional analysis postexpedition. All three Expedition 390 holes display clear polarity reversals that can be tied to Hole U1556A for magnetostratigraphic correlation. Furthermore, Hole U1556C recovered material from depth intervals that were not recovered in Hole U1556A, including around the base of the sediment package, which will allow better constraint of the basal age.

Anisotropy of magnetic susceptibility (AMS) and bulk susceptibility were measured on all discrete cubes. AMS is routinely used as a petrofabric proxy to determine the preferred alignment of the magnetic mineral assemblage under an external field, and bulk susceptibility is used to determine the concentration of magnetic material present. Likewise, all cubes were alternating field (AF) demagnetized, up to 190 mT in some instances. Stepwise demagnetization characterizes, to a first order, the dominant magnetic mineral assemblage and allows determination of the characteristic remanent magnetization (ChRM) of the sample, which reflects the magnetic field direction at or

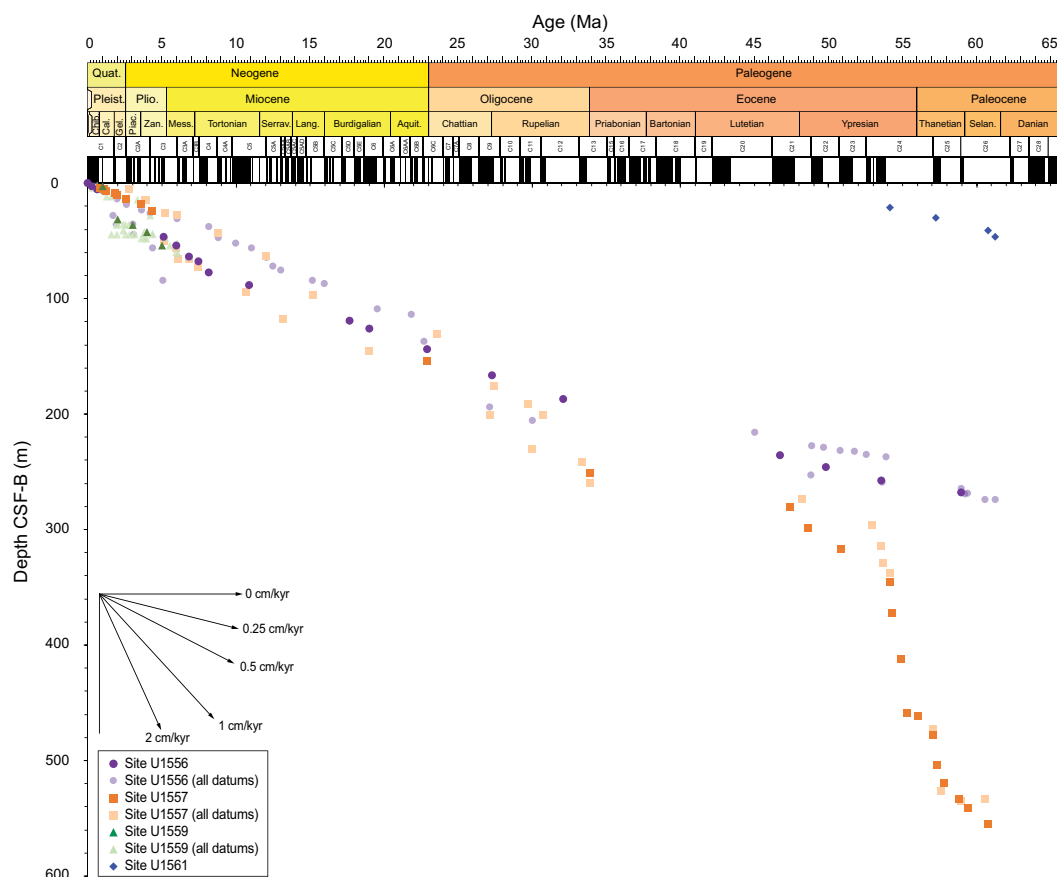


Figure F15. Age-depth plots, Expedition 390 sites. All biostratigraphic and magnetostratigraphic datums are shown in lighter colors; datums used to construct age-depth models at each site are darker. Inset figure to interpret sedimentation rates for the age transect is also shown.

soon after sediment deposition and aids in the magnetostratigraphic interpretation. Acquisition of isothermal remanent magnetization (IRM) and backfield IRM experiments were performed on a subset of discrete samples to characterize the magnetic mineral assemblage. Both the AF demagnetization and IRM experiments suggest the presence of titanomagnetites/titanomaghemites of various oxidation states and/or grain sizes. Of the 59 discrete sediment samples, 49 samples had orthogonal vector plots (OVPs) “clean” enough to contribute to defining the ChRM, and only 28 samples gave maximum angular deviation angles of less than 15°.

9.1.3.5. Sediment age model and mass accumulation rate

The age model for Site U1556 was constructed using calcareous nannoplankton and planktic foraminifera bioevents and paleomagnetic reversal datums from Hole U1556C, which is the best recovered hole at Site U1556 and the most densely sampled for biostratigraphy. Overall, the sediment section ranges in age from middle Paleocene to Holocene, with a ~10 My unconformity/condensed interval spanning the middle Eocene to earliest Oligocene and a ~5 My unconformity spanning the middle Paleocene to early Eocene. Overall sedimentation rates average 0.58 cm/ky from the early Oligocene to Holocene (0–32.1 Ma) and 0.36 cm/ky in the early Eocene between the unconformities (46.7–53.6 Ma; Figure F15). Mass accumulation rates at Site U1556 are generally highest from the late Miocene to Holocene (up to 1.01 g/cm²/ky) and in the early Oligocene (up to 1.3 g/cm²/ky) and tend to covary with carbonate accumulation rate, indicating that sedimentation is primarily driven by pelagic carbonate production. Organic carbon accumulation rates are very low at Site U1556, with a maximum value of 0.003 g/cm²/ky, in the early Eocene.

9.1.3.6. Sediment physical properties and downhole measurements

Physical properties characterization of the sediment section at Site U1556 was based on cores and in situ downhole measurements from Holes U1556A and U1556C and wireline logging data from Hole U1556B. Whole-round core-based measurements included NGR (sensitive to the abundance of minerals containing radioisotopes of K, U, and Th), bulk density from gamma ray attenuation (GRA), magnetic susceptibility (MS; an indicator of the concentration of magnetic minerals), and *P*-wave velocity. Discrete measurements of moisture and density (MAD; to estimate grain density and porosity), thermal conductivity, triaxial *P*-wave velocity, and rheological properties (shear and compressional strength) were made on samples from working-half sections. Trends in the physical properties and downhole logging data generally correlate well with lithologic units.

NGR values are generally low and vary from 6 to 20 counts/s in calcareous nanofossil ooze/chalk and moderate with variability up to 65 counts/s in silty clay (Figure F13). Spectral gamma data from wireline logging show clearly defined intervals of lower and higher values, consistent with the presence of alternating ooze/chalk and silty clay, respectively. At Site U1556, spectral gamma ray logs show that the NGR signal comes largely from the radioactive isotopes of potassium and thorium, with additional contributions from uranium in the higher gamma ray, silty clay layers. Sediment lithologic unit boundaries coincide with sharp changes in NGR, as well as MS. MS values are low (0–60 instrument units [IU]) in carbonate-dominated lithologies and high (up to 250 IU) in silty clays (Figure F13). Bulk density and *P*-wave velocity generally increase with depth in the sedimentary section, which is consistent with a compaction trend. Both are generally locally anticorrelated with natural gamma ray and magnetic susceptibility, indicating that oozes and chinks are denser with higher velocities than silty clay lithologies. Discrete porosity values in sediments decrease downhole, with some variation that is likely related to lithology but also to drilling disturbance in XCB cores. Mean thermal conductivity in sediments ranges from 0.8 to 1.5 W/(m·K).

Eight successful downhole temperature measurements were made in sediments at Site U1556 with the APCT-3 tool. Measurements were made along with Cores 4H, 7H, 10H, and 13H in both Holes U1556A and U1556C, extending temperature data to 123 mbsf. Linear temperature profiles varied between the two holes, with a geothermal gradient of 15°–36°C/km.

Data from cores recovered using the APC/XCB system in Holes U1556A, U1556C, U1556D, and U1556E were correlated to produce a near-continuous shipboard splice for the upper 195.6 m core composite depth below seafloor (CCSF). The correlation is primarily based on changes in MS, NGR, and density in cores from Holes U1556A and U1556C that correspond to lithologic variations between silty clay and nanofossil ooze/chalk. Hole U1556D and U1556E stratigraphy can be correlated to fill gaps in the upper ~40 mbsf of the splice generated between Holes U1556A and

U1556C. The composite depth scale will facilitate future sampling at higher resolution. Deeper than 195 m CCSE, physical properties records from Holes U1556A and U1556C are consistent and can be tentatively correlated, but the construction of a detailed composite section is not possible.

9.1.3.7. Sediment geochemistry

During the sediment drilling in Holes U1556A, U1556C, and U1556E, interstitial water (IW) samples were extracted via squeezing. For APC coring, IW whole-round samples were taken at a frequency of two per core during Expedition 390 (Hole U1556C) and one per core during Expedition 390C (Hole U1556A). One IW sample per core was taken during XCB drilling. Sampling frequency of the squeezed IW increased to two per core within 40 m above the basement. Rhizon IW samples were taken from Holes U1556C and U1556E for postexpedition research. Shipboard analyses of the squeezed IW from Holes U1556A and U1556C include pH, salinity, alkalinity, major cations and anions (sodium, calcium, magnesium, potassium, chloride, and sulfate) using ion chromatography (IC), major and minor elements using inductively coupled plasma–atomic emission spectroscopy (ICP-AES), nutrients (phosphate and ammonium), and sulfide on the spectrophotometer. Carbonate and total carbon measurements were then conducted on the squeeze cake and selected samples from the working half. The remaining IW and squeeze cake were distributed to scientists for postexpedition research. Dissolved oxygen in IW was also measured in Holes U1556C and U1556E using the optical oxygen sensors, with a resolution of ~1–5 m.

Data generated from Hole U1556A and U1556C IW samples are very similar. They both show a strong redox gradient in the top ~100 m, with decreasing sulfate and increasing dissolved manganese and ammonium concentrations consistent with organic carbon respiration. Below ~260 m CSF-B in both holes, sulfate concentrations increase, and dissolved manganese concentrations are minimal (Figure F16). Maxima in silica concentrations at ~5 and ~150 m CSF-B may reflect biogenic silica dissolution. Carbonate contents vary depending on lithology (up to ~93 wt% in the carbonate ooze/chalk and often <1 wt% in the silty clay), whereas the organic carbon concentrations are all below 1 wt%.

9.1.3.8. Sediment microbiology

Microbiological sediment samples were collected from Holes U1556C (Cores 390-U1556C-1H through 31X) and U1556E (Cores 390-U1556E-1H through 5H). The team processed all samples destined for physiology experiments in the anaerobic chamber in the walk-in cold room, whereas samples destined for postexpedition cell counts and nucleic acid analysis were conducted at room temperature between two KOACH air-filtering units to mitigate contamination. This dual setup allowed faster sample processing. To test for potential microbial contamination, drilling fluid was collected during coring of Hole U1556C on 9 May 2022 and Hole U1556E on 10 May. During post-

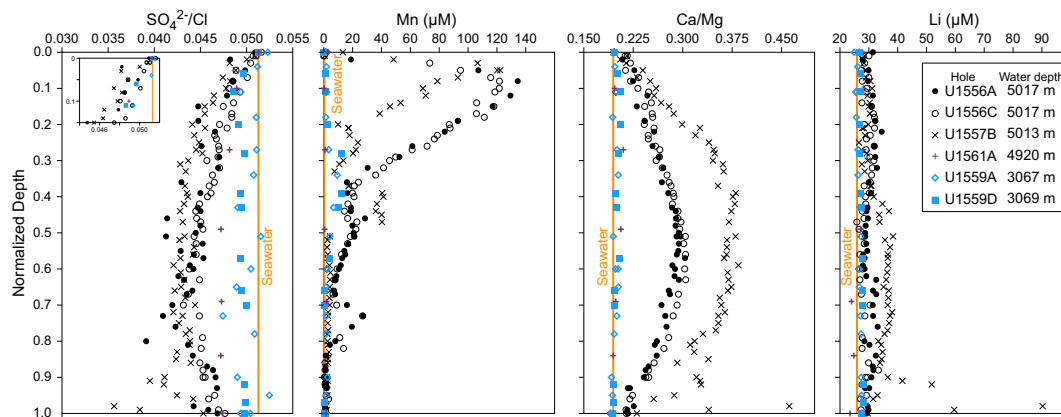


Figure F16. IW chemistry along SAT. Orange = standard seawater values ($SO_4^{2-}/Cl = 28$ mM/546 mM, $Mn = 0.36$ μM , $Ca/Mg = 10.27$ mM/52.7 mM, $Li = 25.9$ μM). Sediment depths were normalized to maximum sediment thickness of each hole to compare variations in IW chemical profiles (0 = near mudline, 1 = near basement). Inset on SO_4^{2-}/Cl plot shows depth dependent decrease in ratios in all holes between 0 and 0.15 normalized depth. Standard seawater values were taken from Monterey Bay Aquarium Research Institute (MBARI) Periodic Table of Elements in the Ocean (<https://www.mbari.org/science/upper-ocean-systems/chemical-sensor-group/periodic-table-of-elements-in-the-ocean>).

expedition research, DNA will be extracted from these samples to create a database of potential contaminants for comparison with cored samples.

9.1.3.9. Basement igneous petrology

In Hole U1556B, 342.3 m of igneous rock, including breccias, were cored after the igneous basement was reached at 291.4 mbsf. The igneous rock succession consists predominantly of pillow lavas, with thin intervals of either more massive lava flows or larger pillows, all punctuated by periodic occurrences of breccias (Figure F17). The igneous sequence was divided into 13 lithologic units based on changes in petrographic type and phenocryst assemblage. The lithologic units were grouped into three overarching stratigraphic sequences (Stratigraphic Sequence A in Sections 390-U1556B-2R-2 through 38R-2; Stratigraphic Sequence B in interval 38R-3 through 54R-3, 130 cm; and Stratigraphic Sequence C in interval 54R-3, 130 cm, through 59R-4; Figure F18). The uppermost 5.1 and 4.7 m of the igneous sequence at Site U1556 were also recovered in Holes U1556A and U1556C, respectively.

The uppermost igneous basement, and the top of Stratigraphic Sequence A, comprises a 11.7 m thick sedimentary breccia (Lithologic Unit 1), which probably represents talus deposits of volcaniclastic debris transported downslope via a gravity flow. Beneath this is a series of sparsely to moderately olivine phyric basalt pillow lava flows interspersed with volcanic breccias in Lithologic Units 2–11. The breccias contain clasts of chilled pillow margins and glass (altered to palagonite) but the proportions of sedimentary matrix and carbonate cement vary significantly between breccia units. Lithologic Unit 12, which has six subunits, corresponds to Stratigraphic Sequence B. It consists of a series of aphyric to very sparsely olivine (micro)phyric basalts that are highly altered. Lithologic Unit 11 is noteworthy in that it records intrusive relationships between the lavas of

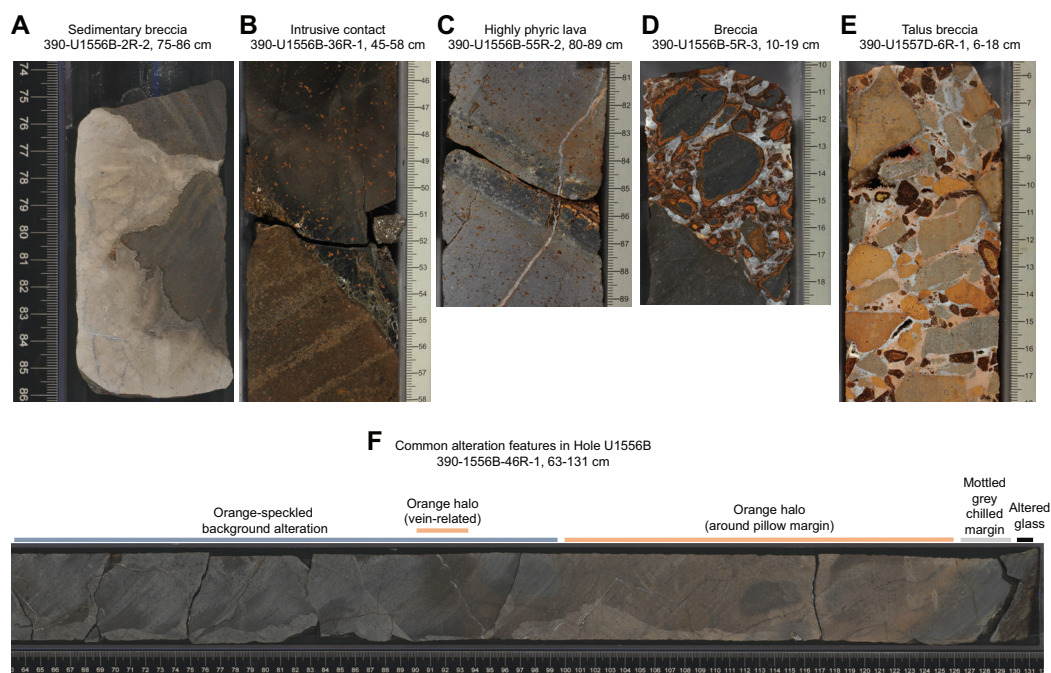


Figure F17. Core photographs of representative samples of uppermost basement rocks, Sites U1556 and U1557. A. Sedimentary breccia from sediment/basement interface, comprising fragments of basaltic lava in micritic limestone matrix. B. Intrusive contact between basalts of Stratigraphic Sequences A and B, Hole U1556B. Moderately olivine phyric basalt (Stratigraphic Sequence A; upper half of image), in which olivine is highly altered to distinctive orange-brown color, intrudes an older, intensely altered pillow basalt (Stratigraphic Sequence B; lower half of image). C. Chilled margins of highly plagioclase-olivine-pyroxene phyric basalts from Stratigraphic Sequence C, Hole U1556B. D. Hyaloclastite breccia with carbonate cement. E. Talus breccia from Hole U1557D, comprising gray, brown, and orange clasts of altered basalt and altered glass cemented by a zeolite ± micritic or microsparry calcite. F. Macroscopic core image illustrating some common alteration types in Hole U1556B and their typical spatial relationship to one another in sequence from margin to interior of large pillow. From chilled margin (right of image) to pillow interior (left of image) these typically include altered glass, a mottled gray cryptocrystalline to variolitic zone, orange halos paralleling the pillow margin and along veins, and orange speckled background in the interior.

Stratigraphic Sequences A and B. Stratigraphic Sequence C corresponds to Lithologic Unit 13, which is a highly plagioclase-olivine-pyroxene phyric basalt that contains cognate inclusions interpreted as cumulates formed in a magma chamber.

9.1.3.10. Basement metamorphic and alteration petrology

All the rocks recovered from Site U1556 are altered to some degree. Alteration manifests as a wide range of styles and extents from slight to moderate background alteration all the way to almost complete oxidation and replacement of groundmass and phenocrysts. The pattern of this alteration is strongly spatially controlled at the scale of individual sections and is primarily related to the locations of veins and the chilled margins of igneous flows/pillows which have provided free surfaces for fluid-rock interactions (Figures F17, F18). The overall degree of alteration broadly increases downhole and is closely related to the igneous stratigraphy and emplacement style of the basalts. Altogether, 5000 veins and vein networks, 600 intervals of breccia cement, and 320 occurrences of filled vesicles were recorded in Hole U1556B. The most abundant fill phases include smectite clays, carbonate, Fe oxyhydroxides, and zeolites. A range of different alteration styles characterize the cores and, together with cross-cutting relationships, indicate a potentially prolonged sequence of alteration under a variety of conditions both oxidative and more reducing.

9.1.3.11. Basement paleomagnetism

Discrete cube samples for paleomagnetic analysis were collected from representative basalts recovered from Hole U1556B, targeting both fresher basalts and those with varying extents and styles of alteration. Both alternating field (AF) demagnetization of the natural remanent magnetization (NRM) and acquisition of IRM indicate a variety of coercivities for the ferromagnetic phases present in samples, requiring fields up to 190 mT to fully demagnetize NRM. The contributing ferromagnetic minerals cannot be determined without additional shore-based work. Most

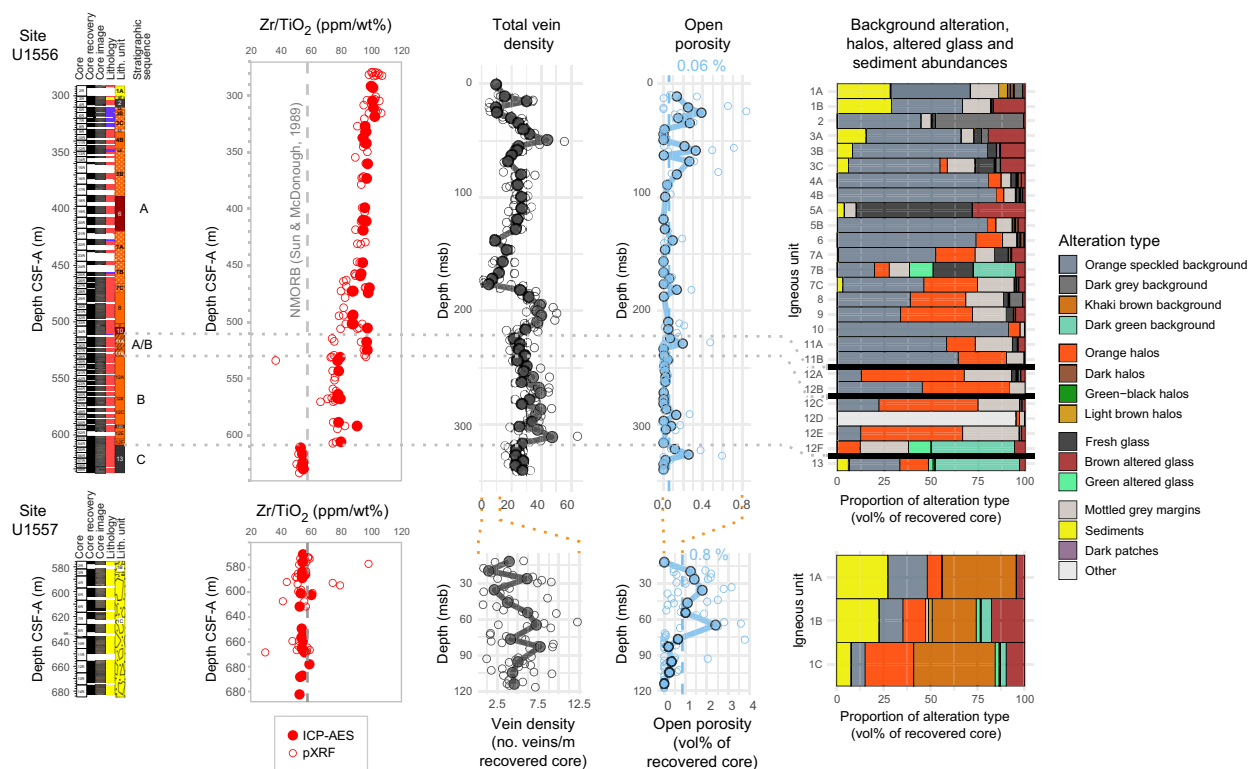


Figure F18. Hard rock core description summary, Sites U1556 and U1557. Summary visual core descriptions showing core recovery and igneous stratigraphy are based on Holes U1556B and U1557D. Zr/TiO₂ shows enriched geochemical signatures in Stratigraphic Sequences A and B at Site U1556 (all geochemical data measured during Expedition 390 are shown; thick dashed line = composition of N-MORB [Sun and McDonough, 1989] for reference). Note that some pXRF data from Holes U1556A and U1557B plot to shallower depth than top of basement in Holes U1556B and U1557D core recovery. Total vein density and open macroscale porosity observed during core logging (thick dashed line = mean as a proportion of all recovered rock, open circles = calculated by section, solid circles = calculated by core, dotted red lines = tie lines indicating differences in x-axis scales for the two holes). Summary of relative proportion of different alteration types recorded for each igneous stratigraphic unit during alteration logging (thick black lines = boundaries between major stratigraphic sequences at Site U1556).

samples carry a well-defined single component remanence with positive inclinations (reversed polarity) compatible with the rock age. An additional component of negative inclination was observed in brecciated orange-colored rocks and some oxidized basalt samples that likely represents a component acquired upon alteration (Figure F19). Because analyzed samples are saturated or close to saturation at the maximum field applied during IRM acquisition (1.2 T), maghemitization of original magnetite-titanomagnetite minerals is suspected. Suitable half core pieces (greater than about 15–20 cm long) from the archive halves have also been measured on the SRM. Finally, a subset of samples were subjected to thermal demagnetization up to 580°C (the temperature used to define magnetite by a loss in magnetization). These data confirm the results of both the AF demagnetization and IRM analyses.

9.1.3.12. Basement physical properties and downhole measurements

Basement physical properties were determined primarily from cores and downhole logging data from Hole U1556B, with additional information from the deepest cores from Holes U1556A and U1556C which extended several meters into basement. Measurements on whole-round and split half sections were compared with each other and with downhole measurements from Hole U1556B for lithostratigraphic characterization and integration of core description and borehole

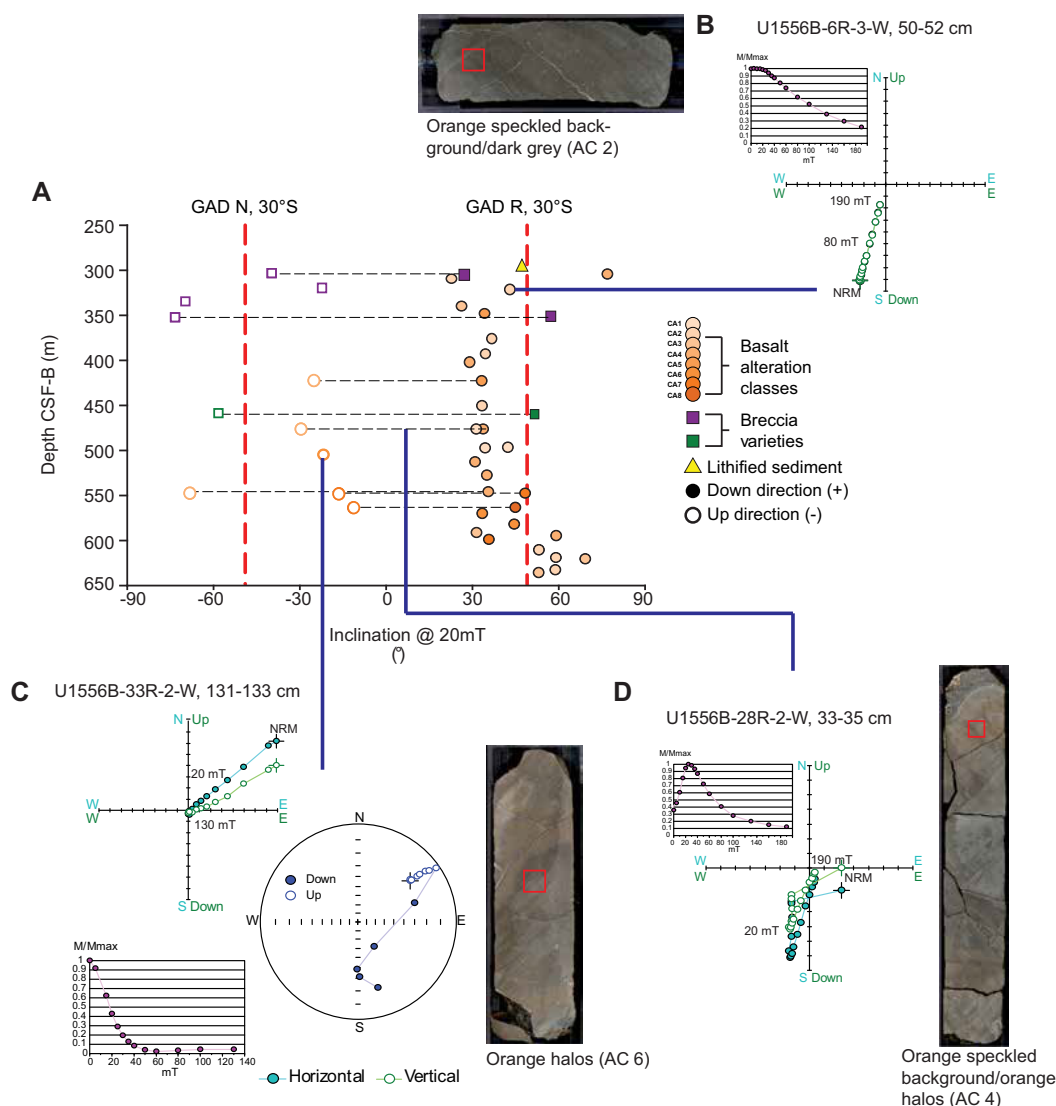


Figure F19. Stepwise demagnetization orthogonal vector plots, decay AF plot, and sampling location of cores for representative samples of different alteration classes along with both (A) ChRM and overprint inclinations of Hole U1556B discrete samples (B: no overprint, C: completely overprinted, D: partially overprinted).

data. In addition to the standard whole-round and discrete measurements, high-resolution 3-D exterior images were also taken from ~170 m of hard rock whole-round cores using the DMT core scanner.

In the basement interval of Site U1556, NGR data show distinct variations that correspond well with the three main stratigraphic igneous units. NGR values range from 0 to 60 counts/s in the uppermost Stratigraphic Sequence A. Between 504 and 529 m CSF-B, mean NGR increases, which corresponds to a transitional zone in basement in which both Stratigraphic Sequence A and B appear together. Below 529 m CSF-B in Stratigraphic Sequence B, NGR decreases and varies between 7 and 25 counts/s. At 609 m CSF-B, NGR decreases abruptly and remains low to the base of the drilled interval, all within Stratigraphic Sequence C. Gamma ray from wireline logging shows similar trends and sharp changes in these data are associated with igneous lithologic sub-unit contacts. MS in the basement interval ranges from 0 to >800 IU, generally increasing with depth in basement. A sharp increase in MS coincides with the change from Stratigraphic Sequence B to C at 609 m CSF-B. Bulk density generally decreases downhole and discrete sample data indicate that the majority of basalt samples have higher density, lower porosity, and higher *P*-wave velocity than hyaloclastite samples. Electrical resistivity and porosity data from wireline logging are both sensitive to formation porosity and show clear distinctions between the more massive basalt flows, which have higher density and resistivity and lower porosity, and the hyaloclastite intervals, which have lower density and resistivity and higher porosity. Thermal conductivity in basement cores ranges from 1.0 to 1.7 W/(m·K), with lower conductivity generally associated with hyaloclastite samples and higher conductivity with basalt samples.

9.1.3.13. Basement geochemistry

For the Hole U1556B basement cores, representative samples were taken from the freshest portions of each lithologic subunit to obtain a downhole record of the primary magmatic compositions. These samples were supplemented with additional basalt samples with different styles and extents of alteration that were considered homogeneous at the scale of sampling to make a preliminary investigation of the alteration effects on elemental abundances. Additionally, lithified sediments, primarily micritic limestone, were sampled from the matrix of sedimentary breccias. Combined, a total of 45 samples were taken for loss on ignition (LOI) and bulk rock geochemical analysis via ICP-AES from Hole U1556B. The 45 samples also included 3 paired basalt samples, with each pair sampling different portions of a single lava flow that display different styles or extents of alteration to investigate the effects of alteration on the bulk rock composition. LOI varies between 0.2 and ~4 wt%, indicating that all selected samples are at least partially altered, with higher LOI suggesting more alteration. Most basalt samples are categorized as basalt and trachybasalt with a transition to lower concentrations for incompatible elements at the bottom of the hole. Comparison of the paired samples suggest addition of Al_2O_3 , Na_2O , K_2O , Ba, and Zn with increased degree of alteration. High field strength element ratios (e.g., Zr/TiO_2) show a transition from normal mid-ocean-ridge basalt (N-MORB) at the bottom of the hole to ocean-island basalt (OIB) at the top of the hole (Figure F18).

9.1.3.14. Basement microbiology

Approximately one microbiological whole-round sample per 10 m advance in Hole U1556B was collected and preserved for shore-based analysis. Before processing the whole rounds, they were imaged using the Foldio lightbox/turntable system (Figure F20). All sampling was done within the KOACH system, a portable air filtration unit that creates a particle-free area for low-contamination sampling. Sample handling was conducted using an ethanol-washed steel rock box and chisels.

Postexpedition research on samples from these microbiology whole rounds includes cell counts; analysis of community DNA, RNA, and lipids; single cell genomics; stable and radioisotope incubation experiments; and generation of enrichment cultures. To test potential contamination of whole rounds by drilling fluid, we collected the inner and outer rock chips containing perfluorocarbon tracer (perfluoromethyldecalin [PFMD]) from each whole round. Preliminary analysis of PFMD samples analyzed via gas chromatography–electron capture detector (GC-ECD) indicated no intrusion of drilling fluid in most samples.

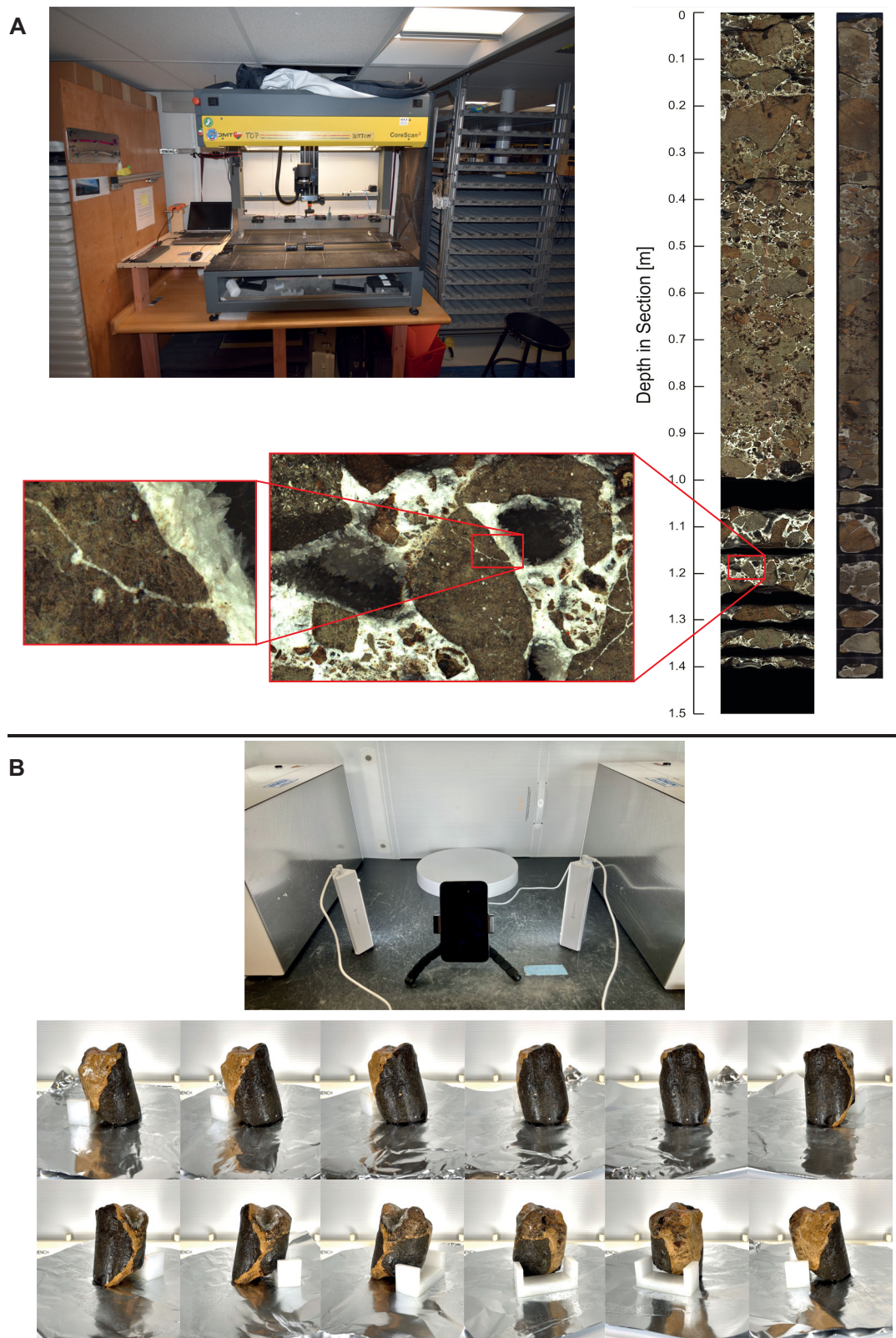


Figure F20. A. DMT CoreScan3 workstation on *JOIDES Resolution* with example of 3-D high-resolution image created using novel methods developed during Expedition 390. B. Foldio workstation with rotating stage and camera positioned to take multiple time-lapsed images of core pieces as it rotates. These images were taken to preserve information on pieces fragmented for microbiological sampling.

9.2. Site U1557

9.2.1. Background and objectives

Site U1557 is in the western South Atlantic Ocean ~1250 km west of the MAR at a depth of ~5000 mbsl. Site U1557 was previously occupied during engineering Expeditions 390C and 395E, during which the sediment succession and uppermost <6 m of basement were cored with the APC/XCB system in Hole U1557B and a reentry system was installed with casing that extends into the uppermost basement in Hole U1557D. The main objectives of revisiting Site U1557 during Expedition 390 were to (1) core up to 250 m into basement with the RCB system in Hole U1557D to collect material that addresses the petrological, geochemical, and microbiological objectives of the SAT expeditions and (2) collect wireline geophysical logging data through the basement section (Figure F12).

Site U1557 is located 6.7 km east of Site U1556, with basement predicted to have formed at ~60.7 Ma, slightly younger than the 61.2 Ma age calculated for Site U1556, at a half spreading rate of ~13.5 mm/y. Oceanic crust at these sites is the oldest that was drilled during the SAT expeditions. The mineralogy and extent of alteration of the basement rocks at Site U1557, changes in physical properties such as porosity, and the composition of the microbial communities will be compared to the same characteristics at the other sites along the transect to investigate the development of hydrothermal circulation and the crustal aging of the upper oceanic crust formed at slow to intermediate spreading rate MORs. The sedimentary succession at Site U1557 is about twice as thick as at Site U1556, and contrasts between these closely spaced sites will allow exploration of the blanketing effect of different sediment thicknesses and basement topography on hydrothermal circulation.

9.2.2. Operations

Site U1557 was first visited during engineering Expedition 390C, with the goal of coring a single APC/XCB hole to basement for gas safety monitoring and installing a reentry system with casing through sediment to ~5 m into basement. After a missed mudline in Hole U1557A, Hole U1557B penetrated to 574.0 mbsf, contacting basement at 564.0 mbsf, with an overall recovery of 414.94 m of sediment as well as the sediment/basement interface (72%). In Hole U1557C, a jet-in test determined that we would not be able to jet in the Dril-Quip reentry system and five joints of 16 inch casing prior to drilling a 10¾ inch casing string into basement. Instead, the reentry system and 16 inch casing was drilled in to Hole U1557D. The casing could not be extended during Expedition 390C because of a subsea camera system failure; Expedition 395E returned to the site, installing casing to 571.6 mbsf with the hole reaching 576.6 mbsf (Table T1).

Expedition 390 arrived at Site U1557 on 12 May 2022 after moving over from Site U1556 in dynamic positioning (DP) mode. We reentered Hole U1557D with the bottom-hole assembly (BHA) for RCB coring and began operations. Core 390-U1557D-2R was the first recovered core in this hole following the two drilled intervals completed during Expeditions 390C and 395E. Coring continued smoothly through Core 8R; Core 9R had advanced only 1 m when we had to pull out of the hole to wait on weather. After 1.5 days waiting on weather, we continued coring from 637.1 mbsf, with Core 10R. Core 14R was the final core for the site and advanced to 684.7 mbsf; after its recovery, we began tripping out of the hole to drop the bit on the seafloor and reenter the hole for logging. Excluding Cores 2R, 3R, and 9R, all cores were full length. A mud sweep was pumped after every core following Core 5R. Penetration rates were <2.5 m/h throughout the hole. In total, coring in Hole U1557D during Expedition 390 advanced 109.1 m and recovered 71.28 m (65%; Table T2; Figure F12).

After dropping the bit on the seafloor using the mechanical bit release, we reentered the hole to log with the triple combo tool string. The string included tools for measuring NGR, borehole diameter, formation density, resistivity, and magnetic susceptibility. Two upward passes covering the basement section of the hole were completed and then the sediment section of the hole was logged through casing while the tools were pulled back to surface. The logging tools were recovered, and we departed Site U1557 to transit to Site U1559. Operations time at Site U1557 totaled 7.6 days during Expedition 390.

9.2.3. Principal results

During Expedition 390, the science party described APC/XCB cored material as well as the sediment/basement interface from Holes U1557A and U1557B, collected during Expedition 390C. Expedition 390 additionally cored 109.1 m of basement in Hole U1557D. Both sediment and basement results are summarized here.

9.2.3.1. Stratigraphic unit summary

The cores recovered at Site U1557 comprise two sedimentary units overlying a single basement unit, identified on the basis of macro- and microscopic visual observations combined with mineralogical analyses by XRD, color reflectance, and magnetic susceptibility data. The units are numbered from the top of the hole, with units in the sedimentary section designated by Roman numerals and basement units designated by Arabic numerals; subunits are designated with letters. The sediment/basement interface was recovered at 564.8 mbsf in Hole U1557B; installation of casing into basement in Hole U1557D prevented recovery of the interval in that hole. The interface was therefore defined as the shallowest recovered occurrence of basalt in Hole U1557B.

9.2.3.2. Sedimentology

The sedimentary column at Site U1557 is composed of two units: alternating silty clays and nannofossil ooze (Unit I; Eocene–Holocene; ~290 m thick) laying over nannofossil/calcareous chalk deposits (Unit II; Paleocene–Eocene; ~275 m thick; Figure F13). The contact between Units I and II is marked by the first substantial (>25 m thick) deposit of siliciclastic sediments (dark brown silty clays) at the Eocene–Oligocene transition. The color of the sediment primarily reflects its lithologic characteristics; sediments composed mainly of nannofossil ooze/chalk are generally pinkish white or light gray, whereas silty clays range from brown/dark brown where carbonate is absent to reddish brown where the carbonate content is higher. In addition to the major lithologies (nannofossil ooze/chalk and silty clay), several minor local sedimentological features are observed, including greenish white foraminifera-rich layers/lenses (especially at the contact between silty clays and nannofossil ooze intervals), microstructural deformation (faulting and folding), and a unique clay-bearing layer (<0.8 m thick; identified as the PETM interval; Figure F21) in the long sequence of nannofossil chalk of Unit II.

9.2.3.3. Sediment biostratigraphy

The ~564.8 m thick sedimentary succession of pelagic ooze, chalk, and clay in Hole U1557B ranges in age from Pleistocene to middle Paleocene. Planktic and benthic foraminifera and calcareous nannoplankton are present in varying abundance in the oozes and chinks but are mostly absent from the clays (Figure F14). Preservation and abundance of calcareous nannoplankton and planktic foraminifera are better in the Paleocene and Eocene than in the Oligocene and Neogene. Sedimentation is continuous from the early Oligocene to Pleistocene (Figure F15). A 12.94 m thick condensed interval or hiatus composed of dark brown pelagic clay and spanning the middle Eocene to early Oligocene occurs in Cores 390C-U1557B-29X through 31X. Below this hiatus/condensed interval, sedimentation again appears to be continuous, although there are significant gaps in core recovery and some evidence for reworking in the early Eocene. We interpret a prominent reddish brown clay in Core 50X to represent the PETM based on the occurrence of the calcareous nannofossil genus *Rhombaster*, which is characteristic of the PETM interval, as well as sedimentological and physical properties data indicating a significant drop in carbonate content (Figure F21). These observations are strong evidence that a complete PETM section was recovered in Section 50X-3. Below this hyperthermal event, continuous sedimentation is observed through to the sediment/basement interface. A sample taken directly above basement (Sample 63X-2, 78–80 cm; 564.15–564.17 m CSF-B) was assigned to planktic foraminifera Zone P4a (between 60.54 and 60.76 Ma) and calcareous nannofossil Zones NP5/CNP7 (between 60.76 and 61.27 Ma), both of which are in good agreement with the projected crustal age of ~60.7 Ma at Site U1557. No samples were analyzed from the limestone-basalt breccia that characterizes the transition from pelagic sediment to basement.

9.2.3.4. Sediment paleomagnetism

The sediment package at Site U1557 was cored in Holes U1557A and U1557B during engineering Expedition 390C, during which most cores were split, and remanence measurements were made using the SRM. The NRM of core sections was measured prior to applying three AF steps (5, 10,

and 20 mT), where the remanence was measured after each step. Measurements were made at 2 cm intervals. Because the working halves of Site U1557 cores were not on the ship during Expedition 390, no discrete samples were taken from the majority of the sediment sequence. The sediment/basement interface cores from Hole U1557B were split and analyzed during Expedition 390, with the archive halves run on the SRM and two discrete samples collected from the interface.

Measured inclinations for Hole U1557B cluster around -52.2° and 49.8° . The inclinations for Hole U1557A are slightly shallower (but within error) than the inclination expected for this latitude for a geocentric axial dipole (GAD; $\pm 49.1^\circ$ at 30°S), whereas those for Hole U1557B are in good agreement with GAD inclination. For all sites, magnetic susceptibility and intensity correlate well with lithologic variations—high values correspond to the silty clays and lower values correspond to the biogenic carbonates. The remanence intensities for the sediment packages at Site U1557 are relatively strong for pelagic material. Throughout Lithologic Units I and II in Hole U1557B, intensity averages are on the order of 10^{-2} A/m for both the NRM and 20 mT intensity. Unit I intensities are roughly twice what they are for Unit II. Three intervals of normal polarity are identified in Core 390C-U1557A-1H that we correlate to the Brunhes, Jaramillo, and Cobb Mountain chrons, respectively. Similar normal polarity intervals are also identified in the uppermost cores of Hole U1557B. Unfortunately, the depth of the Brunhes/Matuyama chron boundary in Hole U1557B is only an estimate because the sediment interval that contained the transition from normal to reversed polarity was not recovered.

A smooth demagnetization curve and an interpretable OVP were observed for the lithified sediment sample from the sediment/basement interface, whereas the nonlithified sediment returned

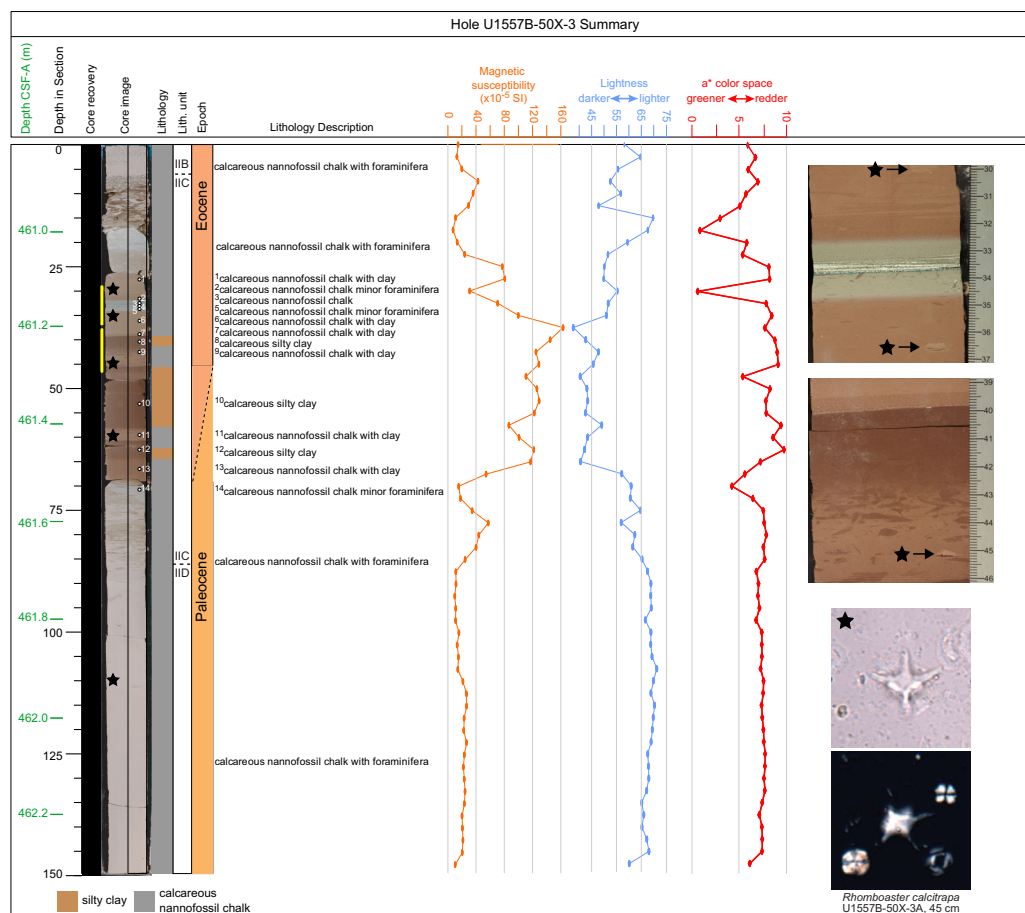


Figure F21. Summary of changes in 390-U1557B-50X-3, inferred to contain sediments deposited during PETM. Stars = locations of samples for nannofossil analyses, 1–14 = levels of closely spaced lithologic descriptions, yellow = two stratigraphic levels where close-up images are provided on right side of figure. Magnetic susceptibility is from point source. Photomicrographs show *Rhomboaster calcitrapa* under (top) plane-polarized and (bottom) cross-polarized light.

spurious results. The magnetic field direction of the lithified discrete sediment sample (inclination of $\sim 37^\circ$, declination of $\sim 128^\circ$) calculated from the ChRM using principal component analysis (PCA) between 30 and 60 mT is lower than that expected for a GAD at this latitude (30°S). This result cannot be accounted for by magnetic secular variation and is likely due to inclination shallowing because of compaction by the overlying sediment column. Analysis of further discrete samples should help elucidate this inclination discrepancy. The median destructive field (MDF) and coercivity spectra for this sample suggest a magnetite-like phase is the dominant magnetic carrier.

9.2.3.5. Sediment age model and mass accumulation rate

The most obvious feature of the age model for Site U1557 is a large hiatus or condensed interval spanning the early Oligocene to middle Eocene. This interval also separates the relatively low sedimentation rates of the Holocene to the Oligocene with the high sedimentation rates of the Eocene and Paleocene. Sedimentation rates average 0.77 cm/ky in Unit I (except in the condensed interval, Subunit IE, which has a sedimentation rate of 0.17 cm/ky and would bring the overall Unit I average down to 0.57 cm/ky) and 2.24 cm/ky in Unit II (Figure F15). The highest sedimentation rate (11.53 cm/ky) occurs in the late Paleocene of Unit II. Mass accumulation rates at Site U1557 are primarily driven by carbonate accumulation, with periods of CCD shoaling resulting in less carbonate dilution of eolian dust flux. A surprising result at Site U1557 is the elevated organic carbon content. Total organic carbon (TOC) values as high as 3 wt% are generally not expected in a mid-latitude gyre setting, and the organic carbon accumulation rate suggests that the Paleocene and Eocene were characterized by high organic carbon production and preservation, with a peak near 0.1 g/cm²/ky. The general correspondence of high organic carbon accumulation rates with high carbon accumulation rates indicates overall high productivity in surface waters during this time interval.

9.2.3.6. Sediment physical properties and downhole measurements

Physical properties characterization of the sediment section at Site U1557 is based on cores and in situ downhole measurements from Holes U1557A and U1557B. Whole-round core-based measurements include NGR (sensitive to the abundance of minerals containing radioisotopes of K, U, and Th), bulk density from GRA, MS (an indicator of the abundance of magnetic minerals), and *P*-wave velocity. Trends in the physical properties recorded downhole in Hole U1557B correlate with lithologic units.

NGR values in Unit I show high-frequency variability between 7 and 50 counts/s reflecting the alternating carbonate and silty clay layers (Figure F13). In contrast, Unit II is characterized by uniformly lower NGR, with a mean of 6 counts/s. Similar trends are present in MS data, which alternate between ~ 40 – 50 and 100 – 150 IU in Unit I and are generally below ~ 50 IU and less variable in Unit II, reflecting the more uniform, carbonate chalk-dominated lithology (Figure F13). In Unit II, concomitant abrupt increases in NGR and MS suggest short-lived possible carbonate dissolution events, likely associated with shoaling of the CCD at the time of deposition of these sediments. Bulk density and *P*-wave velocity generally increase with depth in the sedimentary section, which is consistent with carbonate lithologies being denser than the silty clays and an overall compaction trend.

Data from cores recovered using the APC/XCB system in Holes U1557A and U1557B are correlated based on changes in bulk density, MS, NGR and luminosity (L^*) data. The lack of correspondence in the physical properties between Cores 390C-U1557A-1H and 390C-U1557B-1H, suggests at least 4.1 m is missing from the top of Core 390C-U1557A-1H, which was a missed mudline core. A shipboard splice for the upper 15 m CCSF at Site U1557 is produced with a small splice gap between the bottom of Core 390C-U1557B-1H and the top of Core 390C-U1557A-1H.

Three downhole temperature measurements were made in Hole U1557B using the APCT-3 tool, and a geothermal gradient of $34^\circ\text{C}/\text{km}$ is calculated, similar to the reported upper range at Site U1556. A total of 60 thermal conductivity measurements yield an average of 1.4 ± 0.25 W/(m·K) with a discernible downhole increase to 1.6 W/(m·K) near the sediment/basement interface. Using temperature and thermal conductivity measurements, a heat flow of 48 W/m² for Hole U1557B is calculated.

9.2.3.7. Sediment geochemistry

Approximately 565 m of sediment was cored in Hole U1557B during Expedition 390C, with head-space gas and IW whole rounds taken once per core. A total of 61 IW samples were squeezed under a laboratory atmosphere. During Expedition 390C, shipboard IW analyses included pH, salinity, alkalinity, major cations and anions (sodium, calcium, magnesium, potassium, chloride, and sulfate) using IC, major and minor elements using ICP-AES, and nutrients (phosphate and ammonium). Carbonate and TOC were then analyzed on the squeeze cakes. Depth profiles of redox-sensitive elements in Hole U1557B suggest dissolved oxygen depletion in the upper ~100 m. We observed decreasing sulfate concentrations, a dissolved Mn peak, and increasing ammonium associated with organic carbon decay. Increasing sulfate concentrations combined with Mn concentrations near the limit of detection below 280 mbsf may suggest input of oxygenated fluids from basement (Figure F16). A sharp change in measured alkalinity, as well as calcium, magnesium, boron, and lithium concentrations near the bottom of the hole (~540 mbsf) could also be associated with basement fluid flow. Elevated dissolved Si concentrations at ~3 and ~150 mbsf may be indicative of biogenic silica dissolution at those depths.

9.2.3.8. Basement igneous petrology

Two holes at Site U1557 recovered basement rocks in the form of sedimentary breccia (Figure F17). In Hole U1557B, 9.5 m of sedimentary breccia was cored after basement was reached at 564.8 mbsf. Expedition 390 cored 109.1 m of basement in Hole U1557D, recovering sedimentary breccia throughout the cored interval of the hole. The breccia consists of a range of basaltic clast types derived predominantly from pillow lavas. The clasts are all moderately to highly altered, obscuring many aspects of primary igneous lithology. Therefore, for the purposes of macroscopic core description, we have distinguished between altered glass and basalts (cryptocrystalline to microcrystalline) and grouped the basalts into three categories based on color that broadly reflect different degrees of alteration: gray, brown, and orange. In general, gray basalts are the least altered and most diverse lithologically; they range from cryptocrystalline to microcrystalline and from aphyric to highly plagioclase-olivine-clinopyroxene phyric, although aphyric is most common. Brown and orange basalts are typically aphyric to sparsely plagioclase or olivine phyric. In addition, orange basalts are associated with textures indicative of an origin in a pillow chilled margin. With few exceptions, basaltic glass is completely altered throughout the core. Although some variation in clast lithology is observed downhole, systematic variations were not identified, and the entire sequence of rocks recovered has been defined as a single lithologic unit. It has been divided into three lithologic subunits based on variations in breccia matrix and cement.

9.2.3.9. Basement metamorphic and alteration petrology

Alteration of the breccias at Site U1557 is variable, with evidence of alteration prior to brecciation and redeposition, as well as overprinting alteration in the breccia pile itself. The overall range of alteration is very similar in color, extent, and mineralogy to what was observed at Site U1556 ~6.5 km away, with the major difference at Site U1557 being that clasts of variable alteration have been fragmented and juxtaposed in a breccia where they are further altered in situ (Figure F18). Veins are rare, with only ~300 logged and just under 50 occurrences of vesicles recorded in total. Most of the logged mineral fill consists of breccia cements. The interclast space of the breccias is filled by pelagic sediment, fine grained igneous material (glass and basalt), carbonate, and/or authigenic zeolite “sediment,” with open porosity common throughout much of the hole. The volume proportion of porosity and cement decreases downhole.

9.2.3.10. Basement paleomagnetism

Progressive AF demagnetization of basement split-core sections and discrete samples are used to characterize the paleomagnetic signal and resolve the magnetization components recorded in Site U1557 cores. The NRM of core sections was measured at 2 cm intervals on the SRM. Three AF steps (5, 10, and 20 mT) were applied, and the remanence was measured after each step. Discrete sampling was accomplished for Hole U1557D with 13 discrete cubes (8 cm³) collected across the 14 recovered cores from sufficiently big clasts that displayed diverse grades of alteration. Here, we use these data to primarily characterize the magnetic mineral assemblage. AMS was measured on all collected discrete samples to characterize the fabric. Acquisition of IRM and backfield IRM experiments were performed on two representative discrete samples.

Histograms of the inclinations measured on the SRM suggest that the inclinations in Hole U1557D sweep the full spectrum of values from -90° to 90° and cluster around 7° . This is much shallower than the inclination expected for this latitude for a GAD ($\pm 49.1^{\circ}$ at 30° S). This large departure from that GAD inclination is likely a function of sampling the large clasts from the sedimentary breccia, which should produce randomly oriented directions if the ChRM was blocked before clast emplacement. Every discrete breccia sample displayed stable demagnetization data of a single component that describes a straight line to the origin, which defines the ChRM. Inclinations from the calculated ChRM directions verify the inclinations measured from the SRM. Additionally, all discrete samples gave maximum angular deviation angles $<15^{\circ}$. IRM and backfield IRM experiments illustrate the “softness” of the ferromagnetic assemblage. The coercivity of remanence (B_{cr}) values are around 20 mT, the S ratios are equal to 1, and the $SRM_{100}/SIRM$ ratios are 0.99 and 1, respectively, in the two studied samples. These values are indicative of the presence of soft ferromagnetic phases as remanence carriers likely dominated by either titanomagnetite or titanomaghemite. AMS indicated the presence of both oblate (planar) and prolate (linear) ellipsoids with no consistent directions or particular distribution along the basement rock package.

The “conglomerate test” was employed to test whether the clasts’ ChRM was blocked prior to their emplacement in the sedimentary breccia or reset at a later stage. ChRM directions plot randomly about the stereonet, indicating the conglomerate test was passed and that the ChRM of the clasts has been stable since before their incorporation in the clastic rock. However, the soft nature of the ferromagnetic assemblage suggests that the actual measured components may represent an earlier remagnetization, resulting from alteration (maghemitization) of the original magnetic component on the parent rocks. This result likely means no secondary alteration events that affected magnetization took place between clast emplacement and core retrieval.

9.2.3.11. Basement physical properties and downhole measurements

Basement physical properties were determined primarily from cores and downhole logging data from Hole U1557D, with additional information from the deepest cores from Hole U1557B, which extended several meters into basement. Measurements on whole-round and split half sections were compared with downhole measurements from Hole U1557D for lithostratigraphic characterization and integration of core description and borehole data. In addition to the standard whole-round and discrete measurements, high-resolution 3-D exterior images were also taken from ~ 70 m of hard rock whole-round cores using the DMT core scanner.

In the basement interval of Site U1557, NGR, MS, and GRA bulk density from core data show no obvious trends with depth in basement. NGR ranges from 0 to ~ 30 counts/s, MS ranges from 0 to 800 IU, and GRA clusters around ~ 2.5 g/cm³. Bulk density, porosity, and P -wave velocity from discrete samples show good agreement with the alteration described for the basalt clasts in the breccia. Additionally, discrete samples show the breccia matrix porosity increases with depth, whereas the P -wave velocity of the matrix samples decreases with depth. Electrical resistivity from wireline logging is sensitive to formation porosity and qualitatively agrees with the trends seen in the discrete samples. Thermal conductivity in basement cores ranges from 1.1 to 1.8 W/(m·K) and qualitatively appears to decrease with depth in agreement with the discrete sample porosity and wireline resistivity data.

9.2.3.12. Basement geochemistry

For the Hole U1557B and U1557D basement cored during Expeditions 390C and 390, respectively, representative samples were taken from the least macroscopically altered basaltic clasts in the sedimentary breccia to obtain a downhole record of the primary magmatic compositions. Lithology of clasts includes aphyric basalt, yellow-brown phyric basalt, and equigranular basalt. Additional basalt samples with different styles of alteration were chosen to investigate alteration effects on elemental abundances. A total of 20 samples were selected from Hole U1557D and 1 sample was taken from Hole U1557B for LOI and bulk rock geochemical analysis using ICP-AES. LOI varies between 0.09 and ~ 3.85 wt%, with higher LOI in Hole U1557D samples indicating more alteration. Because of the high degree of alteration, traditional classification methods, such as total alkalis versus silica, cannot be applied. Based on high field strength element ratios (e.g., Zr/TiO₂; Figure F18), the rocks can be classified as N-MORBs. Alteration leads to enrichment in some transition

metals (e.g., TiO_2 , Fe_2O_3 , Sc, and V) and large-ion lithophile elements (e.g., Na_2O , K_2O , and Ba) with lower MgO concentrations.

9.2.3.13. Basement microbiology

Microbiology sampling in basement at Site U1557 during Expedition 390 was focused on exploring evidence for life in basement using microscopy, culture-based approaches, and culture-independent approaches. No microbiology samples were collected from Hole U1557B, which was drilled during Expedition 390C, because there were no scientists on the ship to process the ephemeral microbiology samples. For Hole U1557D, sampling efforts were focused on collecting a single whole-round core sample from each 9.5 m advance that would be processed and subsampled for different analyses. The aim was to generate a suite of samples that were representative of the different rock types and alteration styles that compose the basement stratigraphy of the site. In total, 12 whole-round samples (8–15 cm long) were collected for microbiological analysis. The lithology of all samples collected was sedimentary breccia.

A total of 12 samples were processed for cell counts, shore-based DNA (polymerase chain reaction [PCR] amplicon-based and metagenomes), and/or RNA (PCR amplicon-based and/or metatranscriptomes) analyses; 8 samples were preserved for single cell genomics; and 7 samples were collected for lipid analysis. Microbial isolation experiments using enrichment media in petri dishes were initiated for Samples 390-U1557D-5R-5, 37.5–48.5 cm, and 7R-3, 0–9.5 cm, on petri dishes with 1/10 ZoBell Marine Agar media. This media selects for heterotrophic marine microorganisms and is commonly used to isolate new microorganisms. Samples 6R-3, 39–49 cm, and 8R-3, 52–63 cm, were used to initiate stable isotope probing (SIP) experiments to determine proportions of the microbial community that use specific carbon and nitrogen compounds. Three samples of drill fluid were collected from a pipe on the rig floor during coring operations in Hole U1557D: during coring of Cores 2R (586 mbsf), 11R (645 mbsf), and 14R (676 mbsf). Samples were collected for cell counts and shore-based molecular biology analysis to determine the microorganisms present in drilling fluid.

9.3. Site U1561

9.3.1. Background and objectives

Site U1561 is in the western South Atlantic Ocean ~1250 km west of the MAR at a depth of ~5000 mbsl. Site U1561 was only occupied during engineering Expedition 395E, during which the sediment succession and uppermost <5 m of basement were cored with the APC/XCB system (Hole U1561A), but the sediment and sediment/basement interface acquired enhances petrologic, paleoceanographic, and chemical investigations as part of the SAT. Site U1561 is located 24 km north of Site U1556. The basement at Sites U1556 and U1561 is predicted to have formed at ~61.2 Ma at a half spreading rate of ~13.5 mm/y. Oceanic crust at these sites is the oldest that was drilled during the SAT expeditions. The mineralogy and extent of alteration of the basement rocks at Site U1561 and changes in physical properties such as porosity will be compared to the same characteristics at the other sites along the transect to investigate the development of hydrothermal circulation and the crustal aging of the upper oceanic crust formed at slow to intermediate spreading rate MORs. The sedimentary succession at Site U1561 is substantially thinner than at Sites U1556 and U1557 and will provide information on sediment accumulation patterns and pore water chemical profiles of this local area. Contrasts between these closely spaced sites will allow exploration of the blanketing effect of different sediment thicknesses on hydrothermal circulation. Basement topography between the sites may also affect circulation; Site U1561 appears to sit on a local high.

9.3.2. Operations

Site U1561 was visited during Expedition 395E. Following reentry system installation at Site U1556 and the extension of casing into basement at Site U1557, the remaining 2.5 days of operations time was used to core a single hole at an alternate SAT site on ~61 Ma crust. Holes U1561B and U1561C were missed mudline cores, where seafloor depth was uncertain because of the malfunctioning of the 3.5 kHz precision depth recorder signal and a discrepancy between the reading from the 12.5 kHz signal and what was indicated in the *Scientific Prospectus* (Coggon et al., 2020)

as the estimated water depth. These single-core holes were curated as Holes U1561B and U1561C despite being cored before Hole U1561A. Hole U1561A was spudded at 2335 h on 11 May 2021, with Core 395E-U1561A-1H recovering 6.7 m. Core 6H encountered hard rock at 46.2 mbsf, bending the APC cutting shoe. We switched to the XCB system for capturing the sediment/basement interface; however, Core 7X was empty. Cores 8X and 9X advanced to 48.9 mbsf and recovered 2.39 m. Overall, Cores 1H–9X recovered 45.4 m (93%; Table T1).

9.3.3. Principal results

During Expedition 390, the science party described APC/XCB cored material as well as the sediment/basement interface from Holes U1561A–U1561C, collected during Expedition 395E.

9.3.3.1. Stratigraphic unit summary

The cores recovered at Site U1561 compose two sedimentary units overlying a single basement unit, identified on the basis of macro- and microscopic visual observations combined with mineralogical analyses by XRD, color reflectance, and magnetic susceptibility data. The units are numbered from the top of the hole, with units in the sedimentary section designated by Roman numerals and basement units designated by Arabic numerals; subunits are designated with letters. The sediment/basement interface was recovered at 46.5 mbsf in Hole U1561A; the interface is defined as the shallowest recovered occurrence of basalt in the hole, even though drilling parameters indicate a hard layer at 46.2 mbsf that was not recovered.

9.3.3.2. Sedimentology and petrology

In the three holes cored at Site U1561, the sedimentary column consists of two main lithologies and hence units: silty clays and calcareous nannofossil ooze (Figure F13). Unit I is ≤ 24 m thick and composed mainly of reddish brown silty clay with a variable amount of zeolite. Some organic-rich spots occur in Unit I. Unit II (Paleocene–Eocene) is ~ 24 m thick; it is mainly composed of light yellowish calcareous nannofossil ooze and hosts a variable abundance of foraminifera. The boundary between Units I and II is a gradational transition, defined by a reduction in the proportion of siliciclastic material down through a < 75 cm interval. Unit II was only recovered in Hole U1561A. Units I and II contain $< 5\%$ and $> 90\%$ calcite (weight percent), respectively, and differences in mineral assemblages are relatively small with increasing burial depth within the silty clay and ooze lithologies, respectively.

Basalts collected from the sediment/basement interface are aphyric and were emplaced as a pillow lava flow. Analysis by portable X-ray fluorescence (pXRF) suggests that the basalts are chemically similar to the alkali basalts at the top of the basement section of Hole U1556B. Chilled contacts between pillows contain brecciated and altered glass interlaid with pinkish gray to white sediment, which contains fossil foraminifera.

9.3.3.3. Biostratigraphy

Calcareous nannofossil biostratigraphy was performed on core catcher samples with additional toothpick samples taken from the archive halves of split sections from Hole U1561A (collected during Expedition 395E). Site U1561 comprises a ~ 45 m thick sedimentary sequence of pelagic clay and calcareous ooze that is dated to the Paleocene and early Eocene, with the lowermost samples equivalent in age to the oldest assemblages observed at nearby Sites U1556 and U1557. Calcareous nannoplankton are absent from the clays of Unit I but abundant in the ooze that characterizes Unit II and are moderately preserved throughout the carbonate sequence (Figure F14). A hiatus or extremely condensed interval of up to ~ 5 My is recorded between the late Paleocene and earliest Eocene and is also observed at Site U1556 at the westernmost end of the SAT. The sample taken directly above the basement interface at Site U1561 is assigned to Zones NP4/CNP7–CNP6, agreeing with the predicted basal age (~ 61.2 Ma) and correlating to nearby Sites U1556 and U1557. Planktic foraminifera data are not yet available for this site.

9.3.3.4. Paleomagnetism

Paleomagnetic results from Site U1561 include data collected using the SRM. Because only the archive halves were available shipboard during Expedition 390, analyses of discrete sediment samples could not be conducted. During Expedition 395E, the NRM of core sections was measured at 2 cm intervals. Three AF steps (5, 10, and 20 mT) were applied, and the remanence was measured

after each step. Paleomagnetic inclinations after the 20 mT demagnetization step are bimodal, reflecting intervals of reversed and normal polarity during sediment deposition, and conform well to the expected GAD for this site latitude (49.1° at 30°S). However, reversed polarity inclinations in selected intervals from Hole U1561A are somewhat steeper than the expected 49.1° inclination. This may reflect steeper inclinations in the interval below 26 m CSF-B that are of uncertain origin, but are perhaps due to drilling disturbances. Basement rocks from Cores 395E-U1561A-8X and 9X consistently provide positive (reversed) inclinations compatible with the GAD field at the site latitude and their expected age of 61.2 Ma in the Selandian (Paleocene) in Chron C26r.

9.3.3.5. Physical properties and downhole measurements

Physical properties characterization of the sediment section at Site U1561 is based primarily on cores from Hole U1561A with additional data provided by one core from Hole U1561B and one core from Hole U1561C. Whole-round core-based measurements include NGR, bulk density from GRA, MS, and *P*-wave velocity. Discrete measurements included MS on split-core section halves and thermal conductivity. Formation temperature was also measured at 35.2 m CSF-B with the APCT-3 tool.

Both NGR and MS exhibit two general downhole trends at Site U1561 (Figure F13). Initially, both are relatively high (~35 counts/s and ~110 IU, respectively) from the seafloor to ~24 m CSF-B. Below ~24 m CSF-B, both NGR and MS are relatively low (~5 counts/s and ~40 IU, respectively) to the sediment/basement interface at ~45 m CSF-B. The trends in NGR and MS are reflective of the dominant lithologies: carbonate ooze from the seafloor to ~24 m CSF-B and silty clay from ~24 m CSF-B to the sediment/basement interface (Figure F13). Bulk density and *P*-wave velocity both increase downhole from ~1.4 g/cm³ and ~1500 m/s, respectively, at the seafloor to ~1.8 g/cm³ and ~1550 m/s, respectively, at the sediment/basement interface.

Stratigraphic correlation was completed using the cores from Hole U1561A and Cores 395E-U1561B-1H and 395E-U1561C-1H to create a splice that is mostly complete, with only 3 small gaps, to ~42 m CCSF and a larger gap between ~42 and ~48 m CCSF.

The one downhole temperature measurement of 8.19°C was used along with a calculated mudline temperature and the thermal conductivity of the cored sediment to estimate conductive heat flow at Site U1561 at 227.56 mW/m². This heat flow is higher than expected, but the calculation from only two temperature data points increases uncertainty.

9.3.3.6. Geochemistry

IW samples were collected at a frequency of one per core in Cores 395E-U1561A-1H through 6H for a total of 7 water samples including the mudline. During Expedition 395E, shipboard IW analyses included pH, salinity, alkalinity, major cations and anions (sodium, calcium, magnesium, potassium, chloride, and sulfate) using IC, major and minor elements using ICP-AES, and nutrients (phosphate and ammonium). Carbonate and TOC were then analyzed on the squeeze cakes. The pore waters at Site U1561 have Br/Cl molar ratios (~1.5 × 10⁻³) that are consistent with seawater. Sodium has a similar shape profile to Br and Cl. Sulfate concentrations decrease from ~29.6 mM in the mudline sample to 26.5 mM in the upper 22 m of sediment and then remain stable through the rest of the sediment column. Dissolved manganese concentrations are low in all samples; dissolved iron is likewise low, but, notably, this site is the only one sampled thus far as part of the SAT where iron was detected at all. Carbonate content varies with lithology, with an average of 0.25 ± 0.06 wt% (±1 standard deviation, *n* = 3) in Unit I (silty clay) and 85.9 ± 4.6 wt% (±1 standard deviation, *n* = 3) in Unit II (calcareous nannofossil ooze or clayey nannofossil ooze).

9.4. Site U1559

9.4.1. Background and objectives

Site U1559 is in the central South Atlantic Ocean, ~130 km west of the MAR in a water depth of ~3050 m. Site U1559 was previously occupied during engineering Expedition 390C, during which the complete sediment succession and uppermost ~2 m of basement were cored with the APC/XCB system in Hole U1559A and a reentry system was installed in Hole U1559B to within ~10 m of basement. The main objectives of revisiting Site U1559 during Expedition 390 were to

(1) core two to three holes with the APC/XCB system to recover the complete sediment succession and sample the sediment/basement interface to collect samples that address the microbiological, geochemical, and paleoceanographic objectives of the SAT expeditions; (2) core 250 m into basement with the RCB system in Hole U1559B to collect material that addresses the petrological, geochemical, and microbiological objectives of the SAT expeditions; and (3) collect wireline geophysical logging data through the basement sections (Figure F12).

The basement at Site U1559 is predicted to have formed at ~6.6 Ma at a half spreading rate of ~17.0 mm/y. This site was selected as the young crustal end-member of the SAT and will be compared to older crustal material cored at sites further west. The mineralogy and extent of alteration of the basement rocks at Site U1559, changes in physical properties such as porosity, and the composition of the microbial communities will be compared to the same characteristics at the other sites along the transect to investigate the development of hydrothermal circulation and the crustal aging of the upper oceanic crust formed at slow to intermediate spreading rate MORs. Additionally, the site is similar in age to Hole 504B in the eastern equatorial Pacific (6.9 Ma) that formed at an intermediate (36 mm/y) half spreading rate and is covered by 275 m of sediment, as well as DSDP Hole 395A and Integrated Ocean Drilling Program Sites U1382 and U1383 in the North Atlantic (8.1 Ma) that formed at a slow (~17 mm/y) half spreading rate. As such, material from Site U1559 will allow comparison of how alteration progresses at different spreading centers and with different thicknesses of overlying sediment and sedimentation histories. Overlying sediment from Site U1559 is primarily carbonate ooze and will be used in paleoceanographic and microbiological studies.

9.4.2. Operations

Site U1559 was first visited during engineering Expedition 390C, with the goal of coring a single APC/XCB hole to basement for gas safety monitoring and installing a reentry system with casing. These activities were successful, with a single APC/XCB hole (U1559A) cored to 66.2 mbsf, contacting a hard layer at 64.0 mbsf, and a reentry system and casing installed in Hole U1559B to 55.31 mbsf, ~9 m above basement (Table T1).

Hole U1559C is located 30 m south of Hole U1559B and was spudded on 22 May 2022 using the APC/XCB system in a water depth of 3058.0 m. Cores 390-U1559C-1H through 6H advanced to 51.8 mbsf, recovering 52.08 m (100%). Because we expected to penetrate basement in the next core, we transitioned to using the XCB system. Core 7X encountered a hard layer at ~59 mbsf that was assumed to be the sediment/basement contact. However, no basement material was recovered in the core, only 4.82 m of sediment out of the 9.1 m advance (57%). We ended coring in Hole U1559C, and pulled out of the hole to the seafloor at 1545 h, aiming for better recovery of the sediment/basement interface in Hole U1559D. All Hole U1559C APC cores were oriented; APCT-3 tool formation temperature measurements were made while collecting Cores 4H, 5H, and 6H. For Hole U1559D, the vessel was offset 20 m south. Cores 390-U1559D-1H through 6H advanced to 49.9 mbsf and recovered 42.01 m of sediment (84%). During drilling of Core 7X, we contacted a hard layer and recovered some small rubbly pieces of basement. Core 8X advanced 2 m to a final hole depth of 59.4 mbsf and recovered 0.37 m of material (18%). All Hole U1559D APC cores were oriented; perfluorocarbon microbial contamination tracer was pumped during the circulation of drilling fluid. In total, 2.0 days of expedition time was spent coring at Site U1559 (Table T2; Figure F12).

During the pipe trip back to the surface after finishing operations in Hole U1559D, the bearings failed on the forward electromagnetic drawworks brake. The brake was disconnected from the drawworks and isolated. Tripping back to the surface was finished using the single remaining brake. However, it was not possible to continue operations at Site U1559, and the decision was made to end operations for Expedition 390.

9.4.3. Principal results

9.4.3.1. Sedimentology

In the three APC/XCB holes cored at Site U1559 during Expeditions 390C and 390, lithology is composed almost entirely of biogenic deposits of calcareous nannofossil ooze with foraminifera

(Figure F13). Because of the consistent composition, only member-like subunits are defined, and they are numbered from the top of the hole. Subunit definitions are based on relatively small changes in color, sedimentary structures, bioturbation, and general appearance, combined with microscopic examination of smear slides, bulk mineralogical analysis by XRD, and physical properties data including magnetic susceptibility and color reflectance. Subunit IA consists of pale brown calcareous nannofossil ooze with trace siliciclastic material; Subunit IB is similar but has a high foraminifera content (>25% bulk sediment volume). Both date to the Pleistocene. Subunits IC and ID are reversed in age, with Subunit IC consisting of white calcareous nannofossil ooze with foraminifera dating to the early Pliocene and Subunit ID consisting of a very pale brown ooze dating to the late Pliocene. Subunit IE is Messinian to late Pliocene in age and consists of a very pale brown calcareous nannofossil ooze with foraminifera enriched in *Discoaster* sp. Differences in mineral assemblages are relatively small downhole; all samples have a ~95 wt% carbonate composition. Below the sediment/basement interface in Holes U1559A and U1559D, a transitional unit comprises a mix of micritic limestone (lithified ooze) and basalt clasts.

9.4.3.2. Igneous petrology

Igneous basement was recovered in Holes U1559A and U1559D at Site U1559, although recovery of basement material was low. The rocks represent a portion of the sediment/basement interface and include clasts of both basalt and pelagic sediment, some pieces of which preserve contact relationships between the two lithologies. The textural relationship is similar to that seen in breccias from Sites U1556 and U1557 and is consistent with an origin as a sedimentary breccia. However, given the limited recovery at Site U1559, we have not formally ascribed the rocks to such an origin. The basalts recovered are gray (GLEY 1 5/N) and aphyric, although very sparse plagioclase macrocrysts exhibiting sieve textures are observed. Seven samples from Site U1559 were analyzed by pXRF. The data yield $(Zr/Ti)_N$ values (i.e., normalized to N-MORB [Sun and McDonough, 1989]) typical of mid-ocean-ridge basalts (0.97 ± 0.04 ; $n = 7, 1\sigma$).

9.4.3.3. Biostratigraphy, age model, and mass accumulation rate

The 50.95–62.47 m thick sedimentary succession at Site U1559 contains a Holocene to latest Miocene sequence of pelagic ooze. Calcareous nannoplankton and planktic and benthic foraminifera are diverse and abundant throughout, although preservation decreases directly above basement (Figure F14). A coherent late Miocene assemblage in an otherwise late Pleistocene sequence of samples in Holes U1559A and U1559C marks the presence of a 6–8 m thick slump or sequence of slumps in Holes U1559A and U1559C (~8–14 m CSF-B in Hole U1559A and ~6–14 m CSF-B in Hole U1559C). These out-of-place Miocene samples occur in an interval of noticeably lighter colors in the core and a coincident shift in physical properties (particularly *P*-wave velocity) that delimit the full extent of the slump(s) and allow the same interval to be identified in Hole U1559D (~8–14 m CSF-B). The Pleistocene extends well below the slumped interval to roughly 32 m CSF-B in both Holes U1559A and U1559C. Below this level, multiple calcareous nannoplankton and planktic foraminifera datums occur within the same samples, indicating either very slow sedimentation or a series of short unconformities spanning the Pliocene that requires higher sampling resolution postexpedition to confirm.

The sediment/basement interface was recovered in Holes U1559A and U1559D and is inferred in Hole U1559C based on very slow XCB drilling rates, although no basalt was recovered. The depth of basement varies by more than 5 m between these three holes; in the shallower holes, biostratigraphic markers indicate a latest Miocene age of ~6.0 Ma, whereas the deepest hole contains datums that indicate that the sediment/basement interface there must be older than 6.8 Ma (in line with the projected basement age of 6.9 Ma for this site). Sedimentation rates are high (1.97 cm/ky) in the Pleistocene at Site U1559 (and still 1.43 cm/ky when the 6–8 m slump is removed from the calculation). Assuming that the Pliocene is condensed and not truncated by hiatuses, sedimentation rates in the bottom of the hole are around 0.56 cm/ky (Figure F15). Benthic foraminifera indicate gradual subsidence below abyssal depths from the Miocene to the Holocene.

9.4.3.4. Paleomagnetism

Paleomagnetic investigation of Site U1559 sediments included remanence analysis of cores split during engineering Expedition 390C alongside Expedition 390 analyses of the archive halves of Core 390-U1559C-1H through Section 7X-4 and Core 390-U1559D-1H through Section 7X-1.

Discrete sediment samples were taken from Sections 390C-U1559A-8X-2 and 8X-4, as well as from Holes U1559C and U1559D cored during Expedition 390 (26 samples total). These data were used to establish a magnetostratigraphy for the sediment package at Site U1559, which will be refined with additional analysis postexpedition. All discrete sediment cubes were AF demagnetized, in instances up to 190 mT. By demagnetizing samples in a stepwise fashion, we determine the ChRM of the sample, which reflects the magnetic field direction at or soon after sediment deposition and aids in magnetostratigraphic interpretation. Additionally, this demagnetization process helps to characterize, to a first order, the dominant magnetic mineral assemblage. IRM experiments contribute additional background information on the magnetic minerals present, such as coercivity, by “unmixing” the signal and using qualitative relationships between intensities at various field values.

Inclinations after 20 mT demagnetization measured from Holes U1559A, U1559C, and U1559D are bimodal, although histograms indicate significant contributions from inclinations between the two “peaks.” Hole U1559A inclinations cluster around -53° and 43° . Inclinations for Hole U1559C cluster around -41° and 37° and are the shallowest inclinations at this site. Hole U1559D inclinations cluster around -53° and 34° . Except for the two negative modal inclinations in Holes U1559A and U1559D, most of these inclinations are much shallower than that expected for a GAD at this latitude ($\pm 49.1^\circ$ at 30°S). A small number of the discrete sediment samples display noisy OVPs; of the 26 sediment samples, 20 samples had OVPs clean enough to contribute to defining the ChRM. Only 16 of these samples gave maximum angular deviation angles $<15^\circ$, typically considered the cutoff for reliable magnetic field directions.

Because inclination data depicts a clear polarity sequence for most intervals, the magnetostratigraphy for each hole can be confidently determined. Considering the estimated age of the basement (6.6 Ma) and the pattern of the polarity sequence retrieved at Site U1559, which mainly derives from Hole U1559C, a tie to the geomagnetic polarity timescale (GPTS) is proposed. The proposed correlation of the normal polarities at the base of Holes U1559A and U1559C to Miocene Chron C3An is compatible with the crustal age of the basement. Median destructive fields, considered the field at which half of the NRM intensity remains, and IRM up to 1.2 T and backfield IRM experiments suggest that stable single domain or fine pseudosingle domain magnetite/titanomagnetite is the predominant magnetic mineral.

9.4.3.5. Physical properties and downhole measurements

Physical properties characterization of Site U1559 is based on cores and in situ downhole measurements from Holes U1559A, U1559C, and U1559D. Whole-round core-based measurements include NGR, bulk density from GRA, MS, and *P*-wave velocity. Split-core section measurements include point magnetic susceptibility, *P*-wave velocity, MAD, thermal conductivity, and sediment shear and compressional strength.

NGR is relatively low throughout the carbonate-dominated sediments at Site U1559 (Figure F13). MS records high frequency but low amplitude variability, between 1 and 25 IU, reflecting only minor differences in the concentration of magnetic minerals in carbonates from the seafloor to the sediment/basement interface. Bulk density increases from $\sim 1.3\text{--}1.4\text{ g/cm}^3$ at the seafloor to $\sim 1.7\text{--}1.8\text{ g/cm}^3$ at the sediment/basement interface, with punctuated intervals of low bulk density likely a reflection of dislocated slumped sediments or slurries caused by drilling disturbance. *P*-wave velocity corresponds with bulk density, and both are likely associated with porosity changes downhole. Shear strength increases downhole, whereas compressional strength remained relatively constant with depth. Thermal conductivity varies between 1.091 and 1.284 W/(m·K) with no downhole trend, which is expected given the uniformity of the carbonate lithology observed in all three sediment holes. Using downhole temperature and thermal conductivity measurements, a geothermal gradient of 6.3°C/km and a heat flow of 7.73 mW/m^2 through the sediments were calculated. Calculated conductive heat flow is low for 6.6 Ma crust, which may suggest substantial advective heat loss via hydrothermal circulation.

Minor variations in MS and color reflectance data are used to correlate stratigraphy between holes, resulting in an almost continuous spliced record to the sediment/basement interface at 71.4 m CCSE. Three gaps exist in the shipboard splice where core gaps from all three holes coincide.

Proximal to the sediment/basement interface, there is excellent correspondence in the stratigraphy resulting in a robust alignment of the holes.

9.4.3.6. Geochemistry

In addition to a mudline water sample, two whole-round samples per core were collected for IW squeezing and geochemical analyses from Holes U1559A (15 samples) and U1559D (13 samples). Rhizon samples were also taken for postexpedition research at an approximate frequency of one per section prior to core splitting on cores from Holes U1559C and U1559D. No Rhizon samples were taken from intervals with drilling disturbance visible through the core liner. Shipboard analyses of the squeezed IW from Holes U1559A and U1559D include pH, salinity, alkalinity, major cations and anions using IC, major and minor elements using ICP-AES, and nutrients (phosphate and ammonium) using a spectrophotometer. Carbonate and TOC measurements were conducted on squeeze cakes (Holes U1559A and U1559D) and discrete samples from the working half (Holes U1559C and U1559D). IW oxygen was measured in Hole U1559C and U1559D cores using Presens optical oxygen sensors, with a resolution of ~1.5 m. Sulfate concentrations decrease immediately across the sediment/water interface; however, downcore concentrations are highly variable and do not indicate substantial sulfate reduction (Figure F16). Major cation (e.g., Ca, Mg, K, and Sr) concentrations are stable throughout the hole, but Ca and Sr show a gradual decline near the sediment/basement interface that coincides with a Si increase. Sediment carbonate varies between ~86 and ~96 wt%, reflecting the calcareous nannofossil ooze lithology of all three holes, whereas the organic carbon content is low (<0.5 wt%).

9.4.3.7. Microbiology

Sediment microbiological samples were collected from Cores 390-U1559D-1H through 7X. Samples destined for experiments testing physiology were processed in the anaerobic chamber in the walk-in cold room; samples destined for postexpedition cell counts and nucleic acid analysis were processed at room temperature between two KOACH units to mitigate contamination. This dual setup allowed faster sample processing in the collected sediment sections compared to processing time at Site U1556. To test for microbial contamination of whole-round core samples from drilling fluid, we collected sediment samples containing perfluorocarbon tracer PFMD from each microbiology whole round. PFMD analyses demonstrate successful delivery of the tracer to the core exterior and limited penetration of tracer into core interiors, indicating minimal or no contamination during the coring process.

10. Preliminary scientific assessment

The primary operational objective of the SAT expeditions is to drill a transect of sites along a crustal flow line across the western flank of the southern MAR, core the uppermost (150–250 m) ocean crust produced between ~7 and 61 Ma at the slow/intermediate-spreading MAR, and recover complete sections of the overlying sediments. The SAT was designed to target six primary sites on 7, 15, 31, 49, and 61 Ma ocean crust, which will fill critical gaps in our sampling of intact in situ ocean crust with regards to crustal age, spreading rate, and sediment thickness. These sections are required to investigate the hydrothermal evolution of the aging ocean crust, sediment and basement-hosted microbial community variation with increasing substrate age, the paleoceanographic evolution of the South Atlantic Ocean, and the deep-ocean and subtropical gyre responses to changing global climate. Expedition 390 was the first of two scientific SAT expeditions, building on the successful operations of engineering Expeditions 390C and 395E that conducted preliminary sediment coring and installed reentry systems cased to basement at five of the primary SAT sites. The primary operational objective of Expedition 390 was to complete the drilling operations at the oldest (Sites U1556 and U1557) and youngest (Site U1559) sites of the SAT.

The SAT operations on 61 Ma crust were hugely successful, with the entire ~290 m thick sediment succession cored twice at Site U1556 and an expanded (~565 m) succession cored at Site U1557 during Expeditions 390C and 390 (Table T2; Figure F12). These two sites were located close together (6.7 km) in the same fault-bounded localized sedimentary basin to investigate the effects of the significant basement topography and different sediment cover on hydrothermal alteration of the upper crust. The uppermost ~340 and 120 m of basement were cored at Sites U1556 and

U1557, respectively. Hitherto, there were no scientific ocean drilling holes that penetrated >100 m into ocean crust formed between 46 and 100 Ma, despite the discernible conductive heat flow deficit out to 65 Ma crust, globally on average, indicating that there is significant advection of heat from the cooling of the oceanic lithosphere out to this age. Basement cores from Sites U1556 and U1557 therefore provide a 61 My time-integrated record of hydrothermal alteration that will enable us to quantify the magnitude and duration of low-temperature chemical exchange with the overlying oceans and investigate the impact of changing ocean conditions on hydrothermal exchange. At Site U1556, the uppermost basement comprises a volcanic sequence of pillow lavas, massive flows, and hyaloclastite breccias, of which ~340 m was cored (Figures F17, F18). In contrast, at Site U1557 the uppermost ~120 m of basement was found to comprise a basaltic talus breccia consistent with its location in the deeper portion of the localized sedimentary basin adjacent to a fault scarp (Figures F4, F17, F18). Such breccias are likely a common feature of slow-spreading ridge flanks, which are characterized by fault-bounded basement basins like the one in which Hole U1557D is located. Breccias from Site U1557 had significant primary porosity, now partially to completely cemented by carbonate and zeolite.

The sediments collected from Sites U1556 and U1557 during Expeditions 390C and 390, along with a ~45 m section cored to basement at Site U1561 during Expedition 395E and described during Expedition 390, capture key paleoclimate intervals from the Paleocene to the Holocene (Figure F13). The significant basement topography between these closely spaced sites will allow exploration of the effects of water depth and accommodation space on their sedimentation histories and their records of past ocean conditions and currents. A ~15 My unconformity or condensed interval spanning the early Oligocene to early Eocene at Sites U1556 and U1557, at a depth coincident with a seismic reflector identified by Estep et al. (2020) as representing a regional unconformity, limits investigations of that time interval in this area, but its presence and extent raise further research questions about both global and regional conditions at that time.

Expedition 390 also successfully completed sediment operations at the youngest SAT site (U1559), started during Expedition 390C, with three APC/XCB holes cored to basement in total. The sediment/basement interface was recovered in Holes U1559A and U1559D. The unfortunate failure of the forward drawworks electromagnetic brake after APC/XCB coring was completed prevented deeper basement coring in Hole U1559B. However, the uppermost volcanic rocks recovered in the interface (<2 m) were significantly fresher than the volcanic rocks recovered from 61 Ma Sites U1556, U1557, and U1561, offering a tantalizing glimpse of the effects of crustal aging to be revealed when Expedition 393 completes operations at Site U1559 and the intermediate age SAT sites.

Microbiological samples were collected from both sediment and basement in all holes cored during Expedition 390 and were preserved for postexpedition analyses. The high porosity of the 61 Ma basement samples suggests a suitable basement environment for microbes, and sediment chemical profiles of oxygen, manganese, and sulfate concentrations indicate an extended redox gradient that should allow for a diversity of microorganisms and metabolisms.

The operations planned during Expedition 393 will complete the SAT (Figure F12B), allowing integration of results across crustal ages and laterally across the ocean basin. Here, we document progress toward the primary objectives.

10.1. Objective 1. Quantify the timing, duration, and extent of ridge flank hydrothermal fluid-rock exchange.

With the exception of fresh glass from chilled margins, all volcanic rocks recovered from Sites U1556, U1557, and U1561 are slightly to completely altered. Given that all the samples analyzed are affected by alteration to some degree, the immobile element Zr/Ti ratio was used to discriminate between magma types. Zr/Ti ratios reveal three types of basalts were recovered from Site U1556 (61.2 Ma): OIB, N-MORB, and an intermediate composition (Figure F18). Basalt from Site U1561 (61.2 Ma) has OIB-like compositions, whereas only N-MORB composition basalts were recovered from Sites U1557 (61.2 Ma) and U1559 (6.6 Ma).

Our quantitative logging of the variations in the style and extent of alteration of the volcanic rocks recovered at Sites U1556 and U1557 (Figure F18) in conjunction with analyses of cores recovered at other crustal ages along the SAT during Expedition 393 will allow us to evaluate hydrothermal contributions to global biogeochemical cycles. Postexpedition analyses will include radiometric dating of hydrothermal minerals to determine the timing and hence duration of hydrothermal exchange.

Hydrothermal alteration of the lavas was shown to affect their physical properties, using analyses of a suite of discrete samples that were representative of the variations in lithology and styles of alteration observed in Hole U1556, classified by the degree of alteration. This classification scheme revealed a robust relationship whereby porosity increases and *P*-wave velocity decreases with alteration extent (Figure F22). The observed relationships have important implications for improving interpretations of seismic data and using such data to map variations in hydrothermal alteration and model permeability and hence fluid flow on ridge flanks. Paleomagnetic data will also contribute to reconstructing alteration history. A negative inclination is expected in 61 Ma lavas if the ChRM has been preserved. However, analyses of the same suite of discrete lava samples from Hole U1556B revealed a normal polarity (positive inclination) overprint of the ChRM that is most strongly developed in samples of hyaloclastite breccia or samples with the greatest extent of alteration (Figure F19).

Expedition 390 benefited from the addition of two nonstandard imaging systems (Figure F20). The DMT CoreScan3 system, loaned by the International Continental Scientific Drilling Program (ICDP), was used to capture high-resolution images of basement core exteriors prior to cutting. The images collected preserve key information about the orientations of contacts and structures in the core that may be lost because of fracturing during core splitting and can be integrated with wireline borehole images during postexpedition analysis to establish a more complete stratigraphy through intervals of low recovery. These data will also allow development of novel computer visualization approaches for automated quantitative core logging. Samples fragmented as part of the basement microbiological sampling were also imaged using the Foldio turntable system prior to breaking them open with a hammer. This system generates a series of 36 images captured at 10° intervals as a core sample is rotated on a stage and will allow scientists to gain insight into the composition and structure of removed core material (Figure F20).

Sediment IW chemistry reveals ongoing chemical reactions in the sediment and basement, including mineral dissolution or precipitation, diagenesis, microbial metabolisms, and circulation of basement fluid. Concentration profiles with depth suggest fluid flow between the sediment and basement. IW sulfate normalized to chloride ($\text{SO}_4^{2-}/\text{Cl}$) increases toward the basement in Holes U1556A, U1556C, and U1557B, indicating an increase in sulfate below the sulfate reduction zone

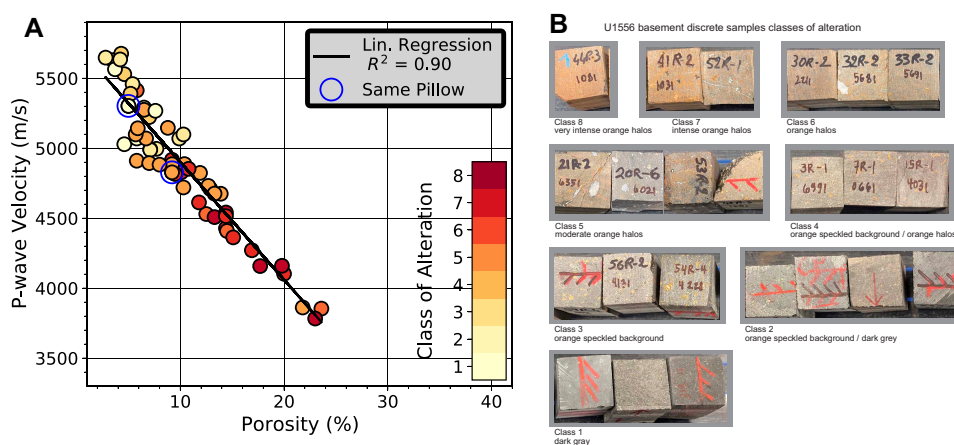


Figure F22. Comparison of porosity, *P*-wave velocity, and alteration for discrete samples of basalt, Site U1556. A. *P*-wave velocity vs. porosity with symbols colored by class of alteration. Blue circles = samples taken from same pillow. B. Selected images of basalt cubes to illustrate different classes of alteration. Class 1 is least altered and Class 8 is most altered. Class descriptions are directly comparable to core alteration description of basement sequence at Site U1556.

detected in the upper portions of the sediment (described further in primary Objective 2; Figure F16). Coincident with this change, the decrease in Ca/Mg toward basement suggests the flow of seawater-derived basement fluid into the basal sediments (Figure F16, where depths have been normalized to sediment thickness to make profiles comparable across sites). The dilute seawater sulfate concentrations ($\text{SO}_4^{2-}/\text{Cl}$), low Mg concentrations (high Ca/Mg), and excess lithium in Hole U1557B suggest an intriguing interaction between those pore fluids and the basement that can be further studied with Sr isotopes and other geochemical tracers.

10.2. Objective 2. Investigate sediment- and basement-hosted microbial community variation with substrate composition and age.

Samples were collected for postexpedition analysis of cell counts, nucleic acid-based analysis of microbial community composition and function, and lipid-based microbial composition throughout the sediment columns in Holes U1556C, U1556E, and U1559D, as well as from basement cores from Holes U1556B and U1557D. In addition, incubation experiments targeting uptake of carbon and nitrogen compounds, sulfate reduction rates, and enrichment of anaerobic Archaea were begun on the ship and will be analyzed during shore-based research. Altogether, the work initiated during Expedition 390 will allow postexpedition work to analyze changes in microbial community abundance, composition, function, and activity from the seafloor to the deepest basement sampled.

Pore water chemical profiles of sulfate normalized to chloride ($\text{SO}_4^{2-}/\text{Cl}$) and of Mn suggest an intriguing overlap of redox zones with implications for active microbial metabolisms. As commonly observed in reducing sediments, the pore water $\text{SO}_4^{2-}/\text{Cl}$ decreases with depth, indicating sulfate consumption. Sulfate is not completely reduced at any of the sites visited during Expedition 390. Increased dissolved Mn, indicative of Mn oxide reduction, typically appears above the sediment depths of maximum depletion of sulfate but also appears below the sulfate reduction zone at Site U1556 (Figure F16). Postexpedition sulfate reduction rate measurements may better characterize the zones of active microbial activity at these sites.

10.3. Objective 3. Investigate the responses of Atlantic Ocean circulation patterns and the Earth's climate system to rapid climate change, including elevated atmospheric CO_2 during the Cenozoic.

The recovery of alternating clay and carbonate intervals in sedimentary units near the top of Sites U1556 and U1557 indicates shoaling and deepening of CCD at these sites from the Oligocene through the Holocene (Figure F13). Planktic foraminifera and calcareous nannoplankton were rare or poorly preserved in pelagic clay intervals (Figure F14), but the abundant, well-preserved microfossils in carbonate intervals supported the construction of robust age models in combination with magnetostratigraphic reversals for all Expedition 390 sites (U1556, U1557, U1561, and U1559; Figure F15). Carbonate dissolution is indicated by high pore water Ca/Mg relative to seawater in the deepwater Holes U1556A, U1556C, and U1557B (Figure F16). This finding partially explains poor preservation of calcareous fossils in some intervals at these sites (Figure F14). Higher resolution biostratigraphic and isotope studies postexpedition will help to refine age models and calculations for mass accumulation rates, carbonate accumulation rates, and organic carbon accumulation rates that will allow us to answer questions regarding ocean productivity and circulation through the Cenozoic.

We recovered a ~0.8 m clay-rich interval that is characteristic of the PETM in Hole U1557B (Figure F21), based on physical properties and sedimentological evidence as well as the presence of diagnostic *Rhomboaster* nannofossils; however, isotope work postexpedition is required to confirm this interpretation. Recovery of the PETM and other Paleogene hyperthermal events will help to address questions regarding Earth's response to rapid intervals of climate change in a particularly expanded Paleogene stratigraphy (~11.5 cm/ky) from Hole U1557B.

10.4. Operational considerations

The SAT objectives were ambitious but achievable owing to the work done during engineering Expeditions 390C and 395E, new developments in drilling capabilities, and the ingenuity of the crew, staff, and scientists. Expeditions 390C and 395E demonstrated that XCB polycrystalline diamond compact (PDC) cutting shoes provide superior recovery of the sediment/basement interface compared to tungsten carbide insert (TCI) cutting shoes, allowing for this critical interval to be sampled multiple times at Sites U1556, U1557, U1561, and U1559. These preliminary engineering expeditions also discovered that the Dril-Quip reentry systems cannot be installed into basement in a single step; when the casing is in basement, weight cannot be removed from the drill string to allow the Dril-Quip release mechanism to operate. To install casing into basement, as planned for the SAT, the hole either needs to be fully drilled out beforehand or a HRT reentry system must be used, which does not allow extension of casing after the initial installation. This finding will aid planning of future expeditions that are considering such installations, which would have cost significant operational time had they been attempted during Expeditions 390 or 393. Having reentry cones with casing installed at five of the six primary SAT sites in advance of Expeditions 390 and 393 expedited basement drilling and allowed for deepening of Hole U1556B beyond the initial target of 250 msb, with ~340 m of basement penetration achieved. Finally, we found that the Transco C-4 RCB drill bits are more durable than drill bits from previous suppliers, allowing for deeper penetration on a single bit and time savings because fewer pipe trips for bit changes are required. The bit brought back to the rig floor and recovered after 61.0 h and 184.6 m of basement drilling in Hole U1556B had minor damage to the TCI insert and a failed bearing seal but was still coring well. We could not inspect the second bit used in this hole because it was dropped at the bottom of the hole after 78.0 h of coring prior to logging. However, up until coring was ended, it was generating good quality core with no sign of a decreasing diameter, which is often the sign of pending bit destruction.

11. Outreach

Expedition 390 had two Onboard Outreach Officers: Marlo Garnsworthy, a nonfiction author/illustrator, photographer, videographer, and science communicator, and Laura Guertin, a university faculty member whose work focuses on increasing student Earth science, information, digital, and geographic literacies. These officers shared the science of the expedition with audiences through ship-to-shore broadcasts, posting on the *JOIDES Resolution* social media channels, authoring entries for the expedition blog, and generating additional education and outreach materials.

11.1. Live broadcasts

Via live video broadcast, the Outreach Officers connected with schools and community groups in nine countries and six languages to share the scientific mission of Expedition 390, a walk-through of the ship, conversations with scientists in the core laboratory and/or geochemistry laboratory, and a question and answer period. The countries included Brazil, China, Germany, Italy, Japan, South Korea, Spain, the United Kingdom, and the United States (13 different states). The school groups ranged from kindergarten classes (students 5 y of age) through graduate school. Class sizes ranged from 11 to 200 students. Special broadcasts were held for museums, university outreach programs, and organizations such as Japan Geoscience Union (JpGU), Pal(a)eoPERCS, Women's Aquatic Network (Champion at Sea Zoom series), the San Diego Geological Society, and the American Helicopter Museum. There was a webinar and tour given from the ship through the National Association of Geoscience Teachers. A special effort was made to recruit community college faculty to sign up for broadcasts. A total of 62 sessions were held, reaching over 2,000 individuals, with one Chinese university admissions event that was live-streamed to an additional 40,000 high school students and family members. Scientist Chris Lowery was additionally featured on a local news broadcast for Fox 7 Austin (<https://www.fox7austin.com/news/ut-researcher-heads-out-on-drill-ship-to-study-earths-past>).

One unique collaboration for the broadcasts was between *JOIDES Resolution* and Media Elementary School in Media, Pennsylvania (USA). The entire school scheduled ship-to-shore sessions for each grade level (K–5), with each grade having a teacher leader that coordinated the curriculum topics with Outreach Officer Guertin. The tours were then customized to match classroom content. Members of the bridge crew, including the Captain, were also part of these sessions. At the conclusion of the expedition, Guertin will be visiting this school as a surprise guest speaker at a school-wide event on the last day of classes. Through this one school 496 students and 23 teachers were reached.

11.2. Social media

The Outreach Officers maintained the ship’s Twitter, Instagram, and Facebook accounts. From 7 April 2022 until the Outreach Officers departed the ship on 4 June, the social media data includes the number of posts, new followers, reactions, and engagements (Table T3). Reactions are defined by how many “likes” each post received, and an engagement is any action on a post that includes reactions, comments, shares, saves, video views, bookmarking, etc. There were 129 posts to Twitter resulting in 4,078 reactions, 10,069 engagements, and 417 new followers. Instagram activity resulted in 3,935 reactions and 7,994 engagements, and Facebook postings yielded 4,623 reactions and 12,271 engagements. The video series generated by Outreach Officer Garnsworthy was also placed on the *JOIDES Resolution* YouTube channel at the end of the expedition.

Outreach Officer Guertin completed several social media “takeovers” and guest postings on the social media pages of other organizations. Each posting described the duties of an Onboard Outreach Officer and included content specific to Expedition 390. There was a 1 day Instagram takeover for the National Marine Educators Association with 3 posts (26 May), a 1 day Twitter takeover for the American Geophysical Union (AGU) Sharing Science program with 14 posts (27 May), and 2 single #GuestGrammer posts to the AGU Instagram account (26 April and 16 May). A full week takeover of the Twitter account for @IAmSciComm was completed with 62 posts (9–14 May).

11.3. Expedition blog

A total of 30 blog posts were written for the *JOIDES Resolution* Expedition 390 web page: 26 by the Outreach Officers and 4 by members of the science party. Blog post topics included comparisons to the voyage of the HMS. *Challenger* 150 y ago, ocean literacy, how science is done at sea, and life on the ship. Eleven of the blog posts featured a video series highlighting a particular part of the expedition. Text-based blog posts included an audio file at the beginning of each post that was a reading of the text on the page to increase the accessibility of the content. Eight of the blog posts were reposted to AGU’s geoscience education blog GeoEd Trek.

11.4. Educational materials

The first blog post for Expedition 390 was a resource page for educators, designed to assist classroom instructors as they prepare their students for ship-to-shore broadcasts. The resource material included a link to several IODP overview and career videos, including the introduction to

Table T3. Summary of social media posts and engagements during Expedition 390.

Week	Twitter				Facebook				Instagram				Broadcasts			
	Posts	New followers	Reactions	Engagement	Posts	New followers	Reactions	Engagement	Posts	New followers	Reactions	Engagement	Events	Institutions	Participants	Number of nations
1	9	28	298	1247	9	31	581	1974	5		472	566	4	4	160	2
2	17	62	438	1180	12	23	482	1100	5	9	427	1356	9	9	360	2
3	15	45	609	2002	13	11	730	1900	9	11	507	1485	10	10	285	2
4	36	36	570	1363	13	10	696	1605	13	9	555	1200	8	6	350	3
5	20	66	664	1589	16	19	855	2301	12	7	509	1299	9	8	480	2
6	16	40	271	1285	10	10	499	1473	7	13	347	634	11	11	497	3
7	12	51	300	892	13	19	569	1710	7	12	390	680	8	8	384	5
8	4	89	192	511	6	19	211	208	5	1	256	208	3	4	132	3

IODP. Additional links were compiled to assist instructors of all grade levels to use existing activities on the *JOIDES Resolution* website, such as an activity that utilizes data from DSDP Leg 3. Five blog posts were designed around data reported in the *JOIDES Resolution* Daily Operations Report. Information on cloud cover, ship speed, wind speed and direction, heave, fuel usage, etc. were placed into data tables along with suggested questions and activities for classrooms. For example, two kindergarten classes that connected for ship-to-shore broadcasts were studying clouds. After their broadcast and meeting the bridge crew member that makes the cloud observations each day, the students started doing daily cloud measurements at their school following the information in the blog post so they could carry out the same activity as someone they met on the ship. In collaboration with the Outreach Officer from IODP Expedition 391, active learning worksheets that students could complete during ship-to-shore broadcasts were designed. The template was shared with teachers that signed up for broadcasts during Expedition 390.

Outreach Officer Garnsworthy generated a series of 11 videos telling the story of Expedition 390 and posted under the hashtag #EXP390Story, with the final few videos to be completed post-expedition, and worked on an animated video science explainer (to be completed).

11.5. Media coverage

The Pennsylvania State University (PSU) newswire did a story on “Brandywine’s Nature Narratives writing contest celebrates natural world” (8 May 2022), where there was a broadcast and original expedition-specific haiku featured as the keynote for the writing contest virtual awards ceremony given by one of the Outreach Officers. The PSU newswire also highlighted the Science at Sea keynote given from *JOIDES Resolution* by an Outreach Officer in “Brandywine hosts local students for exploration of STEM careers” (12 May). The National Marine Educators Association (NMEA) featured “My journey as a JR Onboard Outreach Officer – Laura Guertin” (24 May) on their News & Events page. The Institution IES Delicias (Valladolid, Spain) published an article after their ship-to-shore broadcast, “Videoconferencia <<Joides Resolution>>” (16 May).

11.6. Continuing dissemination

Outreach Officer Garnsworthy is currently producing educational material for students of all ages and the general public, including an animated video with a script written by Co-Chief Scientist Rosalind Coggon. Garnsworthy also conducted research for a book about scientific ocean drilling, IODP, and *JOIDES Resolution*, aimed at upper elementary through early high school. The book proposal and sample chapters will be finished postexpedition. She will continue public and school presentations, with her next one to the American Museum of Natural History in New York, New York (USA) immediately after the expedition.

Outreach Officer Guertin is preparing manuscript submissions for geoscience education outlets, working on a quilt collection that will be displayed for science storytelling about Expedition 390, and submitting scientist profiles for the Scientist Spotlights Initiative database (<https://scien-tistspotlights.org>). She also plans on presenting her Expedition 390 outreach activities at conferences such as the AGU Fall Meeting and/or Ocean Sciences Meeting and to community groups around the Greater Philadelphia region of Pennsylvania (USA). She will continue to maintain contact with the teachers from the tours she gave on the ship.

References

- Alt, J.C., 1995. Subseafloor processes in mid-ocean ridge hydrothermal systems. In Humphris, S.E., Zierenberg, R.A., Mullineaux, L.S., and Thomson, R.E. (Eds.), *Seafloor Hydrothermal Systems: Physical, Chemical, Biological, and Geological Interactions*. Geophysical Monograph, 91: 85–114. <https://doi.org/10.1029/GM091p0085>
- Alt, J.C., and Teagle, D.A.H., 1999. The uptake of carbon during alteration of ocean crust. *Geochimica et Cosmochimica Acta*, 63(10):1527–1535. [https://doi.org/10.1016/S0016-7037\(99\)00123-4](https://doi.org/10.1016/S0016-7037(99)00123-4)
- Andrén, T., Jørgensen, B.B., Cotterill, C., Green, S., Andrén, E., Ash, J., Bauersachs, T., Cragg, B., Fanget, A.-S., Fehr, A., Granoszewski, W., Groeneveld, J., Hardisty, D., Herrero-Bervera, E., Hyttinen, O., Jensen, J.B., Johnson, S., Kenzler, M., Kotilainen, A., Kotthoff, U., Marshall, I.P.G., Martin, E., Obrochta, S., Passchier, S., Quintana Krupinski, N., Riedinger, N., Slomp, C., Snowball, I., Stepanova, A., Strano, S., Torti, A., Warnock, J., Xiao, N., and Zhang, R., 2015. Expedition 347 summary. In Andrén, T., Jørgensen, B.B., Cotterill, C., Green, S., and the Expedition 347 Sci-

- entists, Proceedings of the Integrated Ocean Drilling Program, 347: College Station, TX (Integrated Ocean Drilling Program). <https://doi.org/10.2204/iodp.proc.347.101.2015>
- Antonelli, M.A., Pester, N.J., Brown, S.T., and DePaolo, D.J., 2017. Effect of paleoseawater composition on hydrothermal exchange in midocean ridges. Proceedings of the National Academy of Sciences of the United States of America, 114(47):12413–12418. <https://doi.org/10.1073/pnas.1709145114>
- Bach, W., and Edwards, K.J., 2003. Iron and sulfide oxidation within the basaltic ocean crust; implications for chemolithoautotrophic microbial biomass production. *Geochimica et Cosmochimica Acta*, 67(20):3871–3887. [https://doi.org/10.1016/S0016-7037\(03\)00304-1](https://doi.org/10.1016/S0016-7037(03)00304-1)
- Barker, P.F., and Thomas, E., 2004. Origin, signature and palaeoclimatic influence of the Antarctic Circumpolar Current. *Earth-Science Reviews*, 66(1–2):143–162. <https://doi.org/10.1016/j.earscirev.2003.10.003>
- Barrera, E., Savin, S.M., Thomas, E., and Jones, C.E., 1997. Evidence for thermohaline-circulation reversals controlled by sea-level change in the latest Cretaceous. *Geology*, 25(8):715–718. [https://doi.org/10.1130/0091-7613\(1997\)025<0715:EFTCRC>2.3.CO;2](https://doi.org/10.1130/0091-7613(1997)025<0715:EFTCRC>2.3.CO;2)
- Becker, K., Fisher, A.T., and Tsuji, T., 2013. New packer experiments and borehole logs in upper oceanic crust: evidence for ridge-parallel consistency in crustal hydrogeological properties. *Geochemistry, Geophysics, Geosystems*, 14(8):2900–2915. <https://doi.org/10.1002/ggge.20201>
- Berner, R.A., Lasaga, A.C., and Garrels, R.M., 1983. The carbonate-silicate geochemical cycle and its effect on atmospheric carbon dioxide over the past 100 million years. *American Journal of Science*, 283(7):641–683. <https://doi.org/10.2475/ajs.283.7.641>
- Billups, K., 2002. Late Miocene through early Pliocene deep water circulation and climate change viewed from the sub-Antarctic South Atlantic. *Palaeogeography, Palaeoclimatology, Palaeoecology*, 185(3–4):287–307. [https://doi.org/10.1016/S0031-0182\(02\)00340-1](https://doi.org/10.1016/S0031-0182(02)00340-1)
- Bohaty, S.M., Zachos, J.C., Florindo, F., and Delaney, M.L., 2009. Coupled greenhouse warming and deep-sea acidification in the middle Eocene. *Paleoceanography and Paleoclimatology*, 24(2):PA2207. <https://doi.org/10.1029/2008PA001676>
- Borrelli, C., Cramer, B.S., and Katz, M.E., 2014. Bipolar Atlantic deepwater circulation in the middle-late Eocene: effects of Southern Ocean gateway openings. *Paleoceanography and Paleoclimatology*, 29(4):308–327. <https://doi.org/10.1002/2012PA002444>
- Broecker, W.S., 1991. The great ocean conveyor. *Oceanography*, 4(2):79–89. <http://www.jstor.org/stable/43924572>
- Coggon, R.M., Sylvan, J.B., Teagle, D.A.H., Reece, J.S., Christeson, G.L., Estes, E.R., and Williams, T., 2022. Expedition 390/393 Scientific Prospectus Addendum: South Atlantic Transect. International Ocean Discovery Program. <https://doi.org/10.14379/iodp.sp.390393add.2022>
- Coggon, R.M., Christeson, G.L., Sylvan, J.B., Teagle, D.A.H., Estes, E., Williams, T., and Alvarez Zarikian, C.A., 2020. Expedition 390/393 Scientific Prospectus: The South Atlantic Transect. International Ocean Discovery Program. <https://doi.org/10.14379/iodp.sp.390393.2020>
- Coggon, R.M., and Teagle, D.A.H., 2011. Hydrothermal calcium-carbonate veins reveal past ocean chemistry. *TrAC Trends in Analytical Chemistry*, 30(8):1252–1268. <https://doi.org/10.1016/j.trac.2011.02.011>
- Coggon, R.M., Teagle, D.A.H., Cooper, M.J., and Vanko, D.A., 2004. Linking basement carbonate vein compositions to porewater geochemistry across the eastern flank of the Juan de Fuca Ridge, ODP Leg 168. *Earth and Planetary Science Letters*, 219(1–2):111–128. [https://doi.org/10.1016/S0012-821X\(03\)00697-6](https://doi.org/10.1016/S0012-821X(03)00697-6)
- Coggon, R.M., Teagle, D.A.H., Smith-Duque, C.E., Alt, J.C., and Cooper, M.J., 2010. Reconstructing past seawater Mg/Ca and Sr/Ca from mid-ocean ridge flank calcium carbonate veins. *Science*, 327(5969):1114–1117. <https://doi.org/10.1126/science.1182252>
- Coogan, L.A., Parrish, R.R., and Roberts, N.M.W., 2016. Early hydrothermal carbon uptake by the upper oceanic crust: Insight from in situ U-Pb dating. *Geology*, 44(2):147–150. <https://doi.org/10.1130/G37212.1>
- Cramer, B.S., Toggweiler, J.R., Wright, J.D., Katz, M.E., and Miller, K.G., 2009. Ocean overturning since the Late Cretaceous: inferences from a new benthic foraminiferal isotope compilation. *Paleoceanography and Paleoclimatology*, 24(4):PA4216. <https://doi.org/10.1029/2008PA001683>
- Davis, A.C., Bickle, M.J., and Teagle, D.A.H., 2003. Imbalance in the oceanic strontium budget. *Earth and Planetary Science Letters*, 211(1–2):173–187. [https://doi.org/10.1016/S0012-821X\(03\)00191-2](https://doi.org/10.1016/S0012-821X(03)00191-2)
- Devey, C., 2014. SoMARTerm: the Mid-Atlantic Ridge 13–33°S – Cruise No. MSM25 – January 24–March 5, 2013 – Cape Town (South Africa) – Mindelo (Cape Verde). *MARIA S. MERIAN-Berichte*, MSM25(80). https://doi.org/10.2312/cr_msm25
- D’Hondt, S., Inagaki, F., Alvarez Zarikian, C., Abrams, L.J., Dubois, N., Engelhardt, T., Evans, H., Ferdelman, T., Gribsholt, B., Harris, R.N., Hoppie, B.W., Hyun, J.-H., Kallmeyer, J., Kim, J., Lynch, J.E., McKinley, C.C., Mitsunobu, S., Morono, Y., Murray, R.W., Pockalny, R., Sauvage, J., Shimono, T., Shiraishi, F., Smith, D.C., Smith-Duque, C.E., Spivack, A.J., Steinsbu, B.O., Suzuki, Y., Szpak, M., Toffin, L., Uramoto, G., Yamaguchi, Y.T., Zhang, G.-l., Zhang, X.-H., and Ziebis, W., 2015. Presence of oxygen and aerobic communities from sea floor to basement in deep-sea sediments. *Nature Geoscience*, 8(4):299–304. <https://doi.org/10.1038/NGEO2387>
- D’Hondt, S., Pockalny, R., Fulfer, V.M., and Spivack, A.J., 2019. Subseafloor life and its biogeochemical impacts. *Nature Communications*, 10(1):3519. <https://doi.org/10.1038/s41467-019-11450-z>
- Dickens, G.R., Castillo, M.M., and Walker, J.C.G., 1997. A blast of gas in the latest Paleocene: simulating first-order effects of massive dissociation of oceanic methane hydrate. *Geology*, 25(3):259–262. [https://doi.org/10.1130/0091-7613\(1997\)025%3C0259:ABOGIT%3E2.3.CO;2](https://doi.org/10.1130/0091-7613(1997)025%3C0259:ABOGIT%3E2.3.CO;2)
- Engelen, B., Ziegelmueller, K., Wolf, L., Köpke, B., Gittel, A., Cypionka, H., Treude, T., Nakagawa, S., Inagaki, F., Lever, M.A., and Steinsbu, B.O., 2008. Fluids from the oceanic crust support microbial activities within the deep biosphere. *Ge microbiology Journal*, 25(1):56–66. <https://doi.org/10.1080/01490450701829006>

- Estep, J., Reece, R., Kardell, D.A., Christeson, G.L., and Carlson, R.L., 2019. Seismic Layer 2A: evolution and thickness from 0- to 70-Ma crust in the slow-intermediate spreading South Atlantic. *Journal of Geophysical Research: Solid Earth*, 124(8):7633–7651. <https://doi.org/10.1029/2019JB017302>
- Estep, J., Reece, R., Kardell, D.A., Perez, N.D., Christeson, G.L., and Carlson, R.L., 2020. Intraplate deformation of oceanic crust near the Rio Grande Rise in the South Atlantic. *Tectonophysics*, 790:228543. <https://doi.org/10.1016/j.tecto.2020.228543>
- Estes, E.R., Williams, T., Midgley, S., Coggon, R.M., Sylvan, J.B., Christeson, G.L., Teagle, D.A.H., and the Expedition 390C Scientists, 2021. Expedition 390C Preliminary Report: South Atlantic Transect Reentry Systems. International Ocean Discovery Program. <https://doi.org/10.14379/iodp.pr.390C.2021>
- Expedition 301 Scientists, 2005. Expedition 301 summary. In Fisher, A.T., Urabe, T., Klaus, A., and the Expedition 301 Scientists, Proceedings of the Integrated Ocean Drilling Program, 301: College Station, TX (Integrated Ocean Drilling Program Management International, Inc.). <https://doi.org/10.2204/iodp.proc.301.101.2005>
- Expedition 308 Scientists, 2006. Expedition 308 summary. In Flemings, P.B., Behrmann, J.H., John, C.M., and the Expedition 308 Scientists, Proceedings of the Integrated Ocean Drilling Program, 308: College Station, TX (Integrated Ocean Drilling Program Management International, Inc.). <https://doi.org/10.2204/iodp.proc.308.101.2006>
- Expedition 309/312 Scientists, 2006. Expedition 309/312 summary. In Teagle, D.A.H., Alt, J.C., Umino, S., Miyashita, S., Banerjee, N.R., Wilson, D.S., and the Expedition 309/312 Scientists, Proceedings of the Integrated Ocean Drilling Program, 309/312: Washington, DC (Integrated Ocean Drilling Program Management International, Inc.). <https://doi.org/10.2204/iodp.proc.309312.101.2006>
- Expedition 313 Scientists, 2010. Expedition 313 summary. In Mountain, G., Proust, J.-N., McInroy, D., Cotterill, C., and the Expedition 313 Scientists, Proceedings of the Integrated Ocean Drilling Program, 313: Tokyo (Integrated Ocean Drilling Program Management International, Inc.). <https://doi.org/10.2204/iodp.proc.313.101.2010>
- Expedition 325 Scientists, 2011. Expedition 325 summary. In Webster, J.M., Yokoyama, Y., Cotterill, C., and the Expedition 325 Scientists, Proceedings of the Integrated Ocean Drilling Program, 325: Tokyo (Integrated Ocean Drilling Program Management International, Inc.). <https://doi.org/10.2204/iodp.proc.325.101.2011>
- Expedition 327 Scientists, 2011. Expedition 327 summary. In Fisher, A.T., Tsuji, T., Petronotis, K., and the Expedition 327 Scientists, Proceedings of the Integrated Ocean Drilling Program, 327: Tokyo (Integrated Ocean Drilling Program Management International, Inc.). <https://doi.org/10.2204/iodp.proc.327.101.2011>
- Expedition 329 Scientists, 2011. Expedition 329 summary. In D'Hondt, S., Inagaki, F., Alvarez Zarikian, C.A., and the Expedition 329 Scientists, Proceedings of the Integrated Ocean Drilling Program, 329: Tokyo (Integrated Ocean Drilling Program Management International, Inc.). <https://doi.org/10.2204/iodp.proc.329.101.2011>
- Expedition 330 Scientists, 2012. Expedition 330 summary. In Koppers, A.A.P., Yamazaki, T., Geldmacher, J., and the Expedition 330 Scientists, Proceedings of the Integrated Ocean Drilling Program, 330: Tokyo (Integrated Ocean Drilling Program Management International, Inc.). <https://doi.org/10.2204/iodp.proc.330.101.2012>
- Expedition 335 Scientists, 2012. Expedition 335 summary. In Teagle, D.A.H., Ildefonse, B., Blum, P., and the Expedition 335 Scientists, Proceedings of the Integrated Ocean Drilling Program, 335: Tokyo (Integrated Ocean Drilling Program Management International, Inc.). <https://doi.org/10.2204/iodp.proc.335.101.2012>
- Expedition 336 Scientists, 2012. Expedition 336 summary. In Edwards, K.J., Bach, W., Klaus, A., and the Expedition 336 Scientists, Proceedings of the Integrated Ocean Drilling Program, 336: Tokyo (Integrated Ocean Drilling Program Management International, Inc.). <https://doi.org/10.2204/iodp.proc.336.101.2012>
- Frank, T.D., and Arthur, M.A., 1999. Tectonic forcings of Maastrichtian ocean-climate evolution. *Paleoceanography and Paleoclimatology*, 14(2):103–117. <https://doi.org/10.1029/1998PA900017>
- Gillis, K.M., and Coogan, L.A., 2011. Secular variation in carbon uptake into the ocean crust. *Earth and Planetary Science Letters*, 302(3–4):385–392. <https://doi.org/10.1016/j.epsl.2010.12.030>
- Gradstein, F.M., Ogg, J.G., Schmitz, M.D., and Ogg, G.M. (Eds.), 2020. *The Geologic Time Scale 2020*: Amsterdam (Elsevier BV). <https://doi.org/10.1016/C2020-1-02369-3>
- Harris, M., Coggon, R.M., Smith-Duque, C.E., Cooper, M.J., Milton, J.A., and Teagle, D.A.H., 2015. Channelling of hydrothermal fluids during the accretion and evolution of the upper oceanic crust: Sr isotope evidence from ODP Hole 1256D. *Earth and Planetary Science Letters*, 416:56–66. <https://doi.org/10.1016/j.epsl.2015.01.042>
- Harris, M., Coggon, R.M., Teagle, D.A.H., Roberts, N.M.W., and Parrish, R.R., 2014. Laser ablation MC-ICP-MS U/Pb geochronology of ocean basement calcium carbonate veins. Presented at the 2014 American Geophysical Union Fall Meeting, San Francisco, CA, 15–19 December 2014. <https://agu.confex.com/agu/fm14/meetingapp.cgi/Paper/12488>
- Inagaki, F., Nunoura, T., Nakagawa, S., Teske, A., Lever, M., Lauer, A., Suzuki, M., Takai, K., Delwiche, M., Colwell, F.S., Nealson, K.H., Horikoshi, K., D'Hondt, S., and Jørgensen, B.B., 2006. Biogeographical distribution and diversity of microbes in methane hydrate-bearing deep marine sediments on the Pacific Ocean margin. *Proceedings of the National Academy of Sciences of the United States of America*, 103(8):2815–2820. <https://doi.org/10.1073/pnas.0511033103>
- Inagaki, F., and Orphan, V., 2014. Exploration of seafloor life and the biosphere through IODP (2003–2013). In Stein, R., Blackman, Donna K., Inagaki, Fumio, and Larsen, Hans-Christian (Eds.), *A Decade of Science Achieved by the Integrated Ocean Drilling Program (IODP)*. Developments in Marine Geology. R. Stein (Series Ed.), 7: 39–63. <https://doi.org/10.1016/B978-0-444-62617-2.00002-5>
- Jungbluth, S.P., Grote, J., Lin, H.-T., Cowen, J.P., and Rappé, M.S., 2013. Microbial diversity within basement fluids of the sediment-buried Juan de Fuca Ridge flank. *The ISME Journal*, 7(1):161–172. <https://doi.org/10.1038/ismej.2012.73>
- Kallmeyer, J., Pockalny, R., Adhikari, R.R., Smith, D.C., and D'Hondt, S., 2012. Global distribution of microbial abundance and biomass in seafloor sediment. *Proceedings of the National Academy of Sciences of the United States of America*, 109(40):16213–16216. <https://doi.org/10.1073/pnas.1203849109>

- Kardell, D.A., Christeson, G.L., Estep, J.D., Reece, R.S., and Carlson, R.L., 2019. Long-lasting evolution of Layer 2A in the western South Atlantic: evidence for low-temperature hydrothermal circulation in old oceanic crust. *Journal of Geophysical Research: Solid Earth*, 124(3):2252–2273. <https://doi.org/10.1029/2018JB016925>
- Katz, M.E., Cramer, B.S., Toggweiler, J.R., Esmay, G., Liu, C., Miller, K.G., Rosenthal, Y., Wade, B.S., and Wright, J.D., 2011. Impact of Antarctic Circumpolar Current development on late Paleogene ocean structure. *Science*, 332(6033):1076–1079. <https://doi.org/10.1126/science.1202122>
- Kennett, J.P., and Stott, L.D., 1990. Proteus and proto-oceanus: ancestral Paleogene oceans as revealed from Antarctic stable isotopic results; ODP Leg 113. In Barker, P.F., Kennett, J.P., et al., *Proceedings of the Ocean Drilling Program, Scientific Results, 113*: College Station, TX (Ocean Drilling Program), 865–880. <https://doi.org/10.2973/odp.proc.sr.113.188.1990>
- Kennett, J.P., and Stott, L.D., 1991. Abrupt deep-sea warming, palaeoceanographic changes and benthic extinctions at the end of the Palaeocene. *Nature*, 353(6341):225–229. <https://doi.org/10.1038/353225a0>
- Koppers, A., and Coggon, R. (Eds.), 2020. *Exploring Earth by Scientific Ocean Drilling: 2050 Science Framework*: San Diego, CA (UC San Diego Library). <https://doi.org/10.6075/J0W66J9H>
- Lee, M.D., Walworth, N.G., Sylvan, J.B., Edwards, K.J., and Orcutt, B.N., 2015. Microbial communities on seafloor basalts at Dorado Outcrop reflect level of alteration and highlight global lithic clades. *Frontiers in Microbiology*, 6:1470. <https://doi.org/10.3389/fmicb.2015.01470>
- Lever, M.A., Rogers, K.L., Lloyd, K.G., Overmann, J., Schink, B., Thauer, R.K., Hoehler, T.M., and Jørgensen, B.B., 2015. Life under extreme energy limitation: a synthesis of laboratory- and field-based investigations. *FEMS Microbiology Ecology*, 39(5):688–728. <https://doi.org/10.1093/femsre/fuv020>
- Lever, M.A., Rouxel, Olivier, Alt, Jeffrey C., Shimizu, Nobumichi, Ono, Shuhei, Coggon, Rosalind M., Shanks, Wayne C., III, Lapham, Laura, Elvert, Marcus, Prieto-Mollar, Xavier, Hinrichs, Kaiwe-Uwe, Inagaki, Fumio, and Teske, Andreas, 2013. Evidence for microbial carbon and sulfur cycling in deeply buried ridge flank basalt. *Science*, 339(6125):1305–1308. <https://doi.org/10.1126/science.1229240>
- Lomstein, B.A., Langerhuus, A.T., D'Hondt, S., Jørgensen, B.B., and Spivack, A.J., 2012. Endospore abundance, microbial growth and necromass turnover in deep sub-seafloor sediment. *Nature*, 484(7392):101–104. <https://doi.org/10.1038/nature10905>
- Mallows, C., and Searle, R.C., 2012. A geophysical study of oceanic core complexes and surrounding terrain, Mid-Atlantic Ridge 13°N–14°N. *Geochemistry, Geophysics, Geosystems*, 13(6):Q0AG08. <https://doi.org/10.1029/2012GC004075>
- Marieni, C., Henstock, T.J., and Teagle, D.A.H., 2013. Geological storage of CO₂ within the oceanic crust by gravitational trapping. *Geophysical Research Letters*, 40(23):6219–6224. <https://doi.org/10.1002/2013GL058220>
- Mason, O.U., Nakagawa, T., Rosner, M., Van Nostrand, J.D., Zhou, J., Maruyama, A., Fisk, M.R., and Giovannoni, S.J., 2010. First investigation of the microbiology of the deepest layer of ocean crust. *PLoS One*, 5(11):e15399. <https://doi.org/10.1371/journal.pone.0015399>
- Matter, J.M., Stute, M., Snæbjörnsdóttir, S.Ó., Oelkers, E.H., Gislason, S.R., Aradottir, E.S., Sigfusson, B., Gunnarsson, I., Sigurdardóttir, H., Gunnlaugsson, E., Axelsson, H.A., Woff-Boenisch, D., Mesfin, K., de la Reguera Taaya, D.F., Hall, J., Diderikson, K., and Broecker, W.S., 2016. Rapid carbon mineralization for permanent disposal of anthropogenic carbon dioxide emissions. *Science*, 352(6291):1312–1314. <https://doi.org/10.1126/science.aad8132>
- Maus, S., Barckhausen, U., Berkenbosch, H., Bournas, N., Brozena, J., Childers, V., Dostaler, F., Fairhead, J.D., Finn, C., von Frese, R.R.B., Gaina, C., Golynsky, S., Kucks, R., Lühr, H., Milligan, P., Mogren, S., Müller, R.D., Olesen, O., Pilkington, M., Saltus, R., Schreckenberger, B., Thébault, E., and Caratori Tontini, F., 2009. EMAG2: A 2–arc min resolution Earth Magnetic Anomaly Grid compiled from satellite, airborne, and marine magnetic measurements. *Geochemistry, Geophysics, Geosystems*, 10(8):Q08005. <https://doi.org/10.1029/2009GC002471>
- Michibayashi, K., Tominaga, M., Ildefonse, B., and Teagle, D.A.H., 2019. What lies beneath: the formation and evolution of oceanic lithosphere. *Oceanography*, 32(1):138–149. <https://doi.org/10.5670/oceanog.2019.136>
- Mottl, M.J., 2003. Partitioning of energy and mass fluxes between mid-ocean ridge axes and flanks at high and low temperature. In Halbach, P.E., Tunnichliffe, V., and Hein, J.R. (Eds.), *Energy and mass transfer in marine hydrothermal systems*. Berlin (Dahlem University Press), 271–286.
- Müller, R.D., Sdrolias, M., Gaina, C., Steinberger, B., and Heine, C., 2008. Long-term sea-level fluctuations driven by ocean basin dynamics. *Science*, 319(5868):1357–1362. <https://doi.org/10.1126/science.1151540>
- Neira, N.M., Clark, J.F., Fisher, A.T., Wheat, C.G., Haymon, R.M., and Becker, K., 2016. Cross-hole tracer experiment reveals rapid fluid flow and low effective porosity in the upper oceanic crust. *Earth and Planetary Science Letters*, 450:355–365. <https://doi.org/10.1016/j.epsl.2016.06.048>
- Norris, R.D., Wilson, P.A., Blum, P., Fehr, A., Agnini, C., Bornemann, A., Boulila, S., Bown, P.R., Cournede, C., Friedrich, O., Ghosh, A.K., Hollis, C.J., Hull, P.M., Jo, K., Junium, C.K., Kaneko, M., Liebrand, D., Lippert, P.C., Liu, Z., Matsui, H., Moriya, K., Nishi, H., Opdyke, B.N., Penman, D., Romans, B., Scher, H.D., Sexton, P., Takagi, H., Turner, S.K., Whiteside, J.H., Yamaguchi, T., and Yamamoto, Y., 2014. Expedition 342 summary. In Norris, R.D., Wilson, P.A., Blum, P., and the Expedition 342 Scientists, *Proceedings of the Integrated Ocean Drilling Program, 342*: College Station, TX (Integrated Ocean Drilling Program). <https://doi.org/10.2204/iodp.proc.342.101.2014>
- O'Connor, J.M., and Duncan, R.A., 1990. Evolution of the Walvis Ridge-Rio Grande Rise hot spot system: implications for African and South American plate motions over plumes. *Journal of Geophysical Research: Solid Earth*, 95(B11):17475–17502. <https://doi.org/10.1029/JB095iB11p17475>
- Orcutt, B.N., Bach, W., Becker, K., Fisher, A.T., Hentscher, M., Toner, B.M., Wheat, C.G., and Edwards, K.J., 2011. Colonization of subsurface microbial observatories deployed in young ocean crust. *The ISME Journal*, 5(4):692–703. <https://doi.org/10.1038/ismej.2010.157>

- Orcutt, B.N., LaRowe, D.E., Lloyd, K.G., Mills, H., Orsi, W., Reese, B.K., Sauvage, J., Huber, J.A., and Amend, J., 2014. IODP Deep Biosphere Research Workshop report – a synthesis of recent investigations, and discussion of new research questions and drilling targets. *Scientific Drilling*, 17:61–66. <https://doi.org/10.5194/sd-17-61-2014>
- Orcutt, B.N., Wheat, C.G., Rouxel, O., Hulme, S., Edwards, K.J., and Bach, W., 2013. Oxygen consumption rates in subsurface basaltic crust derived from a reaction transport model. *Nature Communications*, 4:2539. <https://doi.org/10.1038/ncomms3539>
- Pälike, H., Lyle, M.W., Nishi, H., Raffi, I., Ridgwell, A., Gamage, K., Klaus, A., Acton, G., Anderson, L., Backman, J., Baldauf, J., Beltran, C., Bohaty, S.M., Bown, P., Busch, W., Channell, J.E.T., Chun, C.O.J., Delaney, M., Dewangan, P., Dunkley Jones, T., Edgar, K.M., Evans, H., Fitch, P., Foster, G.L., Gussone, N., Hasegawa, H., Hathorne, E.C., Hayashi, H., Herrle, J.O., Holbourn, A., Hovan, S., Hyeong, K., Iijima, K., Ito, T., Kamikuri, S.-i., Kimoto, K., Kuroda, J., Leon-Rodriguez, L., Malinverno, A., Moore Jr, T.C., Murphy, B.H., Murphy, D.P., Nakamura, H., Ogane, K., Ohneiser, C., Richter, C., Robinson, R., Rohling, E.J., Romero, O., Sawada, K., Scher, H., Schneider, L., Sluijs, A., Takata, H., Tian, J., Tsujimoto, A., Wade, B.S., Westerhold, T., Wilkens, R., Williams, T., Wilson, P.A., Yamamoto, Y., Yamamoto, S., Yamazaki, T., and Zeebe, R.E., 2012. A Cenozoic record of the equatorial Pacific carbonate compensation depth. *Nature*, 488(7413):609–614. <https://doi.org/10.1038/nature11360>
- Palmer, M.R., and Edmond, J.M., 1989. The strontium isotope budget of the modern ocean. *Earth and Planetary Science Letters*, 92(1):11–26. [https://doi.org/10.1016/0012-821X\(89\)90017-4](https://doi.org/10.1016/0012-821X(89)90017-4)
- Penrose Conference Participants, 1972. Report of the Penrose field conference on ophiolites. *Geotimes*, 17:24–25.
- Perfit, M.R., and Chadwick, W.W., Jr., 1998. Magmatism at mid-ocean ridges: constraints from volcanological and geochemical investigations. In Buck, W.R., Delaney, J.A., Karson, J.A. and Lagabriele, Y., *Faulting and Magmatism at Mid-Ocean Ridges*. Geophysical Monograph, 106: 59–115. <https://doi.org/10.1029/GM106p0059>
- Rausch, S., Böhm, F., Bach, W., Klügel, A., and Eisenhauer, A., 2013. Calcium carbonate veins in ocean crust record a threefold increase of seawater Mg/Ca in the past 30 million years. *Earth and Planetary Science Letters*, 362:215–224. <https://doi.org/10.1016/j.epsl.2012.12.005>
- Reece, R., and Estep, J., 2019. Processed MCS (PSTM) data from the Mid-Atlantic Ridge (MAR) to the Rio Grande Rise, South Atlantic Ocean, acquired by the R/V Marcus G. Langseth in 2016 (MGL1601) <https://doi.org/10.1594/IEDA/500255>
- Reese, B.K., Zinke, L.A., Sobol, M.S., LaRowe, D.E., Orcutt, B.N., Zhang, X., Jaekel, U., Wang, F., Dittmar, T., Defforey, D., Tully, B., Paytan, A., Sylvan, J.B., Amend, J.P., Edwards, K.J., and Girguis, P., 2018. Nitrogen cycling of active bacteria within oligotrophic sediment of the Mid-Atlantic Ridge flank. *Geomicrobiology Journal*, 35(6):468–483. <https://doi.org/10.1080/01490451.2017.1392649>
- Ryan, W.B.F., Carbotte, S.M., Coplan, J.O., O'Hara, S., Melkonian, A., Arko, R., Weissel, R.A., Ferrini, V., Goodwillie, A., Nitsche, F., Bonczkowski, J., and Zensky, R., 2009. Global multi-resolution topography synthesis. *Geochemistry, Geophysics, Geosystems*, 10(3):Q03014. <https://doi.org/10.1029/2008GC002332>
- Santelli, C.M., Edgcomb, V.P., Bach, W., and Edwards, K.J., 2009. The diversity and abundance of bacteria inhabiting seafloor lavas positively correlate with rock alteration. *Environmental Microbiology*, 11(1):86–98. <https://doi.org/10.1111/j.1462-2920.2008.01743.x>
- Scher, H.D., and Martin, E.E., 2006. Timing and climatic consequences of the opening of Drake Passage. *Science*, 312(5772):428–430. <https://doi.org/10.1126/science.1120044>
- Schmid, F., Peters, M., Walter, M., Devey, C., Petersen, S., Yeo, I., Köhler, J., Jamieson, J.W., Walker, S., and Sültenfuß, J., 2019. Physico-chemical properties of newly discovered hydrothermal plumes above the southern Mid-Atlantic Ridge (13°–33°S). *Deep Sea Research, Part I: Oceanographic Research Papers*, 148:34–52. <https://doi.org/10.1016/j.dsr.2019.04.010>
- Scientific Party, 1970. Introduction. In Maxwell, A.E., et al., *Initial Reports of the Deep Sea Drilling Project*, 83: Washington, DC (US Government Printing Office), 7–9. <https://doi.org/10.2973/dsdp.proc.3.101.1970>
- Shipboard Scientific Party, 1985. Explanatory notes. In Anderson, R.N., Honnorez, J., Becker, K., et al., *Initial Reports of the Deep Sea Drilling Project*, 83: Washington, DC (US Government Printing Office), 5–11. <https://doi.org/10.2973/dsdp.proc.83.101.1985>
- Shipboard Scientific Party, 1993. Explanatory notes. In Alt, J.C., Kinoshita, H., Stokking, L.B., et al., *Proceedings of the Ocean Drilling Program, Initial Reports*, 148: College Station, TX (Ocean Drilling Program). <https://doi.org/10.2973/odp.proc.ir.148.101.1993>
- Shipboard Scientific Party, 1997. Introduction and summary: hydrothermal circulation in the oceanic crust and its consequences on the eastern flank of the Juan de Fuca Ridge. In Davies, E.E., Fisher, A.T., Firth, J.V., et al., *Proceedings of the Ocean Drilling Program, Initial Reports*, 168: College Station, TX (Ocean Drilling Program), 7–21. <https://doi.org/10.2973/odp.proc.ir.168.101.1997>
- Shipboard Scientific Party, 2002. Leg 199 summary. In Lyle, M., Wilson, P.A., Janecek, T.R., et al., *Proceedings of the Ocean Drilling Program, Initial Reports*, 199: College Station, TX (Ocean Drilling Program). <https://doi.org/10.2973/odp.proc.ir.199.101.2002>
- Shipboard Scientific Party, 2003a. Leg 201 summary. In D'Hondt, S.L., Jørgensen, B.B., Miller, D.J., et al., *Proceedings of the Ocean Drilling Program, Initial Reports*, 201: College Station, TX (Ocean Drilling Program), 1–81. <https://doi.org/10.2973/odp.proc.ir.201.101.2003>
- Shipboard Scientific Party, 2003b. Leg 206 summary. In Wilson, D.S., Teagle, D.A.H., Acton, G.D., et al., *Proceedings of the Ocean Drilling Program, Initial Reports*. 206: College Station, TX (Ocean Drilling Program). <https://doi.org/10.2973/odp.proc.ir.206.101.2003>
- Shipboard Scientific Party, 2004. Leg 208 summary. In Zachos, J.C., Kroon, D., Blum, P., et al., *Proceedings of the Ocean Drilling Program, Initial Reports*, 208: College Station, TX (Ocean Drilling Program). <https://doi.org/10.2973/odp.proc.ir.208.101.2004>

- Spinelli, G.A., Giambalvo, E.R., and Fisher, A.T., 2004. Sediment permeability, distribution, and influence on fluxes in oceanic basement. In Davis, E.E., and Elderfield, H. (Eds.), *Hydrogeology of the Oceanic Lithosphere*. Cambridge, UK (Cambridge University Press), 151–188.
- Staudigel, H., Hart, S.R., Schmincke, H.-U., and Smith, B.M., 1989. Cretaceous ocean crust at DSDP Sites 417 and 418: carbon uptake from weathering versus loss by magmatic outgassing. *Geochimica et Cosmochimica Acta*, 53(11):3091–3094. [https://doi.org/10.1016/0016-7037\(89\)90189-0](https://doi.org/10.1016/0016-7037(89)90189-0)
- Stein, C.A., and Stein, S., 1994. Constraints on hydrothermal heat flux through the oceanic lithosphere from global heat flow. *Journal of Geophysical Research: Solid Earth*, 99(B2):3081–3095. <https://doi.org/10.1029/93JB02222>
- Stommel, H., 1961. Thermohaline convection with two stable regimes of flow. *Tellus*, 13(2):224–230. <https://doi.org/10.1111/j.2153-3490.1961.tb00079.x>
- Sun, S., and McDonough, W.F., 1989. Chemical and isotopic systematics of oceanic basalts: implications for mantle composition and processes. In Saunders, A.D., and Norry, M.J. (Eds.), *Magmatism in the Ocean Basins*. Geological Society Special Publication, 42: 313–345. <https://doi.org/10.1144/GSL.SP.1989.042.01.19>
- Sylvan, J.B., Hoffman, C.L., Momper, L.M., Toner, B.M., Amend, J.P., and Edwards, K.J., 2015. *Bacillus rigilipofundi* sp. nov., an endospore-forming, Mn-oxidizing, moderately halophilic bacterium isolated from deep seafloor basaltic crust. *International Journal of Systematic and Evolutionary Microbiology*, 65(6):1992–1998. <https://doi.org/10.1099/ij.s.0.000211>
- Thomas, D.J., Bralower, T.J., and Jones, C.E., 2003. Neodymium isotopic reconstruction of late Paleocene–early Eocene thermohaline circulation. *Earth and Planetary Science Letters*, 209(3–4):309–322. [https://doi.org/10.1016/S0012-821X\(03\)00096-7](https://doi.org/10.1016/S0012-821X(03)00096-7)
- Tobin, H.J., Kinoshita, M., Ashi, J., Lallemand, S., Kimura, G., Screaton, E.J., Thu, M.K., Masago, H., and Curewitz, D., 2009. NanTroSEIZE Stage 1 expeditions: introduction and synthesis of key results. In Kinoshita, M., Tobin, H., Ashi, J., Kimura, G., Lallemand, S., Screaton, E.J., Curewitz, D., Masago, H., Moe, K.T., and the Expedition 314/315/316 Scientists, *Proceedings of the Integrated Ocean Drilling Program*, 314/315/316: Washington, DC (Integrated Ocean Drilling Program Management, Inc.). <https://doi.org/10.2204/iodp.proc.314315316.101.2009>
- Tripathi, A., Backman, J., Elderfield, H., and Ferretti, P., 2005. Eocene bipolar glaciation associated with global carbon cycle changes. *Nature*, 436(7049):341–346. <https://doi.org/10.1038/nature03874>
- Vance, D., Teagle, D.A.H., and Foster, G.L., 2009. Variable Quaternary chemical weathering fluxes and imbalances in marine geochemical budgets. *Nature*, 458(7237):493–496. <https://doi.org/10.1038/nature07828>
- Westerhold, T., Marwan, N., Drury, A.J., Liebrand, D., Agnini, C., Anagnostou, E., Barnet, J.S.K., Bohaty, S.M., Vleeschouwer, D.D., Florindo, F., Frederichs, T., Hodell, D.A., Holbourn, A.E., Kroon, D., Lauretano, V., Littler, K., Lourens, L.J., Lyle, M., Pälike, H., Röhl, U., Tian, J., Wilkens, R.H., Wilson, P.A., and Zachos, J.C., 2020. An astronomically dated record of Earth's climate and its predictability over the last 66 million years. *Science*, 369(6509):1383–1387. <https://doi.org/10.1126/science.aba6853>
- Wheat, C.G., and Fisher, A.T., 2008. Massive, low-temperature hydrothermal flow from a basaltic outcrop on 23 Ma seafloor of the Cocos plate: chemical constraints and implications. *Geochemistry, Geophysics, Geosystems*, 9(12):Q12O14. <https://doi.org/10.1029/2008GC002136>
- Williams, T., Estes, E.R., Rhinehart, B., Coggon, R.M., Sylvan, J.B., Christeson, G.L., and Teagle, D.A.H., 2021. Expedition 395E Preliminary Report: Complete South Atlantic Transect Reentry Systems. *International Ocean Discovery Program*. <https://doi.org/10.14379/iodp.pr.395E.2021>
- Wright, J.D., Miller, K.G., and Fairbanks, R.G., 1991. Evolution of modern deepwater circulation: evidence from the Late Miocene Southern Ocean. *Paleoceanography and Paleoclimatology*, 6(2):275–290. <https://doi.org/10.1029/90PA02498>
- Wunsch, C., 2002. What is the thermohaline circulation? *Science*, 298(5596):1179–1181. <https://doi.org/10.1126/science.1079329>
- Zachos, J., Pagani, M., Sloan, L., Thomas, E., and Billups, K., 2001. Trends, rhythms, and aberrations in global climate 65 Ma to Present. *Science*, 292(5517):686–693. <https://doi.org/10.1126/science.1059412>
- Zachos, J.C., Dickens, G.R., and Zeebe, R.E., 2008. An early Cenozoic perspective on greenhouse warming and carbon-cycle dynamics. *Nature*, 451(7176):279–283. <https://doi.org/10.1038/nature06588>
- Zachos, J.C., Röhl, U., Schellenberg, S.A., Sluijs, A., Hodell, D.A., Kelly, D.C., Thomas, E., Nicolo, M., Raffi, I., Lourens, L.J., McCarren, H., and Kroon, D., 2005. Rapid acidification of the ocean during the Paleocene-Eocene Thermal Maximum. *Science*, 308(5728):1611–1615. <https://doi.org/10.1126/science.1109004>
- Zeebe, R.E., Zachos, J.C., Caldeira, K., and Tyrrell, T., 2008. Oceans: carbon emissions and acidification. *Science*, 321(5885):51–52. <https://doi.org/10.1126/science.1159124>